DOCTORAL DISSERTATION

Investigating tidal evolution and tide–river runoff interactions in a two-inlet lagoon and multi-channel estuary

（2 つの入口を持つラグーンとマルチチャネル河口における潮汐進化および潮汐と河川流出の相互作用に関する調査研究）

July 2022

Department of Civil and Environmental Engineering

Graduate School of Engineering

Hiroshima University

KHADAMI, FARUQ

Acknowledgement

The members of my supervisory committee deserve the best accolades and my deepest thanks for their expertise, encouragement, and support. First, I would like to thank my supervisor, Prof. Kawanishi, for his excellent guidance, support, and patience during my doctoral studies at Hiroshima University.

I would like to express my sincere appreciation to Nakashita sensei for his help in the laboratory and to Dr. Mohamad Basel Al Sawaf for his excellent guidance, invaluable support, and critical science. I also thank all the laboratory members, Gillang, Xiao, Torigoe, and Hiep, for their help.

In the opportunity, I would thank the Japanese Government (MEXT) scholarship program for supporting my doctoral program at Hiroshima University.

Thanks to all my friends who supported me during my time at Hiroshima. PPI Hiroshima (Indonesian Student Association in Hiroshima) that introduce me to the Indonesian community in Hiroshima. I also thank member group chats WA Les Bahasa for the nice talk and discussion. Many thanks to Mika for the support, understanding, and patience.

Last but not least, Special thanks to my parents, Ibuk Catur Wirononingsih and Bapak Imron Rosyadi, who prayed a lot for me; they deserve great respect. I also thank my sisters, Mbak Novi and Dek Tia, for their support and love.

Tables of Contents

List of Symbols

Symbols	
c	celerity of tidal wave
g	gravitational acceleration
h	water depth
γ	skewness
Q	water discharge
η	elevation of …
Ri_L	Richardson number
ρ	density of …
Fr_f	Freshwater Froude Number
M	Mixing tidal efficiency
C_D	drag coefficient
U_T	amplitude of the tidal velocity
N	buoyancy frequency
S_0	reference salinity
U	current velocity
W	channel width
C	Chézy coefficient

List of Abbreviations

Abbreviations	
TDA	tidal duration asymmetry
PCA	peak current asymmetry
SWA	slack water asymmetry
PLW	Pelawangan West
PLE	Pelawangan East
TMD	Tidal Model Driver
NSE	Nash-Sutchliffe Efficiency
SAL	Segara Anakan Lagoon
ETM	estuarine turbidity maximum
ADCP	acoustic Doppler current profiler
FAT	fluvial acoustic tomography
CWT	continuous wavelet transform
XWT	cross wavelet transform
WTC	coherence wavelet transform
ODC	Ota diversion channel
HWL	high water level
FFT	fast Fourier transform
HA	harmonic analysis

List of Figures

List of Tables

Abstract

Understanding hydrodynamics induced by an interaction between tide and river flow is essential to continuously improve the management of delta and estuarine systems. The investigation of the interaction between tides and river flow could also enhance our understanding of the alteration process of the environment in tidal rivers. This research investigates the spatiotemporal tidal dynamics in various setting topography, aiming to understand the evolution of tidal waves in single-channel, multi-channel and multi-inlet lagoons. The work was divided into two main projects that worked in two site locations: the Segara Anakan Lagoon and the Ota River Estuary.

The first work aims to investigate the tidal dynamics in Segara Anakan Lagoon, which can be the main factor that leads to sedimentation patterns. The Segara Anakan Lagoon (SAL) is a two-inlet lagoon with a high sedimentation rate in the western part. The two-dimensional hydrodynamic model was used to investigate the tidal dynamics. Spatial computation of tidal duration asymmetry, peak discharge asymmetry, and slack water asymmetry are used to identify the tidal dynamics characteristics of the SAL. The model results show that tidal wave propagates to the lagoon from both inlets and amasses in the central part of the lagoon. Analysis of the tidal asymmetry shows that the tidal duration and slack water asymmetry are ebb dominance in both inlets, while the peak discharge is ebb dominance in the western lagoon and flood dominance in the eastern lagoon. However, the tidal duration, peak discharge, and slack water asymmetry show flood dominance in amassing areas. The convergence of tidal waves in the central part of the lagoon results in abrupt changes in the tidal range and near-zero discharge in the amassing area. Moreover, the tidal asymmetry pattern might have implications for the sedimentation pattern in SAL.

The second work aims to investigate the tidal evolution in a multi-channel estuary, in this case, the Ota River Estuary. The Ota River estuary has a straight channel, the Ota diversion channel (ODC), and a branching channel. This study examines tidal distortion, tidal asymmetry, and subtidal water elevation variations in two topographical settings, straight and branching channels, under low-flow conditions. The ratio of the amplitudes of the quarter-diurnal and semidiurnal tidal species shows that the tidal distortions in the straight and branching channels are similar. The skewness of the tidal duration shows a tendency to be flood-dominant in both topographical settings. However, the increase in tidal asymmetry on the branching channel is steeper than that on the straight channel. In addition, changes in bathymetry and channel width also contribute to the steep increase in tidal asymmetry in branching channels. Moreover, the variation in the subtidal water elevation analysed using the decomposition of the subtidal friction term shows that the variation is more influenced by the interaction of the tides and tidal asymmetry in the junction area. In contrast, the variation is more affected by the subtidal flow in the straight channel. Moreover, the interaction between tides and river runoff in the straight ODC shows that the mixing was controlled by neap–spring tidal oscillation; high discharges significantly influence mixing during the neap tide. Furthermore, the results of the wavelet transform indicates that during the spring, tidal straining increases and induces intense mixing, while during the neap, river discharge has a more significant influence on circulation. The interactions between tides and river runoff influence the appearance of a convergence zone and estuarine turbidity maxima that are located approximately 4.8 km from the river mouth.

The tidal evolution mechanism in a branching channel is examined using a barotropic hydrodynamic model in an idealized junction domain, inspired by the Ota River Estuary junction. Even though the model was simplified, it successfully reproduced the increase in nonlinearity at the junction apex. A sensitivity analysis of tidal nonlinearity to the width of the

upstream channel at the junction was performed by varying the upstream channel width from the same width as the branch channel width to three times the branch channel width. The relationship between the upstream channel width at the diversion point and tidal nonlinearity was not linear, whereas tidal nonlinearity was maximized when the width was twice the branch channel width. The convergence of the tides in the narrow junction induces an increase of M4 tidal constituent that raises the tidal nonlinearity, while in the case of a wider channel, which the wide of the upstream channel is more than twice of the branches channel, the river runoff dampens the M2 and M4 tidal constituents that lead to decrease tidal nonlinearity.

Chapter 1: Introduction

1.1. Study Overview

Estuaries are a transition zone of the river environment and marine environment. In recent decades, the estuary has been facing anthropogenic pressure that led to a change in the hydrodynamics and sediment dynamics pattern. These changes potentially cause reforms in the ecological function of the estuary's ecosystem. The critical issues in estuarine zone management are to protect estuaries' ecological function while still giving economic benefits. Hence, understanding the mechanism that drives the hydrodynamics and sediment dynamics changes is essential to solving those issues.

In estuary, of the interaction between the tides and river runoff causes a complex hydrodynamics and water circulation in estuaries. The tides and high salinity water from the seas converges with the fresh water river runoff. The density difference between the fresh water and saline water induces density currents that increase the complexity of the hydrodynamics in the estuary. Moreover, the hydrodynamics and the tidal dynamics in estuary is affected by the topographical setting of the estuary. Thus, understanding interactions between tides and river runoff is important because it has implications in estuary management quality.

Topography settings of the estuary affects interactions between the tides and river run off in estuary significantly. In a single channel estuary, the tides–river runoff interaction is influenced by the width and depth of the channel. In multi-channel estuaries, the interactions are more complex because the interaction is also influenced by the convergence of the tides that coming from two inlets or mores. Therefore, on the lagoon estuaries, the interactions are influenced by the bottom topography during the propagation of tidal waves. A steep changes of bottom topography could induce an abrupt change of the water level and increase of tidal asymmetry. In single-channel, multi-channel, and lagoon estuaries, the tides–rivers runoff interactions induce the nonstationary features in tidal elevations and currents profile.

Explaining the nonstationary features and distinguishing the mechanism are difficult. Thus, it remains a challenge to examine the nonstationary of tide–river runoff interaction, particularly in the various topography settings.

Likewise, studying the tides–river runoff characteristics is necessary to further understanding about the dynamics of the estuary and improve the management of estuary. The nonstationary interactions between tides and river runoff exhibit nonstationary on spatial and temporal all physical feature in estuaries, such as the water elevation, currents, salinity and temperature. Accordingly, characterisation the role of tides and river runoff on the local circulation that affects the physical features is crucial. Thus, in this study, interactions between tides and river runoff are investigated on various setting of topography. Moreover, the nonstationary behavior that was influenced by the interactions are examined. In addition, the survey sites are located in the Ota River network that represents multi-channel estuaries and the Segara Anakan Lagoon that represents lagoon estuaries

1.2.Literature Review

Large estuaries, such as Yangtze and Mahakam Estuaries, are often studied due to their high river flow and sediment rates [1, 2]. Moreover, those rivers influence the social economics of the people that live around the rivers. The river discharge plays a significant role in tidal evolution at estuaries by delaying the wave celerity and reducing the amplitude. Furthermore, the river discharge affected the nonlinearity behaviour of tidal waves by dissipating energy to a higher frequency and increasing the tidal asymmetry [3]. The river flow transports the sediment seaward while the tides transport the sediment landward. The river and tidal flow convergence could induce the ETM [4]. In the water column stratification, the high river flow could block the salinity intrusion, and their interaction with tides plays a role in the mixing variation [1].

In recent centuries, estuaries got massive anthropogenic stress. The estuaries got the human intervention by deepening, dam development, canalization of the rivers, and accommodating larger ships [5]. The large estuaries have been influenced by the development long before the small estuaries, accordingly, the studies about the mechanism of the hydrodynamics parameter changes and the influence of development to the ecology have gotten much attention [5–7]. In recent decades, small estuaries bears the human intervention accommodate social-economic changes. Hence, the research on dynamics in small estuaries has increased in recent years. Studies of tidal regime shifting have been conducted in single channel estuaries or convergence estuaries [8–11]. Mechanism of tidal evolution in difference shape estuaries, such as multi-channel estuaries and lagoon estuaries are not yet well understood. Therefore, studies on tidal evolution and tidal dynamics particularly in various forms of estuaries are necessarily to conduct.

1.2.1. Tidal dynamics in lagoons

Tidal dynamics in tidal lagoons are strongly affected by the geomorphological settings. Geomorphological changes, either natural or anthropogenic influences, can change the tidal wave properties [12–14]. Moreover, the alteration of tidal wave properties induces shifting hydrodynamics and sediment distribution patterns in the estuaries [14]. However, the alteration of tidal wave properties is different in every tidal lagoon depending on the tidal forcing, river runoff, and geometry of the lagoon. Hence, conducting local detail studies of the estuaries is vital to understanding the lagoon's local process.

In multi-inlet lagoon, the tide propagates to the interior of the lagoon from more than one inlet. The meeting of tidal waves from more than one inlet into the lagoon interior leads to a complex hydrodynamics system. During the propagation to in lagoon interior, the tidal wave experiences tidal deformation that changes the tidal regime. For example, in Terminos lagoon,

Mexico, The tidal regime in inlets is mixed diurnal, while in the interior lagoon, the regime is diurnal [15]. Moreover, the convergence of tidal waves could induce a standing wave and eddies current inside the lagoon [16]. Due to the complex hydrodynamics system, quantifying the critical variable that controls the process is difficult. Moreover, because of those specific topography settings, studies about the dynamics of multi-inlet lagoons are limited. Hence, studying tidal dynamics in Segara Anakan Lagoon could give additional knowledge about the dynamics in multi-inlet lagoons. Furthermore, the Sagara Anakan Lagoon is a mangrove fringe; therefore, the study could improve the understanding of tidal dynamics in the mangrove area.

1.2.2. Tides in Channel network

When tidal waves propagate from the sea to estuaries, the tidal wave experiences tidal evolution by dissipating the tidal energy, damping/amplification amplitudes, and shifting the tidal phase. The geometry and bottom topography resolving the bed shear stress influence the evolution of tidal waves [11]. Moreover, river runoff interacts with the tidal wave by increasing the nonlinearity of the behaviour of the tidal waves [11]. High variability affecting the tidal evolution leads to difficulty in determining the key control variable. Some researches applied analytical models to solve the critical variable controlling the tidal evolution in a convergent channels [10, 11]. Several studies used field observation and numerical models to examine the key variable controlling the tidal evolution. In recent years, the study of channel networks has focused on tidal dynamics in distributaries channels. Interaction between tides and river runoff studies in distributary channels using numerical models shows that the branches' length and depth affect tidal range [17]. Wagner et. al. (2019) [2] suggested that tidal convergence of tidal waves from the branches strongly affects the tidal wave properties. In addition, the tide convergence location depends on the distributaries channel's topography settings.

Most of the research in the distributaries channel reviewed above was analysed using numerical models. Numerical models could provide the dynamics of the multi-channel

estuaries spatially and temporally. However, there are limitations to using the numerical model. The numerical model does not efficiently study the small estuaries with narrow and shallow channels. Besides, the dynamics in shallow estuaries are more complex because the channels are extremely shallow during the low water, and the hydrodynamics pattern changes [18]. The processes are difficult to capture in numerical models. Therefore, broad field observation of the physical properties of the estuaries, including salinity, temperature, water lever, and currents, are needed to develop a comprehensive understanding of the dynamics in small channel networks estuaries.

1.3. Research Motivation and Objectives

The tidal evolution and estuarine circulation in various topographical settings have been studied in previous studies. However, most of the studies had been conducted in well-known large estuaries with hundreds of kilometres tidal compartments and a discharge in excess of 1000 m^3/s such as Yangtze and Mahakam River. Limited studies consider small estuaries with limited discharge, whereas small estuaries are most common. For an example, more than 80% of the estuaries in UK have surface areas of less than 50 km^2 and are classified as small estuaries [19]. Hence, understanding tidal dynamics and estuarine circulation in small estuary is crucial.

In recent decades, human intervention in the small estuaries increased due to social-economic development [8]. Research in estuaries enlarges not limited to large estuaries but also to small estuaries. Research in small estuaries increased in recent years. Several studies have been carried out to investigate the detail mechanism of the tidal evolution in small estuaries. However, the detail researches are limited to tidal evolution mechanism in single-channel estuaries [9–11]. Research on tidal dynamics in multi-channel estuaries and lagoons with multi-inlets is still limited. Hence, investigating the mechanism of the tidal evolution in various topography settings of estuaries is needed.

In this research, two small estuaries that have different setting topography are selected to conduct the field studies. The locations are the Segara Anakan Lagoon that is a coastal lagoon with two inlets and Ota River Estuary that is a multi-channel estuary. In a coastal lagoon, variation of bottom topography has a significant role in tidal transformation [20, 21]. Moreover, in a two-inlet lagoon, the convergence of the tides in the inner lagoon could induce the standing wave [16] and the residual currents could induce eddies current [22]. The Segara Anakan Lagoon have unique topography because it is a mangrove fringed with two inlets and it is the river mouth of Citandui River (one of biggest river in Java island, Indonesia). Hence, the Segara Anakan Lagoon is an ideal research area to study the tidal dynamics in the lagoon due to the uniqueness of geographical setting. Furthermore, the Ota river estuary is an ideal location to study interactions between tide and river discharge in small estuary with multi-channel and limited discharge. The main channel of the Ota River estuary is the Ota diversion channel that is a 9 km straight channel. The discharge of the Ota diversion channel is controlled by the Gion Gate. The channel is suitable for researching the interactions between tides and river runoff in tidal dominated and limited discharge estuary. Moreover, the Ota River is branching in the delta. Thus, the river is suitable for studying multi-channel estuary.

Hence understanding the temporal and spatial tidal evolution in various geographic setting is important to achieve clear understanding the role of tides, river runoff, and the setting of topography for the tidal evolution. Moreover, this understanding can improve the management of estuarine system.

From those point of view, the main objectives of this study are:

- To characterize and demonstrate the effects of various topographical settings, including single channel, multi-channel and multi-inlet lagoon to tidal evolution.

- To understand the response of the estuarine circulation in tidal dominated estuaries caused by the interactions between river runoff and tide, and determine the variables that control the estuarine circulation.

1.4. Novelties of Thesis

The findings of this thesis are to clarify the deformation of the tidal wave in small estuaries with multi-tidal inlets, which most studies in estuaries are conducted in well-known large estuaries. Previous studies in multi-inlet estuaries could not simultaneously present data in a straight and branching channel during the same periods. Their studies focus on tidal wave dynamics, either only on a straight channel or branching channel. Data during the same periods in the straight and branching channel could exhibit the difference in tidal wave deformation in the straight and branching channel. Moreover, previous studies cannot continuously measure the current velocity in the upstream and downstream of the branching channel during the same periods. The lack of continuous data is probably because of (1) the limited number of ADCP that can be used for the observation, and (2) they used the currents velocity data as the reference for the numerical model validation.

The condition motivated the author to study multi-inlets lagoons and multi-channel estuaries. The original work of the studies is we found that the convergence of the tides from the inlets plays a role in the tidal deformation in both lagoon and multi-channel estuaries. Moreover, we continuously observed currents velocity using three ADCPs in upstream and downstream of the branches channel during the same periods to fill the gap in the previous studies.

1.5. Site Location and Research Methods

1.5.1. Site Location

This study was conducted in two site locations: the Segara Anakan Lagoon, Indonesia, and the Ota River Estuary, Japan. The Segara Anakan Lagoon is an estuarine lagoon with two tidal inlets, while the Ota River Estuary is a multi-channel estuary. Both of the estuaries are tidal-dominated. These locations are chosen to represent the various topographical setting, which the study focuses on the tidal dynamics in the various setting of topography.

The Segara Anakan Lagoon is a mangrove-fringed shallow coastal lagoon with two tidal inlets located in Indonesia (Figure 1.1). The tide propagates inside of the lagoon through the eastern and western inlets. The tidal regime is mixed and predominantly semi-diurnal, ranging from 0.8 m during neap tide to 1.9 m during spring tide[23]. The lagoon is the river mouth of the Citanduy river; the river discharge is estimated 78 m^3/s during the dry season and 208 m^3/s during the rainy season [24]. Moreover, smaller rivers are emptying into the lagoon with two orders lower magnitude. The seasonal variation of Citanduy river discharge strongly affects the salinity and maximum turbidity in the western part of the lagoon [23]. During high tide, the central part is dynamically affected by the water exchange between the eastern and western parts. Moreover, the hydrodynamics of the eastern part of the lagoon is strongly affected by tidal exchange from the eastern tidal inlet from the Indian Ocean [24].

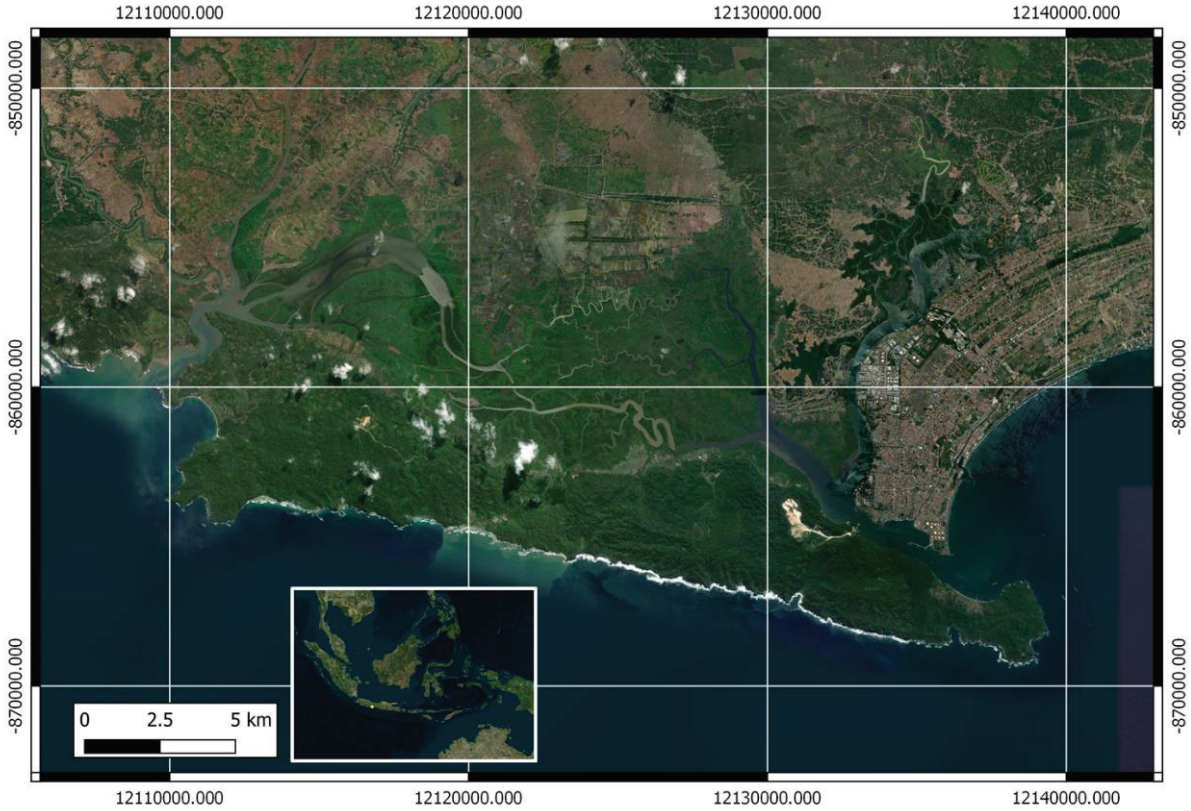

Figure 1.1 Segara Anakan Lagoon; The location of the Segara Anakan Lagoon is shown by the yellow mark in the inset map.

Ota River estuary is a multi-channel estuary located in Hiroshima city, Japan. It consists of two main branches, the Ota diversion channel and the Misasa channel. The Misasa branches into Tenma and Kyu Ota, and then the Kyu Ota channel branches into Kyu Ota and Motoyasu, as shown in Figure 1.2. The tidal compartment in this estuary reaches 13 km from the river mouth. The tidal regime of the estuary is semidiurnal, with the range up to 2 m during neap tide and 3.5 m during spring tide. The hydrological regime shows the discharge maximum during summer with around 70-100 m^3/s and minimum during winter with 20-50 m^3/s [25]. The mean bathymetry of the estuary is approximately 3 m. However, the depth of the river mouth is up to 10 m due to the utilization of the river mouth as a port.

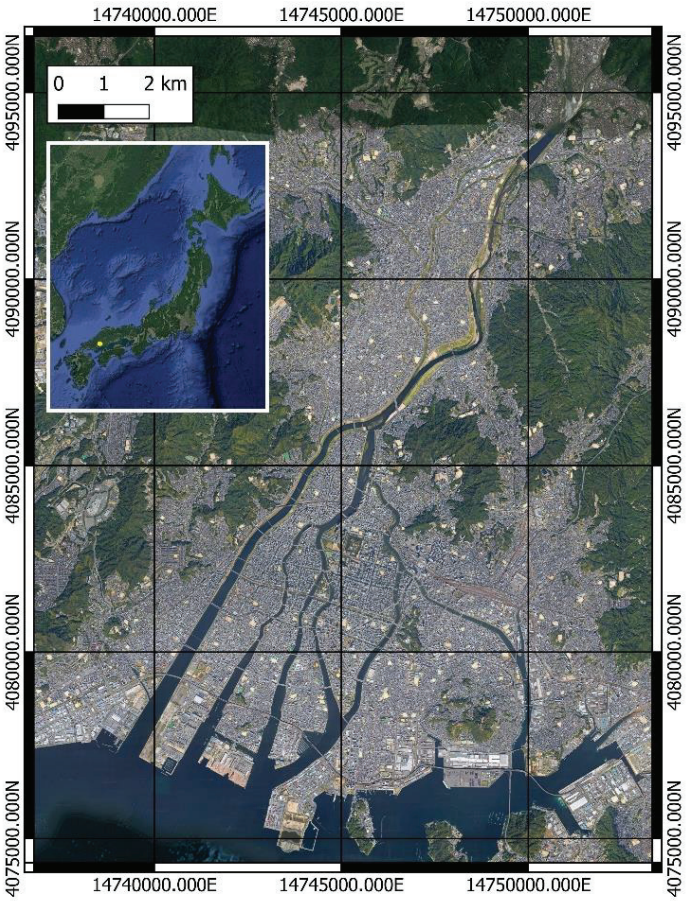

Figure 1.2 Ota River estuary; The location of the Ota River estuary is shown by the yellow mark in the inset map.

1.5.2. Data and Methods

Field observation campaigns and numerical model are utilized to conduct this research. Two field campaigns were carried out during 22 Dec 2007–16 Jan 2008 and 13-28 July 2021 in the Ota river estuary to explore the tidal evolution and estuarine circulation. During the campaigns, the currents, salinities, and temperatures were collected. The two-dimensional depth average model from Delft 3D is utilized to examine the tidal propagation and evolution inside the Segara Anakan Lagoon. Moreover, the model is applied in a synthetical branching channel domain to explain the tidal evolution mechanism in Ota River Estuary.

Chapter 2 examines tidal dynamics in the Segara Anakan Lagoon with two tidal inlets. In this chapter, a two-dimensional depth average hydrodynamic model from Delft 3D is

utilized. The model is forced by river discharge from the Citanduy River and other small rivers and tides in the open boundary. The simulation is run during the dry season to minimalize the effects of the river discharge. The model is validated using data observation from Holterman et. Al. (2009). Furthermore, the tidal range, tidal wave celerity, bed shear stress, and tidal asymmetry are calculated to discuss the mechanism of tidal evolution inside the lagoon.

Chapter 3 presents the interactions between the tides and river discharge and the effects of the mixing and the currents spatial and temporally. The mixing is evaluated using several methods to analyze the intensity and dominance of the driving variable that induces the mixing. Richardson number and Freshwater Froude Number are applied to examine the dominant driving variables in the mixing process, while the mixing tidal efficiency is used to investigate the mixing intensity. Moreover, continuous wavelet transform analysis is applied to analyze the dominant frequency and its variation over time. The cross-wavelet transform and coherence wavelet transform examine the dependency of circulation on stratification and river discharge.

Chapter 4 is an extension of Chapter 3 that examines the interactions between tides and river runoff in a straight channel. Chapter 4 examines the tidal evolution in a straight and branching channel. In this chapter, the tidal elevation data in the straight and branching channel were utilized to discuss the effect of the topographical setting, particularly a junction, on the tidal evolution in the estuary. Harmonic analysis and the variation of tidal asymmetry are applied to discuss the tidal oscillation before and after propagating to the estuary. Moreover, the subtidal elevation on the junction is discussed using the decomposition of subtidal friction from ADCP data.

Numerical model is used in Chapter 5 to examine the effect of the changing of channel width into the tidal nonlinearity. As an extension of Chapter 4, Chapter 5 focuses on the behavior of the tidal oscillation on varying upstream channel width. In the investigation, 5 scenario were simulated by varying the width of upstream channel of the junction. The width

is variated from the same width as the branch channel width to three times the branch channel width.

1.6. Research Outline

The study's main objective is to characterize and understand the tidal evolution in different topographical settings. The evolution of tides are examined in a multi-inlet lagoon estuary and multi-channel estuary. The physical mechanism involved in the tidal dynamics in those locations is elaborated in the four following chapters. The last chapter presents the study's summaries and suggestions for further research.

In chapter 2, we used a two-dimensional hydrodynamic model to investigate the tidal dynamics in the Segara Anakan Lagoon (SAL). The main purpose of this chapter is to clarify the dynamics of tidal propagation inside the lagoon by calculating the tidal duration asymmetry, peak discharge asymmetry, and slack water asymmetry. This chapter has been reproduced with minor changes from *Khadami, Faruq, Kiyosi Kawanisi, and Ayi Tarya. 2020. "Tidal Asymmetry in Two-Inlet Lagoon: A Case Study on Segara Anakan Lagoon, Central Java, Indonesia." Journal of Japan Society of Civil Engineers, Ser. B1 (Hydraulic Engineering) 76 (2): I_1411-I_1416. https://doi.org/10.2208/jscejhe.76.2_i_1411*.

In chapter 3, Observational data are used to investigate the response of currents and mixing to the interactions between tides and river runoff in a single straight channel. The main purpose is to examine the interactions between tides and currents, as well as river runoff and currents, in a small-sized estuary with a low discharge range. This chapter is reproduced with minor changes from *Khadami, Faruq, Kiyosi Kawanisi, Mohamad Basel Al Sawaf, Gillang Noor Nugrahaning Gusti, and Cong Xiao. 2022. "Spatiotemporal Response of Currents and Mixing to the Interaction of Tides and River Runoff in a Mesotidal Estuary." Ocean Science Journal, no. 0123456789. https://doi.org/10.1007/s12601-022-00056-0*.

In chapter 4, Data observation in the junction is used to examine the evolution of the tidal wave propagation in a tidal-dominated multi-channel estuary. This section discusses tidal distortion, tidal asymmetry, and subtidal water elevation variations in two topographical settings, straight and branching channels, under limited discharge conditions. This chapter is reproduced with minor changes from *Khadami, Faruq, Kiyosi Kawanisi, Mohamad Basel Al Sawaf, Gillang Noor Nugrahaning Gusti, and Cong Xiao. "Propagation of tidal waves in tidal dominated and multi-channel estuary" submitted in Continental Shelf Research*

In chapter 5, the barotropic hydrodynamic model is applied in an idealized junction domain, inspired by the Ota River Estuary junction, to estimate the nonlinearity in the junction quantitatively. A sensitivity analysis of tidal nonlinearity to the width of the upstream channel at the junction is performed by varying the upstream channel width from the same width as the branch channel width to three times the branch channel width. This chapter has been reproduced with minor changes from *Khadami, Faruq, Kiyosi Kawanisi, Mohamad Basel Al Sawaf, and Gillang Noor Nugrahaning Gusti. "Sensitivity of Junction Width to Tidal Nonlinearity on Small and Shallow Tidal Junction" submitted in Indonesian Journal of Science and Technology*

Finally in Chapter 6 presents the summaries of the study and future work related to this study.

.

Chapter 2: Tidal asymmetry in two-inlet lagoon: a case study on Segara Anakan Lagoon, Central Java, Indonesia

2.1. Introduction

Tidal asymmetry is recognized as an important factor that controls residual sediment transport in coastal waters and lagoon systems. Tidal asymmetry induces residual currents that transport sediments. There are three classifications of tidal asymmetry. (1) Tidal duration asymmetry (TDA) estimates the asymmetry of flood and ebb duration, (2) peak current asymmetry (PCA) estimates the asymmetry of the peak currents of flood and ebb, and (3) slack water asymmetry (SWA) computes the asymmetry of high and low water slack duration. The rising and falling durations are strongly related to the peak currents and the slack water duration [26]. A shorter rising tide will induce stronger flood currents and longer high water slack. This system means flood dominance. In the flood dominance system, seawater inflow to the basin is greater than the outflow and vice versa on the ebb dominance system. Sedimentation tends to occur in the flood dominance system, while in the ebb dominance system, erosion tends to occur.

Tidal asymmetry commonly occurs when the tidal wave propagates into a shallow water system. The interference of bottom friction in a shallow water system generates transformations of the tidal wave to be shallow water tide's components, such as M4 [16]. The interaction of principal tides and shallow water tide's components cause tidal asymmetry [27–29]. Non-tidal aspects such as river discharge can also affect tidal dynamics [29–31]. River discharge shortens the flood duration and induces the longer ebb duration [28].

Water circulation in a multi-channel lagoon system has more complex hydrodynamics. Tides can propagate to the lagoon through two open channels or more. Several studies in two-inlet lagoons explain that the tides convergence in a region behaves looks like a standing wave

[16] and the residual currents in the basin induce eddies [22]. A multi-channel lagoon system can show a different tidal asymmetry in every inlet because of the morphology and bathymetry of the inlets.

Segara Anakan Lagoon (SAL) is a semi-enclosed, mangrove-fringed estuary with two outlets located in Cilacap, on the south coast of Central Java, Indonesia (Figure 2.1). The lagoon is the estuary of the Citanduy River. There are nine rivers flowing into the SAL besides the Citanduy River. However, the watershed areas of other rivers are not more than 10% of Citanduy River [24]. The hydrodynamics of the SAL are driven by the interaction of the tides that propagate from the western and eastern channels, as well as the Citanduy River discharge [12, 24]. Seasonal wind and rain affect the current and salinity distribution in the SAL [23]. Satellite imagery and historical maps recorded high sedimentation occurred in the western part of the SAL but not in the eastern part [32, 33].

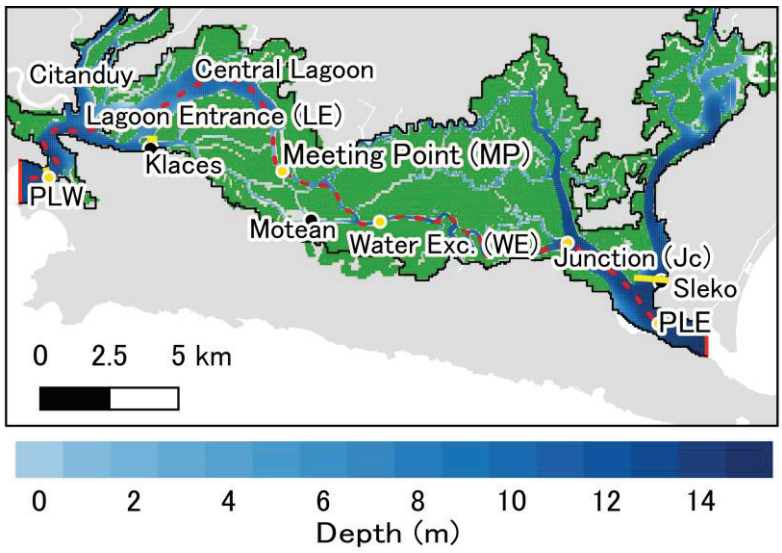

Figure 2.1 Bathymetry of the Segara Anakan Lagoon (SAL); Black dots are the tide gauge stations, and the yellow lines are cross-sections for calculating the discharge. The red dashed line is transecting for spatial change analysis. The grey and green areas show land and mangrove areas, respectively. The computational domain is enclosed by the solid black line. Solid red lines denote open boundaries.

The objective of the present study is to clarify the dynamics of tidal propagation inside the lagoon. A numerical model is used to represent hydrodynamic circulation in the lagoon, and the results of the model are utilized as data to compute the tidal asymmetry. The dynamics of the tides are analyzed using tidal asymmetry computations. The paper presents the followings. Section 2.2 explains the numerical model, asymmetry computation formula, and observation data. Section 2.3 presents the results of the numerical model and the computations of tidal asymmetry. In section 2.4, we discuss the cause in the spatial changes of the asymmetry and the implication of the changes.

2.2. Data and Methods

2.2.1. Data

Field observation data from Holtermann et al., (2009)[24] are utilized in this study. We use bathymetry, discharge, and water elevation data that carried out in the multidisciplinary German-Indonesian SPICE (Science for the Protection of Indonesian Coastal Marine Ecosystems) research project as well as additional bathymetry data that measured in 2017 and 2018 in the frame of P3MI ITB project. The data on the dry and rainy seasons are used as the model input as well as to validate the results of the model. The water elevations were measured in Sleko and Klaces from 9 July to 15 August, 2005 and February 2006 to March 2006. The discharges were measured in the Pelawangan West (PLW), Citanduy River, Klaces, water exchange station, and the Pelawangan East (PLE) (Figure 2.1). A more explanation of the measurement method, quality control, and post-processing of observation data are comprehensively written in Holtermann et al., (2009)[24].

2.2.2. Numerical Modelling

Delft3D is hydrodynamics model software developed by Deltares that can be applied for coastal, river and estuaries hydrodynamics simulation. This software has been used for modelling hydrodynamics and sediment transport in various studies [12, 34]. The Delft3D model could simulate the flow and transport resulting from tidal and atmospheric forcing on rectilinear and curvilinear coordinates [35]. The model solves the mass conservation and momentum equation for incompressible fluid under shallow water and hydrostatic assumption. The Delft3D model uses orthogonal curvilinear coordinates that support two coordinate systems in the horizontal direction. The coordinates are (1) Cartesian coordinates (ξ, η) and (2) Spherical coordinates (λ, ϕ), in which ξ and λ are longitudes while η and ϕ are latitudes. Governing equations of Delft3D are presented as follows.

- Continuity Equation

  The depth-averaged continuity equation is derived by the integration of continuity equation for incompressible fluids ($\nabla \cdot \vec{u} = 0$) over total depth and applied kinematic boundary conditions at water surface and bed level into consideration.

$$\frac{\partial \zeta}{\partial t} + \frac{1}{\sqrt{G_{\xi\xi}}\sqrt{G_{\eta\eta}}} \frac{\partial((d+\zeta)U\sqrt{G_{\eta\eta}})}{\partial \xi} + \frac{1}{\sqrt{G_{\xi\xi}}\sqrt{G_{\eta\eta}}} \frac{\partial((d+\zeta)V\sqrt{G_{\xi\xi}})}{\partial \eta} = (d+\zeta)Q \quad (1.1)$$

  with U and V are the depth averaged velocities

$$U = \frac{1}{d+\zeta}\int_d^\zeta u dz = \int_{-1}^0 u d\sigma \quad (1.2)$$

$$V = \frac{1}{d+\zeta}\int_d^\zeta v dz = \int_{-1}^0 v d\sigma \quad (1.3)$$

  The each variable has meaning as,

  ζ : free surface elevation above reference plane ($z = 0$)

  t : time

  $G_{\xi\xi}$: $R \cos \phi$, with $R = G_{\eta\eta}$ is radius of the Earth

  d : the depth below the reference plane

The Q representing the contributions per unit area due to the discharge or withdrawal of water.

$$Q = \int_{-1}^{0}(q_{in} - q_{out})d\sigma + P - E \tag{1.4}$$

with q_{in} and q_{out} are the local sources and sinks of water per unit volume (1/s), respectively, P represents non-local source term of precipitation and E is non-local sink term due to evaporation.

- Momentum equations in horizontal direction

  The momentum equations in ξ- and η- direction are respectively given by

$$\frac{\partial u}{\partial t} + \frac{u}{\sqrt{G_{\xi\xi}}}\frac{\partial u}{\partial \xi} + \frac{v}{\sqrt{G_{\eta\eta}}}\frac{\partial u}{\partial \eta} + \frac{w}{d+\zeta}\frac{\partial u}{\partial \sigma} - \frac{v^2}{\sqrt{G_{\xi\xi}}\sqrt{G_{\eta\eta}}}\frac{\partial \sqrt{G_{\eta\eta}}}{\partial \xi} + \frac{uv}{\sqrt{G_{\xi\xi}}\sqrt{G_{\eta\eta}}}\frac{\partial \sqrt{G_{\xi\xi}}}{\partial \eta} - fv =$$
$$-\frac{1}{\rho_0\sqrt{G_{\xi\xi}}}P_\xi + F_\xi + \frac{1}{(d+\zeta)^2}\frac{\partial}{\partial \sigma}\left(\upsilon_V \frac{\partial u}{\partial \sigma}\right) + M_\xi \tag{1.5}$$

$$\frac{\partial v}{\partial t} + \frac{u}{\sqrt{G_{\xi\xi}}}\frac{\partial v}{\partial \xi} + \frac{v}{\sqrt{G_{\eta\eta}}}\frac{\partial v}{\partial \eta} + \frac{w}{d+\zeta}\frac{\partial v}{\partial \sigma} - \frac{uv}{\sqrt{G_{\xi\xi}}\sqrt{G_{\eta\eta}}}\frac{\partial \sqrt{G_{\eta\eta}}}{\partial \xi} + \frac{u^2}{\sqrt{G_{\xi\xi}}\sqrt{G_{\eta\eta}}}\frac{\partial \sqrt{G_{\xi\xi}}}{\partial \eta} - fu =$$
$$-\frac{1}{\rho_0\sqrt{G_{\eta\eta}}}P_\eta + F_\eta + \frac{1}{(d+\zeta)^2}\frac{\partial}{\partial \sigma}\left(\upsilon_V \frac{\partial v}{\partial \sigma}\right) + M_\eta \tag{1.6}$$

  In which,

  u : flow velocity in ξ- direction

  v : flow velocity in η- direction

  f : Coriolis parameter

  ρ_0 : reference density of water

  $P_{\xi,\eta}$: gradient hydrostatic pressure in ξ- and η- direction

  $F_{\xi,\eta}$: turbulent momentum flux in ξ- and η- direction

  σ : scaled vertical coordinate

  υ_V : vertical viscosity

  $M_{\xi,\eta}$: source or sink of momentum in ξ- and η- direction

- Vertical velocities

  Vertical velocity ω in the adapting σ-coordinate system with taking precipitation and evaporation into consideration can be specified as follows

$$\frac{\partial \zeta}{\partial t} + \frac{1}{\sqrt{G_{\xi\xi}}\sqrt{G_{\eta\eta}}}\frac{\partial((d+\zeta)u\sqrt{G_{\eta\eta}})}{\partial \xi} + \frac{1}{\sqrt{G_{\xi\xi}}\sqrt{G_{\eta\eta}}}\frac{\partial((d+\zeta)v\sqrt{G_{\xi\xi}})}{\partial \eta} + \frac{\partial \omega}{\partial \sigma} = (d+\zeta)(q_{in} - q_{out}) \quad (1.7)$$

with,

q_{in} : local source per unit volume

q_{out} : local sink per unit volume

- Hydrostatic pressure assumption

  Hydrostatic pressure equation is used instead of vertical momentum equation here due to the assumption of shallow water condition. Thus,

  $$\frac{\partial P}{\partial \sigma} = -g\rho H \quad (1.8)$$

  where,

  P : hydrostatic water pressure

  g : gravitational acceleration

  ρ : density of water

  H : total water depth

The computational domain of the model is 26.5 km in the west-east direction and 13.3 km in the north-south direction, gridded by a rectangular grid with 67 m horizontal spatial resolution (Fig. 1). The model is forced by tides through two open channels in the open boundaries at PLW and PLE (Fig. 1) and river discharge from Citanduy and 8 smaller rivers [24]. In the open boundaries, radiation boundary condition is applied to make boundaries less reflective [35]. The water level is formed by 8 major tidal constituents, with K1, P1, O1, and Q1 for diurnal constituents and N2, M2, S2, and K2 for the semi-diurnal constituent. The amplitude and phase of the tidal constituent are obtained from TPXO model using the Tidal Model Driver (TMD)[36]. Constant river discharge is defined for the Citanduy River and the others based on Holtermann et al., (2009)[24]. A spatial change of the Manning's roughness coefficient (n) is considered, i.e., for the mangrove area and non-mangrove area, $n = 0.1$ and

$n = 0.03$ are applied, respectively. In this study, we simulated 2 model scenarios: dry season scenario and wet season scenario. The dry season simulation is run from 15 June, 2005 to 30 August, 2005 while the wet season scenario is run from 1 February, 2006 to 30 March, 2006. Although we validated both model results, the results of the dry season model are used for further analysis.

2.2.3. Model Validation

The model is validated using Nash-Sutchliffe Efficiency (NSE). The NSE formula is shown in equation (2.1)[37].

$$NSE = 1 - \frac{\sum_{i=1}^{N}(x_{obs} - x_{mod})^2}{\sum_{i=1}^{N}(x_{obs} - \overline{x_{obs}})^2} \qquad (2.1)$$

where x_{mod} is the model result, x_{obs} is the data observation, $\overline{x_{obs}}$ is the mean of the data observation, and *N* is the number of observed data. The NSE value is classified as excellent for *NSE*>0.65, very good for 0.5<*NSE*<0.65, good for 0.2<*NSE*<0.5, and poor for *NSE*<0.2 [37].

2.2.4. Asymmetry Quantification

Tidal asymmetry affects the sortation of residual sediment transport during the tidal cycle, that is, controlling the morphological change of the basins over the long-term sedimentation process. Tidal duration asymmetry, peak velocity skew, and slack water difference are the basic tidal asymmetry indexes that mostly control the net sediment transport. In this study, we modify the calculation of peak current asymmetry by calculating the peak discharge asymmetry (PDA) to measure differences in the water flux through the channel. The asymmetries are calculated as follows [27] :

$$\gamma(x) = \frac{\frac{1}{N-1}\sum_{i=1}^{N}(x_i - \bar{x})^3}{\left[\frac{1}{N-1}\sum_{i=1}^{N}(x_i - \bar{x})^2\right]^{3/2}} \qquad (2.2)$$

where γ is skewness, x_i is the time series of sample signals, $\bar{x}$ is the mean value of the samples, and *N* is the number of time-series data. For the TDA calculation, x denotes the time derivative of elevation ($x = \frac{d\eta}{dt}$), for the calculation of PDA x denotes the discharge ($x = Q$), and for SWA *x* denotes the time derivative of discharge ($x = \frac{dQ}{dt}$). Besides, we compute the asymmetry using 14 days window and 25 hours window in the spring and neap conditions. A window of 14 days is enforced to capture the asymmetry on a full tidal cycle, while a window of 25 hours is enforced to capture asymmetry in the neap and spring conditions. The skewness indicators are based on the previous studies [27, 34]

2.3. Results

2.3.1. Model Validation

The results of the numerical model are validated by comparing with the observation data (Figure 2.2). The NSE value for tidal elevation at Sleko station from 9 July to 14 August, 2005 was 0.87, while on 29 February to 29 March, 2006 was 0.81. Comparison of the tidal elevation in Klcaces station shows that the NSE value is 0.74 for the 22 July to 11 August, 2005 period, and 0.71 for the 17 February to 29 March, 2006 periods, respectively. Thus, the tidal model validation shows acceptable results for further analysis.

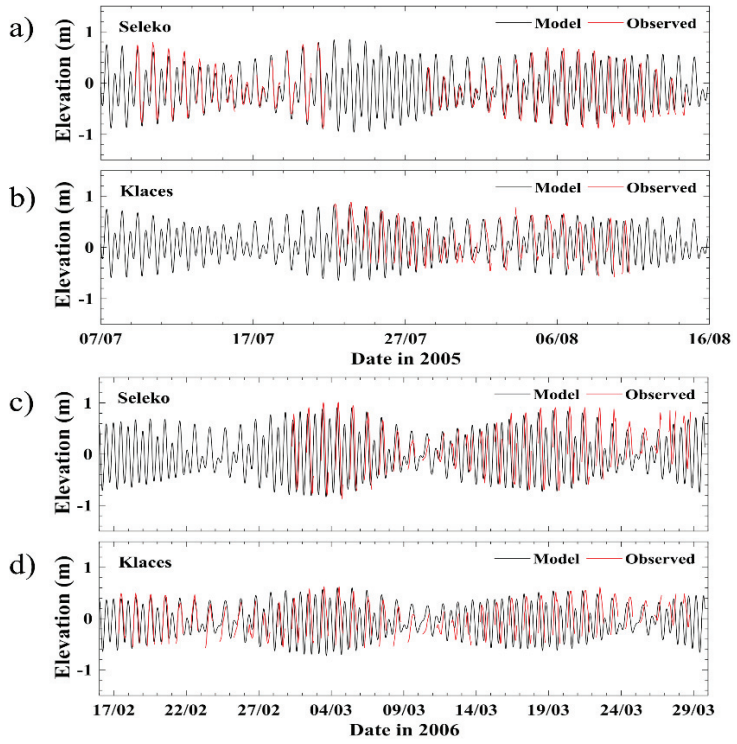

Figure 2.2 Tidal elevation during dry and wet seasons in Sleko (a, c) and Klaces (b, d). The black lines denote the simulation results, and the red lines denote the observation data.

A comparison of the discharges resulted from the model and the observation data is shown in Figure 2.3. The NSE between the model and the observation data for Pelawangan West (PLW) and Klaces during dry season periods were 0.85 and 0.24, respectively. During the wet season periods, the validation of the model is done by comparing the discharge from the model with the observation on the Pelawangan West and the water exchange station. The NSE between the model and the observation at both stations were 0.77 and 0.79, respectively. The comparison indicates that the results of the model are in good agreement with the observation data, except at Klaces during the dry season periods. The utilization of different manning's roughness coefficient for mangrove and non-mangrove areas resulted in good agreement between the model and observation data. However, NSE value in Klaces is low because the number of observation data in Klaces is limited. Hence, small variance of

observation data reduces the NSE value. In spite of that, the discharge in Klaces still shows acceptable judgment on pattern and range visually.

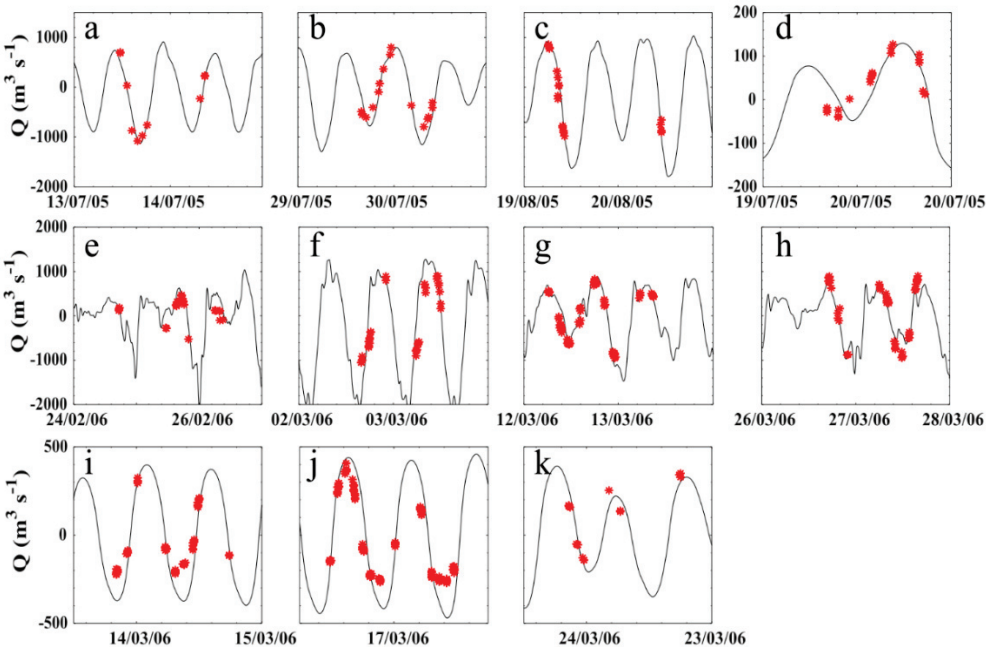

Figure 2.3 Comparisons of the discharge from the model (black line) and observation data (red dots) on the dry season in Pelawangan West (a, b, c) and Klaces (d), while on the wet season in Pelawangan West (e, f, g, h) and water exchange station (i, j, k).

2.3.2. Tidal Level and Discharge

The model results show that the tides in the SAL are mix diurnal types. The maximum tidal range at Sleko is higher than that at Kalces with 1.96 m and 1.82 m, respectively. On the spring tides, the tidal range reaches ~2 m in Klaces and Sleko while in the neap tide condition, the range is ~1m. The phase of the tides shows an opposite phase during the neap and spring (Figure 2.4a,b). The tides propagate to the inner lagoon from the PLW and PLE, with no significant phase difference. However, the tidal levels at Klaces and Sleko station have the phase difference of 20 minutes. The cross-correlation between tides in Motean–Klaces and Motean–Sleko shows that tidal elevation in Motean delays 110 minutes from Klaces and delays 130 minutes from Sleko. These results reveal that tides from PLW propagate eastward while

tides from PLE propagate westward and amass around the middle of the lagoon [12]. Figure 2.4c and d show the variations of discharges at Sleko, Klaces, and Motean stations during the neap and spring conditions. Discharges at Sleko and Klaces clearly show the tidal variation while the discharge at Motean is near zero along the tidal period.

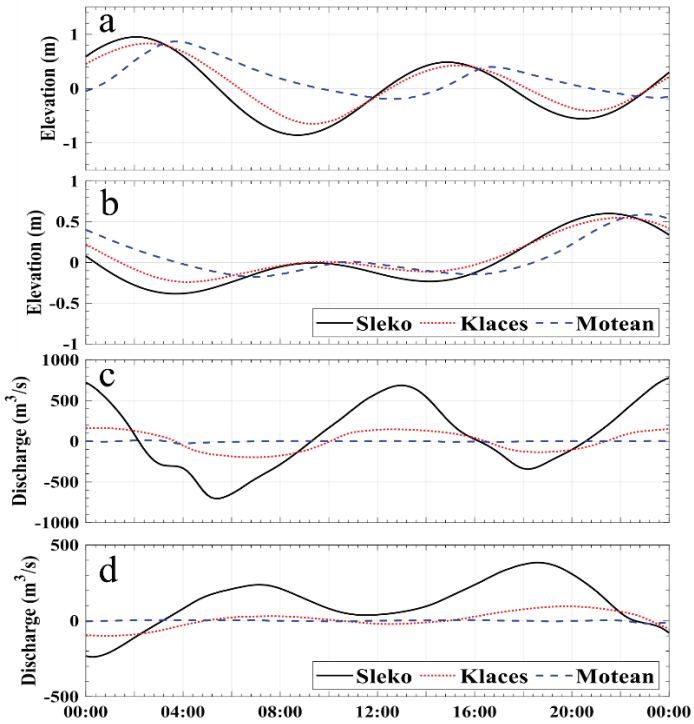

Figure 2.4 Twenty-four hours of the elevation (a, b) and discharge (c, d) during spring condition (a, c) and neap condition (b, d). The black solid line, red dot line, and blue dashed line are model results for Sleko, Klaces, and Motean stations, respectively. The spring/neap condition was on 23 July 2005/31 July 2005.

During the rising periods of tidal elevation, the discharge in Sleko and Klaces flows into the lagoon, while during the falling tidal periods, the discharge flows out from the lagoon (Figure 2.5). Referring to the tidal behavior in the lagoon, during the rising periods, the discharge converges to the inner lagoon and fills the lagoon and during the falling tides, the discharge diverges flowing out of the lagoon. The convergence of the tidal wave in the central

part of the lagoon results in quasi-standing wave that causes near-zero discharge [16] at the Motean station.

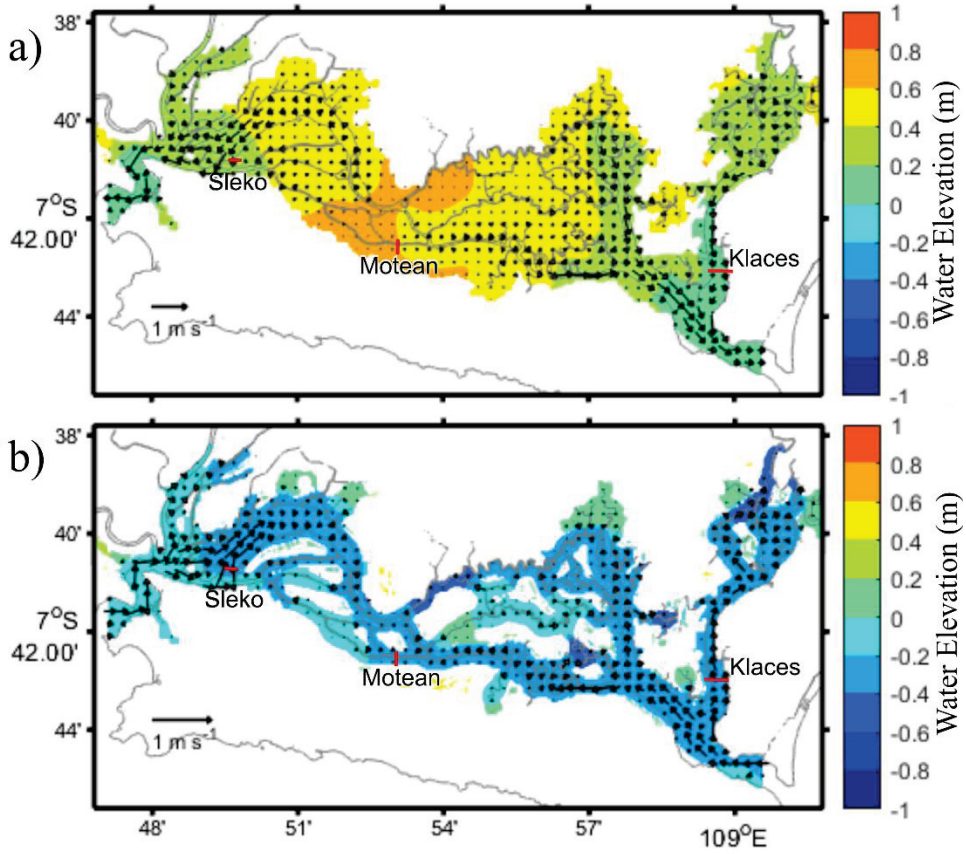

Figure 2.5 Depth average velocity vector fields and water elevation (color shading) in the Segara Anakan Lagoon on spring condition at (a) ebb tide and (b) flood tide. Red lines denote cross-section transects for calculating water volume discharge.

2.3.3. Tidal Asymmetry

We calculated the asymmetry of tidal duration, peak discharge, and slack water in 2 windows: 25 hours on the neap and spring to capture the conditions, and 14 days window to capture the asymmetry on the full tidal cycle. The results of the TDA computation at several stations in the western and eastern parts of the lagoon are shown in Table 2.1. In the spring condition, TDA in PLW, Lagoon, PLE, and Sleko shows an ebb dominance, while in the neap

condition, TDA shows a flood dominance. Despite flood dominance during the neap condition, the TDA value is close to zero. However, the TDA value at Motean station increases significantly and shows flood dominance in spring and neap conditions. Computation of TDA using 14 days window shows the same pattern of TDA in the spring condition.

There are differences in flow direction of the ebb and flood discharges in the western and eastern parts of the lagoon. The flood discharge in the west is eastward, while the flood discharge in east parts of the lagoon is westward. Owing to the definition, for PDA and SWA computation, we multiplied the discharge at the Motean and water exchange station with −1. Using the transformation, we have the same definition that positive discharge is a flood discharge.

The PDA computation shows an ebb dominance on the PLW (Table 2.1). However, the PDA changes spatially to flood dominance in the Motean station. In contrast, the PDA at the PLE station shows flood dominance and then shifts to ebb dominance in the water exchange station and then changes dramatically in the Motean to flood dominance. This pattern is shown in all computation windows. A significant change in the asymmetry from the Motean Station could be caused by the meeting of the tidal wave that propagated from east and west.

Table 2.1 Computation of Tidal Duration Asymmetry (TDA), Peak Duration Asymmetry (PDA), Slack Water Asymmetry (SWA), using a 25 hours window in spring and neap and 14 days.

Station	TDA			PDA			SWA		
	neap	spring	14 days	neap	spring	14 days	neap	spring	14 days
PLW	0.11	-0.19	-0.09	-0.64	-0.84	-0.77	0.05	-0.08	0
Lagoon	-0.08	-0.18	-0.11	-0.4	-0.45	-0.41	-0.92	0.7	-0.04
Klaces	-0.12	-0.16	0	-0.13	-0.14	-0.05	0.13	-0.04	-0.17
Motean	0.59	0.79	0.78	1.87	1.52	1.73	2.08	3.13	2.95

Water exc	0.21	-0.24	-0.19	-0.09	-0.12	-0.09	-0.66	-0.63	-0.67
Sleko	0.04	-0.2	-0.12	0.72	0.45	0.81	-0.16	-0.46	-0.48
PLE	0.04	-0.2	-0.12	0.72	-0.1	0.06	-1.11	-0.99	-1.18

The SWA computation (Table 2.1) shows different results for the eastern and western parts of the lagoon. Generally, in all computation windows, SWA computations at the western part lagoon stations (PLW, Lagoon and Klaces) are near zero. This means that the high and low slack water durations are nearly the same. While the eastern part of the lagoon, the SWA value shows ebb dominance. In the Motean station, the SWA value changed to flood dominance.

2.4. Discussion

The morphological setting of the SAL, which has two open channels, allows the tidal wave to propagate from the east and west to the inner lagoon. The celerity of wave propagation along the red dashed line in Figure 2.1 was calculated (Figure 2.6b) using the equation $c = \sqrt{gh}$, where c is the celerity, g is the gravitational acceleration, and h is water depth. The tidal celerity is related to the shoaling effect which is lower celerity value affects the increase of tidal range Moreover, the bed shear stress was computed by the model using equation $\tau_b = \frac{\rho_0 g U|U|}{C}$, where τ_b is the bed shear stress, ρ_0 is reference density of water, U is depth average velocity and C is the bottom roughness Chezy coefficient. In contrast, the high value of the bed shear stress (Figure 2.6b) is related to the damping of the tidal range. The value of celerity and the bed shear stress is highly correlated with the depth of water column. The lowest value of celerity and the increase of bed shear stress in the meeting point (Figure 2.6b) show concurrently with the drop of tidal range (Figure 2.6a). This mechanism indicates that the

bottom friction effect is more dominant (rising of bed shear stress) than the shoaling effect (lowest value of tidal celerity).

The amassing of a tidal wave significantly changes the tidal asymmetry as well. It can be seen from Figure 2.6c and Table 2.1. Figure 2.6c shows that the TDA values in PLW and PLE are close to zero and then decrease gradually to ebb dominance in the inner lagoon. However, the value increases to flood dominance around the meeting point. In meeting point, a significant change in the TDA to flood dominance is seen in the Motean station (Table 2.1). Significant changes in PDA and SWA were seen in Motean station as well. PDA and SWA showed flood dominance in Motean station, whereas the nearest station from Motean station showed ebb dominance (Table 2.1).

Peak Discharge Asymmetry (PDA) controls the coarse sediment residual transport and Slack Water Asymmetry (SWA) controls the residual transport of fine sediment [26]. In the Segara Anakan lagoon, the sediment source is mainly from the Citanduy River [23] which is deposited in the western area of the lagoon [33]. The Asymmetry pattern might correlate the sedimentation pattern that only happens in the western area. In the western part of the lagoon, PDA and SWA tend to ebb dominance. The tendency of ebb dominance can be induced by river discharge [29]. The ebb dominance in the lagoon leads to the transport of sediment from the river to the seaward. From the Citanduy river mouth, the sediment is spread in the western lagoon and transported to the sea. Due to the very low discharge around the amassing area, the sediment from the western area could not be transported to the eastern part of the lagoon. This mechanism might relate to the sediment dynamics in the Segara Anakan Lagoon. However, a study that focused on sediment transport and sedimentation should be conducted to get a better understanding of sediment dynamics in the Segara Anakan Lagoon.

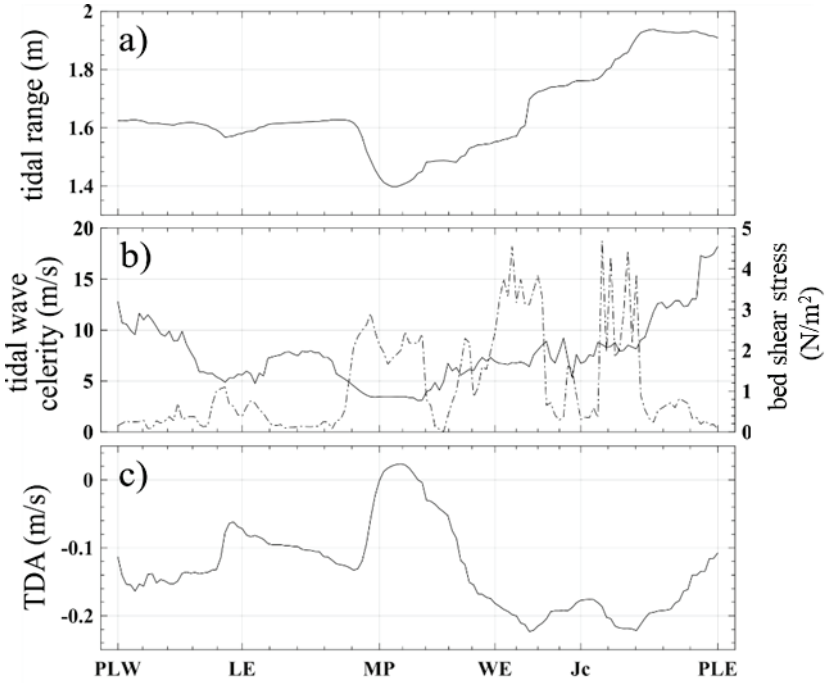

Figure 2.6 (a) Tidal range, (b) tidal wave celerity (solid line) and bed shear stress (dashed line), and (c) Tidal Duration Asymmetry (TDA) along the red dashed line transect in Figure 2.1.

2.5. Conclusions

The tidal wave in the Segara Anakan Lagoon is a mixed semi-diurnal tide with around 2 m maximum in range. The tidal wave virtually simultaneously propagates to the lagoon through two open channels from eastern and western inlets. During the rising tide, the tidal wave converges in the middle of the lagoon and diverges during the falling tides. The amassing tidal wave from eastern and western inlets in the middle of the lagoon induces an abrupt change in the tidal range and the tidal asymmetry. TDA and SWA in the eastern and western parts of the lagoon indicate the ebb dominance but shifts to the flood dominance in the middle of the lagoon. PDA shows that the asymmetry of the western part of the lagoon is the ebb dominance, while the flood dominance in the eastern part of the lagoon. The differences in the asymmetry patterns in eastern and western parts of the lagoon and low discharge in the amassing area could

be the reason for sedimentation only occurring in the western part of the lagoon, but not in the eastern part.

Chapter 3: Spatiotemporal response of currents and mixing to the interactions between tides and river runoff in a multi-channel estuary

3.1. Introduction

Current circulations in estuaries play a vital role in sediment transportation, suspended material deposition, saline water intrusion, and the alteration of water quality and estuarine habitats. The hydrodynamics in estuaries are complex and driven by various forces, including tides, river discharge [38–40], and geographical settings that modify circulation [2, 17, 26, 41]. Estuarine circulation is determined by its dominant forcing mechanism, which may include i) tidally dominated, ii) river-dominated, and iii) mixed tidal–river influence [42]. The interactions between these forcing mechanisms affect the currents, elevation, salinity, mixing, and sediment dynamics patterns within estuaries [30, 43–46].

The effects of tides and river discharge on circulation have been studied comprehensively by characterizing the circulation response to changes in elevation, current and discharge profiles, and sedimentation processes [28, 29, 38, 46–48]. The water level response due to the interactions between river discharge and tides is expressed by the occurrence of higher frequency tidal components [28, 29]. Furthermore, high river flow enhances friction and increases tidal damping [49]. The interactions between river runoff and tides in ebb–flood variation affect mixing, whereas an increase in river runoff may intensify the stratification [40, 48]. Stratification and turbulence, as a response to tide and river discharge convergence, tend to induce the estuarine turbidity maximum (ETM) [50]. In previous researches, several empirical methods [45, 51] and statistical methods [25, 52] have been applied to examine the effects of tides and river runoff on circulation. However, most studies that have considered tide–river discharge interactions with regard to circulation have typically focused on large estuaries with high discharges, i.e., greater than 1000 m^3/s, where tidal oscillations may be up

to several hundred kilometers. In other words, the majority of previous studies have been conducted on well-known rivers with a mean discharge in excess of 1000 m^3/s and up to a hundred kilometers of tidal penetration, such as the Yangtze and Mahakam.

There are only limited studies that have considered small estuaries with short tidal penetration distances, despite small estuaries being the most common type of tidal rivers. For example, more than 80% of the estuaries in the United Kingdom and Wales are small estuaries [53]. In this study, small estuaries are defined as those with surface areas of less than 50 km^2 [19]. Previous studies on small estuaries have focused on tidal straining, saltwater intrusion, and sediment transport; for example, previous researches have highlighted the role of straining and mixing limited to the tidal cycle [44, 54]. Other studies have highlighted the dynamics of the salt wedge during the tidal cycle [55, 56] or investigated variations in sediment concentration in the tidal cycle [25, 57]. However, these studies are generally limited to the effect of tides on circulation, thus interpretation of the driving variables within small estuaries has always varied due to local factors. Therefore, a mixing evaluation based on the driving variables, especially the contribution of tides and river runoff, needs to be conducted to enhance our understanding of circulation in small estuaries.

The Ota River Floodway is a small, mesotidal estuary with an average depth of 3m in the western part of Hiroshima City, Japan. Previous studies of the dynamics of the Ota River Floodway have investigated sediment transport, salinity intrusion, mixing, and turbulence [25, 58–60]. The circulation has been reported to be controlled by flood–ebb and spring–neap tidal variations and modified by river discharge [25]. During the ebb tide, the near-bed currents were smaller than those in the flood tide, and consequently, the near-bed turbulence weakened [61]. In the ebb–flood cycle, stratification increased during ebb [61]. In contrast, in the spring–neap cycle, the stratification weakened during the spring, thereby strengthening tidal mixing [58]. Generally, the aforementioned studies have focused on how tidal oscillations drive circulation.

The river runoff modifies the hydrodynamic patterns; where convergence zones appear, these require extensive analysis to understand the underlying convergence mechanism [25]. Although a considerable amount of research has been conducted in the Ota River Floodway, the majority of studies have considered the effects of tides and river discharge separately. Therefore, the dependency and consequences of the interactions between tide and river runoff on circulation and mixing are imperfectly understood and remain open to study.

In this study, we investigated the interactions between tides and currents, as well as river runoff and currents, in a small-sized estuary with a low discharge range. To address the identified research gaps in studies of low discharge and small estuaries, in this work, we examine the dominance of mixing and currents by applying wavelet analyses to two-week–one-month records of acoustic Doppler current profilers (ADCPs) at three stations along the Ota River Floodway. An enhanced understanding of the processes of tidal fluvial interaction is essential for better river management, especially in small and shallow estuaries.

The paper is structured as follows: a description of the study area is presented in Section 3.2. The data and methods are explained in Section 3.3; Sections 3.4 and 3.5 then present the results and discussion, respectively. Finally, the study's conclusions are summarized in Section 3.6.

3.2. Study Area

The Ota River Estuary is a multiple-branch delta located in the Hiroshima City, Japan. The estuary is mainly utilized for transportation and tourism. The downstream area of the estuary is used for the aquaculture of oysters [62].

The Ota River Floodway is the longest straight channel of the Ota River estuary branch (Figure 3.1). Razaz et al. (2015) [63] reported that the maximum velocity values during the ebb and flood tides were 0.65 m/s and 0.5 m/s, respectively, with tidal wave penetration of up to

13 km from the river mouth. The tidal regime of the Ota River Floodway has a mixed semidiurnal tidal cycle, with a range of 2–4 m. The river discharge of the Ota River Floodway is controlled by the Gion sluice gate, which is located 9 km upstream from the river mouth. The gate is fully opened whenever the discharge at the Yaguchi Station exceeds 400 m^3/s. Yaguchi Station is located 14.6 km from the river mouth (not shown in Figure 3.1).

Discharge observations using the fluvial acoustic tomography (FAT) system showed that ~20–50% of freshwater from Yaguchi flows to the Ota River Floodway through the Gion Gate [64]. The FAT system has demonstrated excellent performance in the Ota River Estuary [65, 66] and mountainous rivers [67–69]. During low discharge, a salt wedge occurs and high levels of stratification develop during the ebb [59].

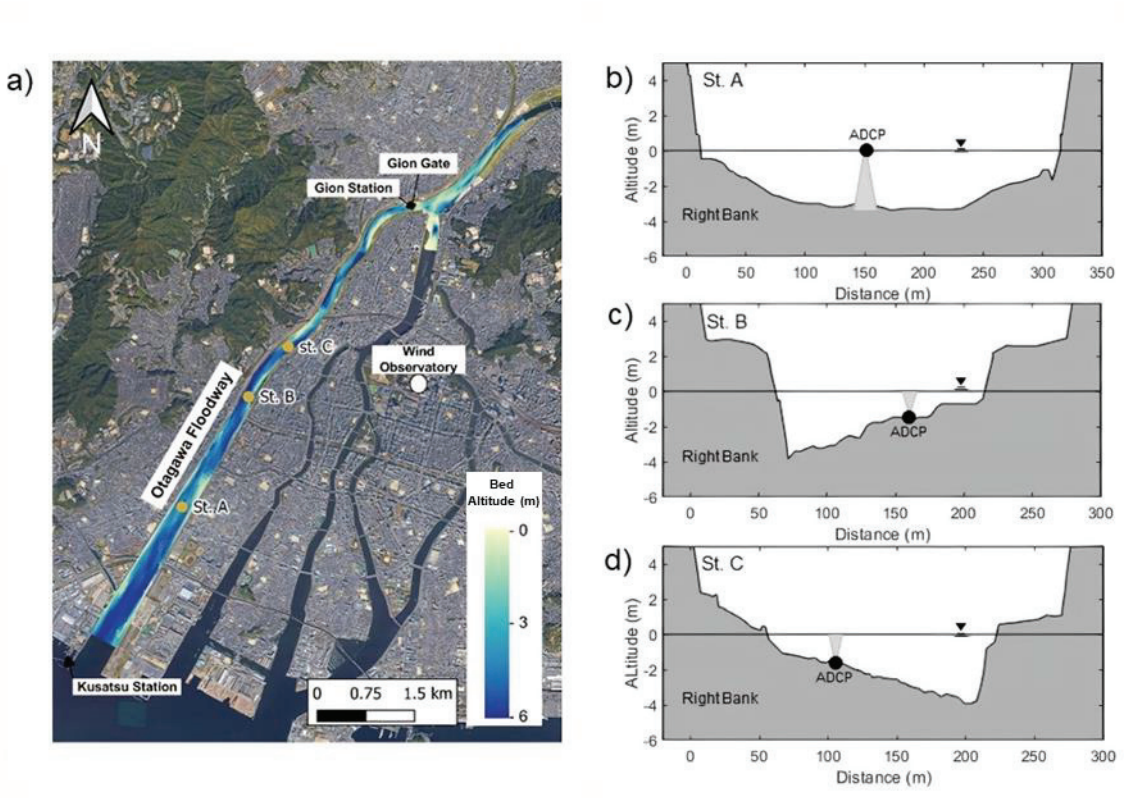

Figure 3.1. Observation sites and bathymetry along the Ota River Floodway, Hiroshima City, Japan (a). Transversal locations of the ADCPs in St. A (b), St. B (c), St. C (d).

3.3. Materials and Methods

3.3.1. Data

The data were taken at distances 2.8 km, 4.8 km, and 6 km upstream from the mouth of the Ota River mouth (Figure 3.1). Current data at stations A, B, and C were obtained using a ADCP Nortek Aquadopp 2-MHz profiler with three beams. The operation settings and deployment of the ADCP are summarized in Table 3.1. Two conductivity, and temperature, sensors (CTs) were installed, each one near the water surface and bottom at St. A from December 22, 2007, to January 16, 2008.

Hourly wind records were obtained from the Japan Meteorological Agency. In addition, the hourly elevation records at Kusatsu Station and the hourly discharge data from the Yaguchi Station were gathered from the Water Information System, Ministry of Land, Infrastructure, Transport, and Tourism (MLIT), Japan. The discharge at Gion Station was calculated from an empirical relationship established between the discharge values at the Gion and Yaguchi stations; the relation was developed in a previous study [64]. The positions of the wind observations are shown in Figure 3.1

Table 3.1. ADCP settings and deployment

Station	Bin size (m)	Blank space (m)	Sampling periods (min)	Installation	Observation periods	Notes
St. A	0.1	0.05	20	Downward looking	22 Dec 2007 –16 Jan 2008	Missing period on 2-7 Jan 2008
St. B	0.1	0.05	20	Upward looking	22 Dec 2007 –16 Jan 2008	
St. C	0.1	0.05	20	Upward looking	27 Dec 2007 –9 Jan 2008	

3.3.2. Methods

3.3.2.1. Evaluation of Mixing

The stability and mixing of the water column were examined using the Richardson number (Ri_L), which is a dimensionless value that expresses the ratio of the buoyancy force to the mechanical force. A high Richardson number indicates that the buoyancy force can suppress the mechanical force, with mixing taking place when the Richardson number is less than 20. The bulk Richardson number [40] was used in this study, which can be estimated as:

$$\boldsymbol{Ri_L = \frac{g'h}{\overline{V}^2}} \text{ and } \boldsymbol{g' = g\frac{\Delta\rho}{\rho}} \qquad (3.1)$$

where g' and g are the reduced gravity and gravitational acceleration (9.8 m/s^2), respectively, $\Delta\rho$ is the density difference between the surface and bottom, ρ is the depth-averaged density of the water column, and $\overline{V}$ is the depth-averaged longitudinal velocity.

Mixing was evaluated based on the dominance of driving factors. River discharge and tidal currents are considered to be the dominant driving variables in the mixing process. The Freshwater Froude Number (Fr_f) is used to distinguish the effects of freshwater flow on mixing in the estuary, where a high Fr_f value indicates an intense contribution of river runoff to mixing. The Fr_f is calculated by scaling the maximum velocity owing to river flow to the maximum speed of propagation gravity wave. The Fr_f is expressed as:

$$\boldsymbol{Fr_f = \frac{U_R}{(\beta g s_{ocean} H)^{1/2}}} \qquad (3.2)$$

$$\boldsymbol{\beta = \frac{\left(\frac{\rho}{\rho_0} - 1\right)}{s}} \qquad (3.3)$$

where U_R is the net velocity due to river flow, which is calculated by applying a 30-hour low-pass filter to the current data. β is the instantaneous buoyancy frequency as a function of the depth-averaged density (ρ) and salinity (s) [70], ρ_0 is the ocean density as a reference density, S_0 is ocean salinity as a reference salinity, and H is the water depth.

Mixing tidal efficiency (M) is used to measure the intensity of mixing in a stratified estuary driven by tidal currents [71]. The effectiveness of tidal mixing is expressed by the following equation:

$$\boldsymbol{M^2 = \frac{C_D U_T^2}{\omega N H^2}} \quad (3.4)$$

where C_D is the drag coefficient (0.0025) [70], U_T is the amplitude of the tidal velocity, ω is the tidal frequency, and N is the buoyancy frequency, expressed as:

$$\boldsymbol{N = \sqrt{\frac{\beta g S_0}{H}}} \quad (3.5)$$

where S_0 is the reference salinity.

The mixing characteristics of estuaries can be applied to classify estuaries. Based on the mixing, estuaries are broadly classified as either stratified, partially mixed, or well-mixed [72]. In terms of circulation, stratified estuaries are classified as either fjord, strongly stratified, or salt wedge [73, 74]. Conventional methods to determine the type of estuaries include measuring the vertical profile of salinity along the estuary over time [56, 75]. However, these methods cannot take into account variations in river discharge and tides in terms of classification. In this study, the combination of two parameters, Fr_f and M, is applied to determine the Ota Floodway estuary regime. The mixing condition occurs when $\alpha^{1/2} Fr_f^{1/3} M^{-2} \approx 1$ with an α value of 3.4 [71], meaning that mixing occurs when this critical threshold value is exceeded. This method has previously been successfully used to map different estuary classes [71].

3.3.2.2. Wavelet Transform

In this study, the wavelet analyses comprise the continuous wavelet transform (CWT), cross wavelet transform (XWT), and coherence wavelet transform (WTC) [76]. The CWT approach is applied to decompose the time series into the time–frequency domain and analyze the dominant frequency and its variation over time. The CWT is applied to the depth-averaged

current, stratification, and discharge data. The XWT and WTC methods are used to determine parameter dependency — we used these approaches to examine the dependency of circulation on stratification and river discharge. XWT exposes the power of the relationship between two time series, whereas the WTC reveals the coherence of the datasets. The WTC results can be significantly coherent, despite having low power on the XWT. The physical relationship shown by XWT and CWT results is uncertain; however, interpretation of the physical association of these results is essential to reveal the dependency of circulation on stratification and river discharge.

3.4. Results

3.4.1. General circulation of Ota River Floodway

The wind, discharge, depth-averaged velocity, salinity, and mean flow profiles are shown in Figure 3.2. The time series of the wind magnitude shows a diurnal pattern with a magnitude of 2–8 m/s (Figure 3.2a) in a northeast –north direction (Figure 3.2b). The wind direction and magnitude (Figure 3.2a, b) changed significantly to the west between December 28, 2007, and January 1, 2008. However, calculation of the coefficient correlation between the along-channel wind and non-tidal flow showed that the wind has no considerable effect. On this basis, we assumed that the wind did not significantly influence circulation, thus, the impact of the wind was ignored in further discussion.

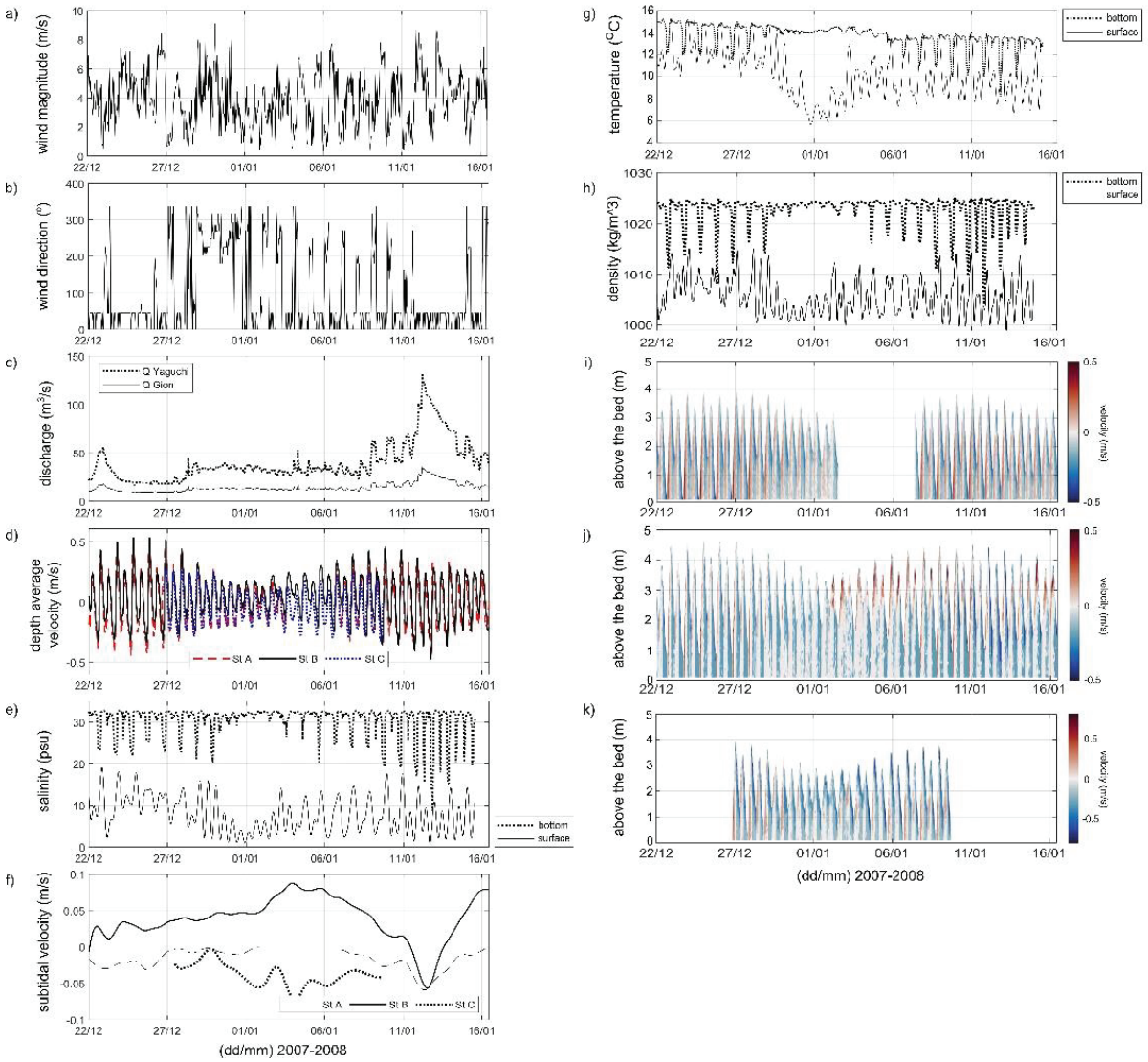

Figure 3.2. Time plots of (a) wind magnitude, (b) wind direction, (c) discharge at Yaguchi and Gion stations, (d) depth-averaged velocity at St. A, St. B, and St. C, (e) salinity at St. A at the water surface and bottom, (f) subtidal velocity, (g) temperature, and (h) density in St. A at the water surface and bottom, and vertical profile along channel currents velocity at (i) St. A, (j) St. B, and (k) St. C. The Yaguchi Station is located around 14.6 km from the river mouth. The wind direction is shown with north as 0°, east as 90°, south as 180°, and west as 270°.

The discharge at Gion was indirectly estimated from the discharge data at Yaguchi Station [64]. During the observation periods, the mean discharge values at Yaguchi and Gion were approximately 40 m^3/s and 13 m^3/s, respectively, while the maximum discharge values

were approximately 132 m^3/s and 36 m^3/s, respectively. Figure 3.2c shows that the discharge increased during January 9–16, 2008. During the high discharge period, the surface salinity was low (Figure 3.2e), the maximum depth-averaged velocity decreased (Figure 3.2d), and the subtidal velocity tended to flow downstream (Figure 3.2f).

Salinity, temperature, and density clearly show a tidal excursion (Figure 3.2e, g, and h). Ebb–flood and neap–spring variations in salinity, density, and temperature are demonstrated from the observation data. During the flood period, the near-bottom salinity and density values are approximately 32 psu and 1023 kg/m^3, respectively, indicating the intrusion of a water mass from the sea. The temperature data shows that the water is warmer at a deeper level. The highest salinity, density, and temperature differences occurs during the neap periods.

A tidal excursion was clearly observed in the depth-averaged velocity data (Figure 3.2d). The subtidal velocity can be seen in Figure 3.2f, which was calculated using a low-pass filter from the depth-averaged velocity, with a 30-hour cut-off period. In general, the subtidal velocities at stations A and B are landward during neap conditions, whereas the mean flow at station C is seaward. The differences in patterns of the daily mean flow at the stations indicated that St. A and St. B are more affected by tidal excursions, whereas St. C is more affected by river runoff. Moreover, because St. C is located on the tidal flat and the exit of curvature, centrifugal acceleration plays a role in displacing the maximum current towards the exit of the curvature [77]. In addition, the residual velocity is influenced by bathymetry, with intense currents located in the shallowest parts of the river cross-section [77]. Vertical profiles of along channel currents at St. A, B, and C are shown in Figure 3.2i, j, and k, respectively. Field data at St. A, B, and C revealed tidal current oscillations, indicating a strong flood-ebb tidal cycle. The tidal currents at St. A and St. B appear to have similar ranges, while that at St. C has larger tidal current. In general, these data indicate that the hydrodynamics of the Otagawa Floodway are dominated by the influence of the tidal cycle.

3.4.1.1. Spring–Neap Tidal Variation

To examine the spring–neap variations in circulation, vertical profiles along the channel currents at St. A, B, and C, and the bottom–surface salinity differences are presented during spring (December 27–28, 2007) and neap conditions (January 1–2, 2008) (Figure 3.3). The discharge conditions during these periods were low, i.e., ~20 m^3/s in spring and ~30 m^3/s in neap, based on observations at the Yaguchi Station (Figure 3.3c). As shown in Figure 3.3a and e, under spring tide conditions, the salinity difference at St. A during flood and ebb was 10–25 psu. The minimum and maximum salinity differences at St. A occur during the first flood and first ebb events, respectively. During the neap tide, the salinity difference during the ebb and flood was stable at approximately 27–30 psu. Overall, the tidal forcing controlls the stratification of the water column.

During the spring tide, the current velocities at St. A and St. B (Figure 3.3b, c) show similar profiles. The upstream velocity during the flood is uniform with depth, whereas during the ebb, the maximum velocity is near the surface. At St. C (Figure 3.3d), the maximum ebb and flood current velocities are higher than those observed at St. A and B. The ebb currents at St. A, B, and C have maximum velocity values near the surface; in contrast, the near-surface ebb currents at St. C preceded the deeper layer currents. The higher downstream current velocities and phase differences indicate that the effect of river runoff at St. C is greater than that at the other stations. The effect of river runoff could also be identified in terms of the asymmetry of the near-surface maximum downstream currents during ebb conditions at St. C.

The tide dominance at St. A and B is observed during neap conditions. During the neap tide, at St. A and St. B (Figure 3.3e, f, g, and h), the flood duration is longer than the ebb duration. The flood duration was 7.6–8.3 hours, whereas the duration of the ebb was 5–6.3 hours. In contrast, the effect of river runoff at St. C caused a longer ebb duration than flood duration, with values of 7–7.6 and 5–5.3 hours, respectively. The observed longer flood

durations at St. A and B suggest that even when tidal force during the neap is low, the tidal straining component is dominant at both St. A and B. Because the locations of St. A and B are near the river mouth, the tides have a predominant effect on circulation at these sites.

At St. C only, two-layer currents, in which the current in near-surface layer is downstream and the current in deeper layer is upstream, are observed during flood and high tides for both neap and spring periods, even though discharge is low (Figure 3.3d and h). This two-layer flow is characteristic of baroclinic circulation in stratified estuaries [78] and usually occurs due to interactions between the river discharge and the horizontal gradient density [45]. However, two-layer flow is only observed at St. C and not at St. A and B; therefore, we hypothesize that the two layers occurs because St. C is located upstream, where the river influence is stronger, and the density at St. C would be lower. As a result, the horizontal density gradient at St. C would be higher than that at St. A and St. B. Moreover, blocking of water flow at the Gion gate leads to lower tidal current velocities and weaker tidal mixing in the upstream region of the floodway; the depth-averaged velocity at St. C is lower than velocities at Sts. A and B as shown in Figure 3.2d.

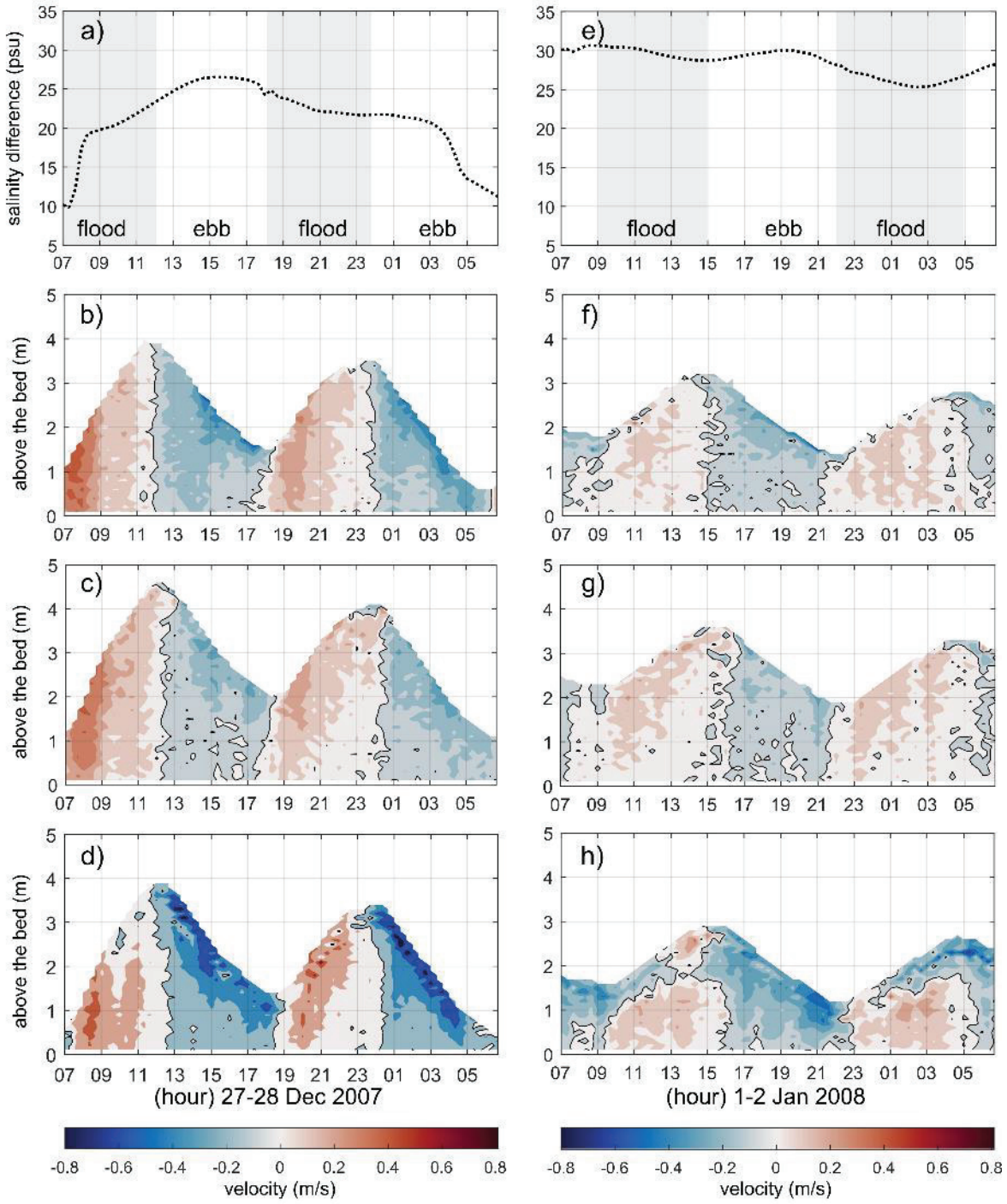

Figure 3.3. Temporal variation of the (a, e) surface-bottom salinity difference profile at St. A and (b-d, f-h) velocity profiles at (b, f) St. A, (c, g) St. B and (d, h) St. C during (a-d) spring and (e-h) neap conditions. Positive values indicate flood and landward currents conditions.

3.4.1.2. Influence of Discharge Variation

The effect of discharge variation was examined by comparing the vertical profile of longitudinal currents during spring tide under low discharge (20 m^3/s) and high discharge conditions (110 m^3/s). The longitudinal velocity data were captured on December 25, 2007, and January 12, 2008. The influence of discharge on the circulation is shown only at St. A and B, as no records were available at St. C during the studied period (Figure 3.4). During the high-discharge condition, the fluctuation in the salinity difference is greater; this parameter fluctuated from 5 psu during the flood to 30 psu during the ebb. During the low discharge period, the maximum flood and ebb currents are 0.51 m/s and 0.46 m/s, respectively, whereas, during the high discharge period, the maximum flood and ebb currents are 0.33 m/s and 0.56 m/s, respectively. Compared with the low discharge condition, under high discharge condition, the currents in the flood tide are weaker, while the currents in the ebb tide are stronger. The non-tidal currents (Figure 3.2f) show that the seaward currents strengthen during the high discharge period, strengthening the ebb currents and damping the flood currents. In addition, during the high discharge period, there is a phase difference between the flow in the upper and deeper layers, where the upper phase propagates into a deeper layer.

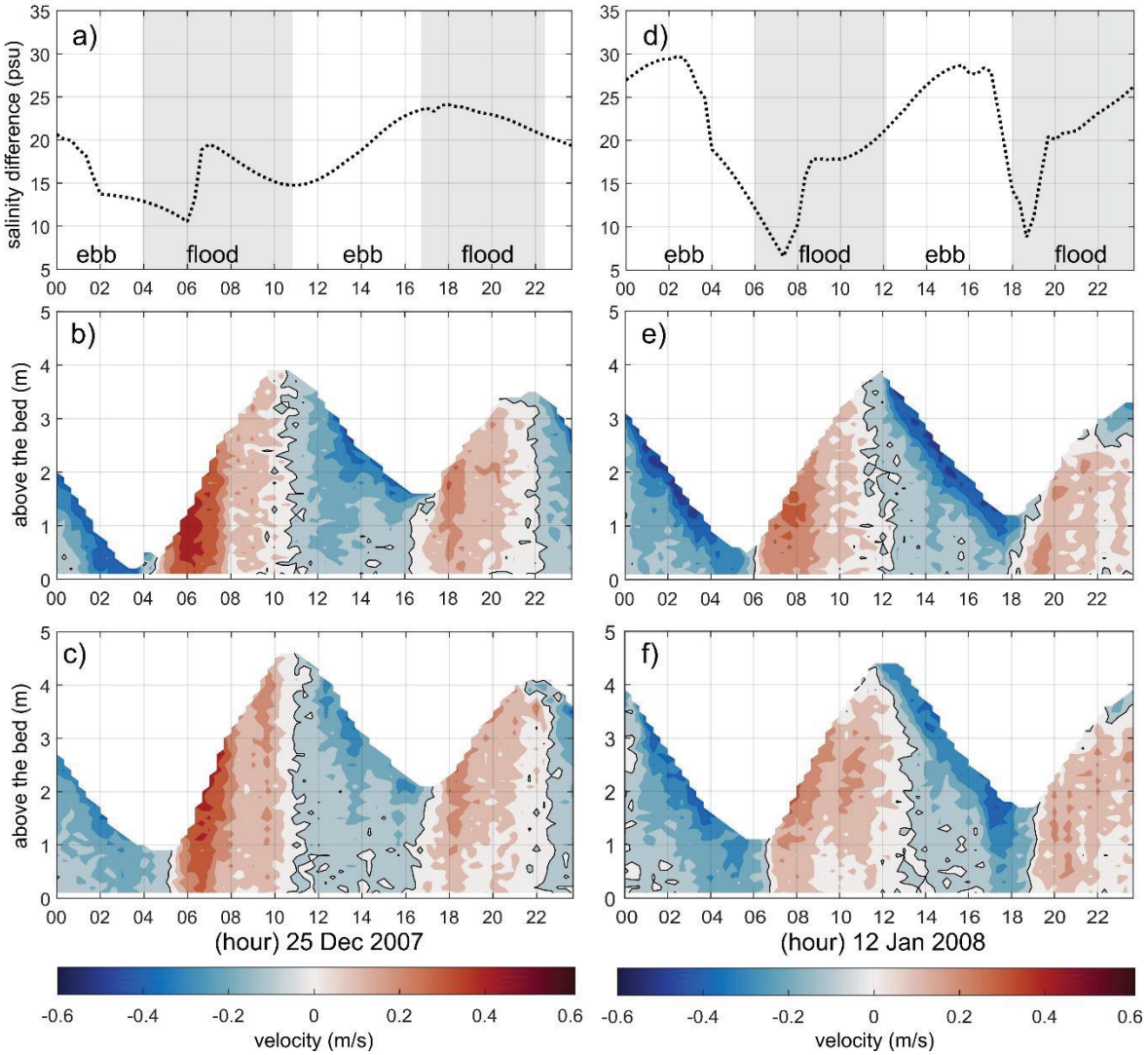

Figure 3.4. Temporal variation of (a, d) the surface-bottom salinity difference profile at St. A and (b, c, e, f) velocity profiles at (b, e) St. A and (c, f) St. B during (a-c) low and (d-f) high discharge conditions. Positive values indicate flood and landward currents conditions.

3.4.2. Mixing

The mixing intensity was measured using the bulk Richardson number (Figure 3.5a). During the neap-spring cycle, the low frequency of the Richardson number increases during the neap period. High stratification and low tidal velocity during the neap condition are related to an increase in the Richardson number (Ri_L); therefore, the observed strong fluctuations of

Ri_L in the spring conditions are mainly caused by the high variability of stratification and current velocity.

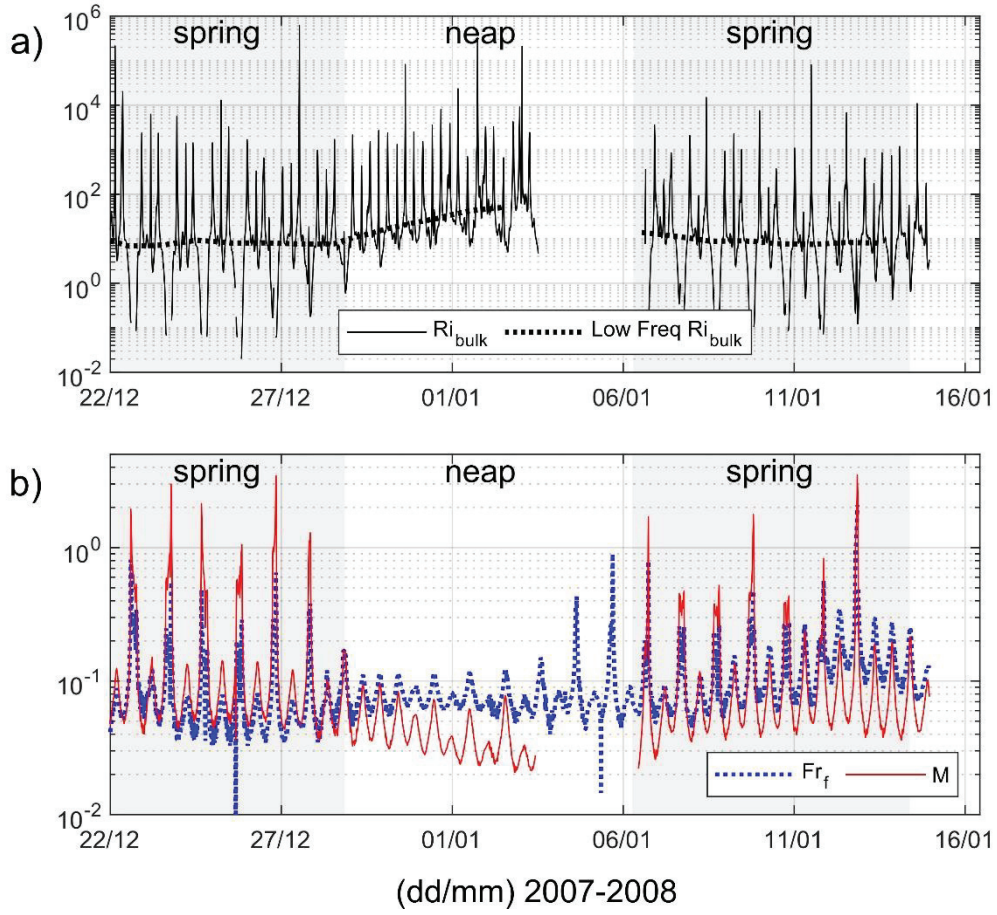

Figure 3.5. Time plot of the (a) bulk Richardson number (Ri_L) and (b) Freshwater Froude Number (Fr_f) — Mixing tidal efficiency (M)

The mixing was evaluated based on the driving forces, which are tidal currents and river runoff, using the mixing tidal efficiency (M) and Freshwater Froude Number (Fr_f). Mixing analysis was performed only at St. A. Variations in both mixing parameters (Figure 3.5b) are affected by fluctuations in salinity, which varied with both ebb–flood and neap–spring cycles. The effect of tidal currents can be seen in the magnitudes of the M value — the tidal velocity is higher during spring, thus, the magnitudes of M increase during the spring period. The effect

of discharge can be seen from the low magnitudes of Fr_f. During the high discharge period, the magnitude of Fr_f increases. During the neap condition, the variation in density is low; hence, the variation in Fr_f is low.

Evaluation of the mixing using the Ri_L, Fr_f and M values suggests that mixing variation is affected by fluctuations in the salinity, which vary during ebb–flood and neap–spring cycles. Horizontal density variations can induce tidal straining, while vertical density variations can suppress vertical mixing [51, 79]. The daily mixing variation is controlled by density fluctuation, which is influenced by tides. Figure 3.5 shows that during flood conditions, the stratification weakens owing to the increasing of the mixing and the current velocity. In the neap and spring cycles, the Fr_f and M values reveal that the role of river discharge in mixing is more significant during the neap tide. Moreover, during high discharge periods, the effect of river flow increased (Figure 3.2f), inducing an increase in the value of Fr_f(Figure 3.5b)— this increase in Fr_f indicates that higher river velocities tend to mix the water column and suppress stratification.

3.4.3 Wavelet Analysis

3.4.3.1. Continuous Wavelet Transform

Wavelet analysis was used to analyze the variability of currents at Sts. B and C, the bottom-surface density difference value at St. A, and river discharge (Figure 3.6). The CWT results for the current data at Sts. B and C (Figure 3.6a, b) clearly show a strong semidiurnal signal during the observation period, except for under the neap condition. Furthermore, strengthening of the diurnal period signal is observed in both CWTs, although the signal is not significant (Figure 3.6a,b). This strengthening indicates the influence of tidal diurnal components on tidal currents. In particular, for the CWT of the data from St. B, signals with

shorter periods (i.e., higher frequencies), such as 0.25 days, showed significant power. Coincident with increased discharge, the signal is slightly strengthened over periods of 2–4 days.

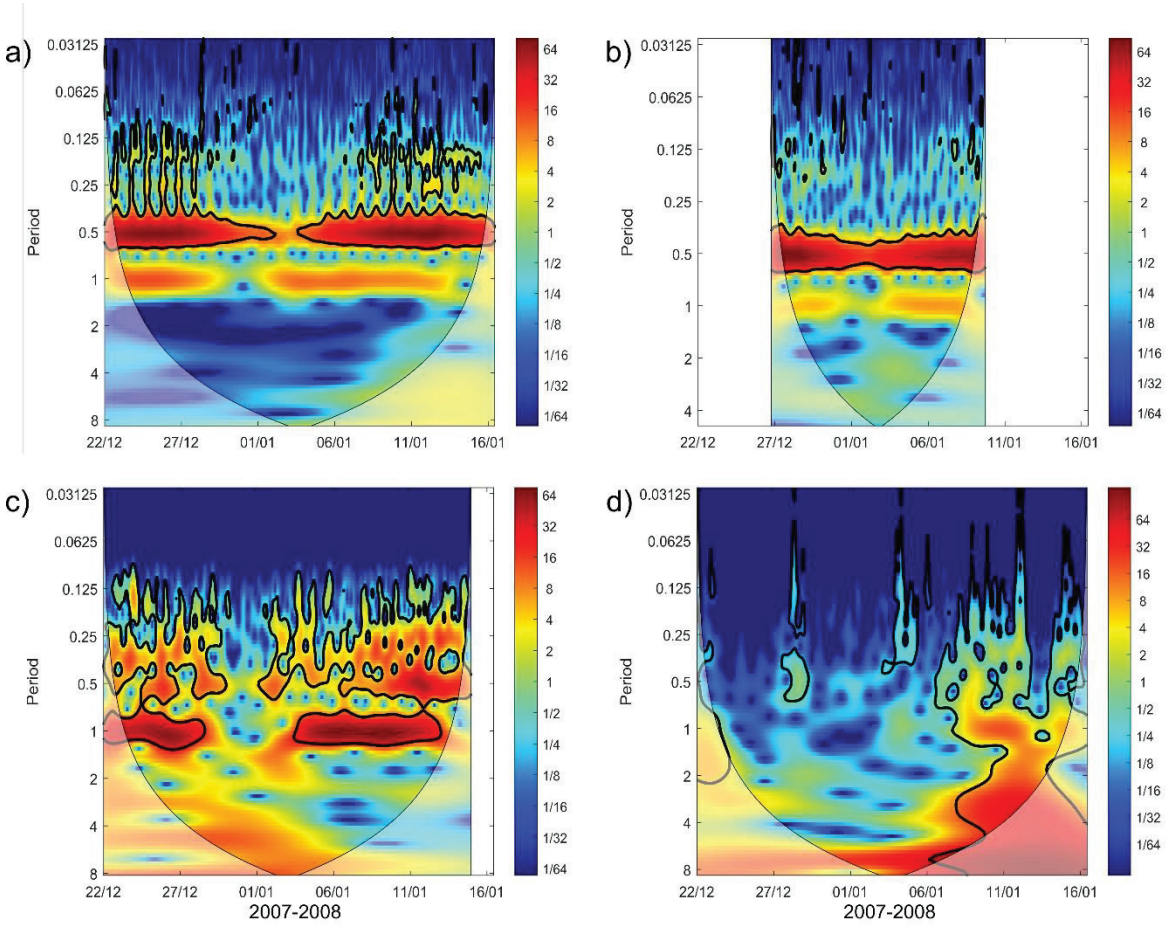

Figure 3.6. Continuous Wavelet Transform (CWT) of depth-averaged velocity at (a) St. B and (b) St. C, (c) surface–bottom density difference, (d) river discharge.

The CWT of the bottom–surface density difference value at St. A (Figure 3.6c) shows a different pattern from the CWT of the currents. The strongest signal of the CWT density difference value is in diurnal periods during the observation period, except during the neap condition. We also note that the power of the CWT weakens significantly during the neap condition. The strong signal during the diurnal periods demonstrates that tidal straining occurs

once in one tidal cycle. This differs from the semidiurnal tidal regime in the Otagawa Floodway, where two flood and ebb events occur per tidal cycle. In addition, the CWT of the discharge data in Figure 3.6d indicates a strengthening of the signal during January 9–16, 2008, coinciding with the increase in discharge.

3.4.3.2. XWT and WTC of the St. B Currents

Wavelet transform coherence (WTC) and cross wavelet transform (XWT) are applied on the currents in St. B, discharge, and vertical density differences to capture the interactions of currents, discharge, and buoyancy during low–high discharge and neap–spring conditions. The XWT and WTC between currents and the vertical density difference (Figure 3.7a, b) show that the power of the XWT is significant in the diurnal and semidiurnal periods in the spring condition. The WTC results show that the signals are coherent with the diurnal frequency in the first spring period (December 22–28, 2007), where the phase of the buoyancy signal influences the current signal. This indicates that buoyancy affects currents by inducing straining. The WTC during the second spring tide (January 8–16, 2008), which coincides with the increase in discharge, shows coherence in the semidiurnal and diurnal periods. The strengthening of the signals indicates an enhancement in tidal straining.

The response of the currents velocity due to fluctuation of the river discharge is examined using the XWT and WTC between the depth-averaged currents and the discharge, as shown in Figure 3.7c and d. At St. B, the power of the XWT is significant in terms of the semidiurnal variation during the observation period, whereas the diurnal frequency is significant during the high discharge condition (e.g., 11–16 January 2008). The WTC indicates a significant signal in diurnal variation during the neap tide. Furthermore, during the high discharge episode, the diurnal variation signal is significant. The coherence of currents and river discharge on the neap tide suggests a strengthening of influence of the river discharge to

the currents velocity when the tidal force is minimal. Moreover, from 11–16 January 2008, when the river runoff was high, the effect of discharge is clearly shown in the results of XWT and WTC.

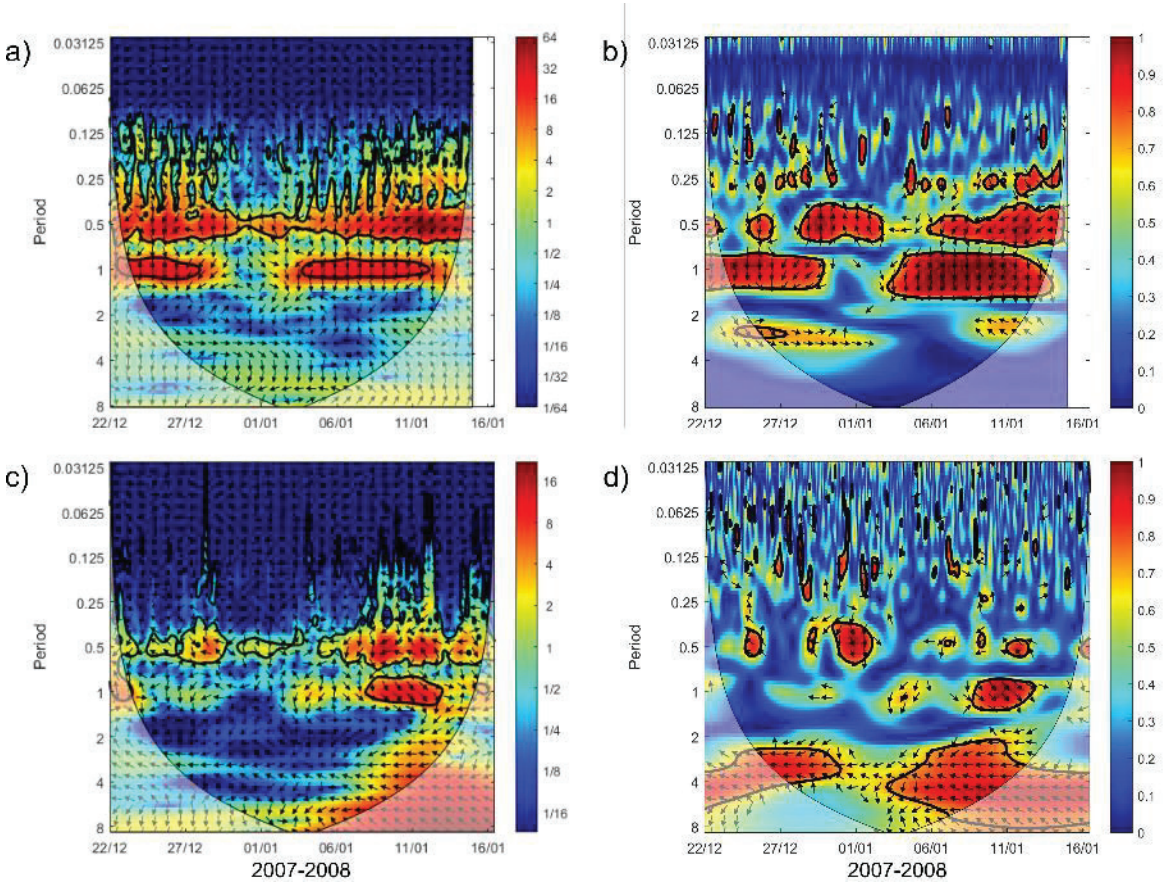

Figure 3.7. Cross wavelet transform (XWT) between currents in St. B with (a) surface–bottom density difference and (c) river discharge. Coherence wavelet transform (WTC) between currents in St. B with (b) surface–bottom density difference and (d) river discharge.

3.4.3.3. XWT and WTC of the St. C Currents

Because the duration of current observations at St. C was limited, the data only captured the neap and spring periods during the low discharge condition. The results of the XWT and WTC between the current and surface–bottom density differences are shown in Figure 3.8a. The XWT analysis shows the significant power of the semidiurnal component throughout the observations and of the diurnal component during the middle to the end of the observation

period (December 28, 2007 –January 2, 2008). The CWT shows coherence signals in the semidiurnal variation from the end of the first spring until the first neap (December 28, 2007 – January 2, 2008); in contrast, during the second period, neap to spring (January 3–10, 2008), the CWT shows significant coherence in both semidiurnal and diurnal periods. However, the phase of the coherence signal in both periods is completely different, indicating an opposing relationship between currents and buoyancy.

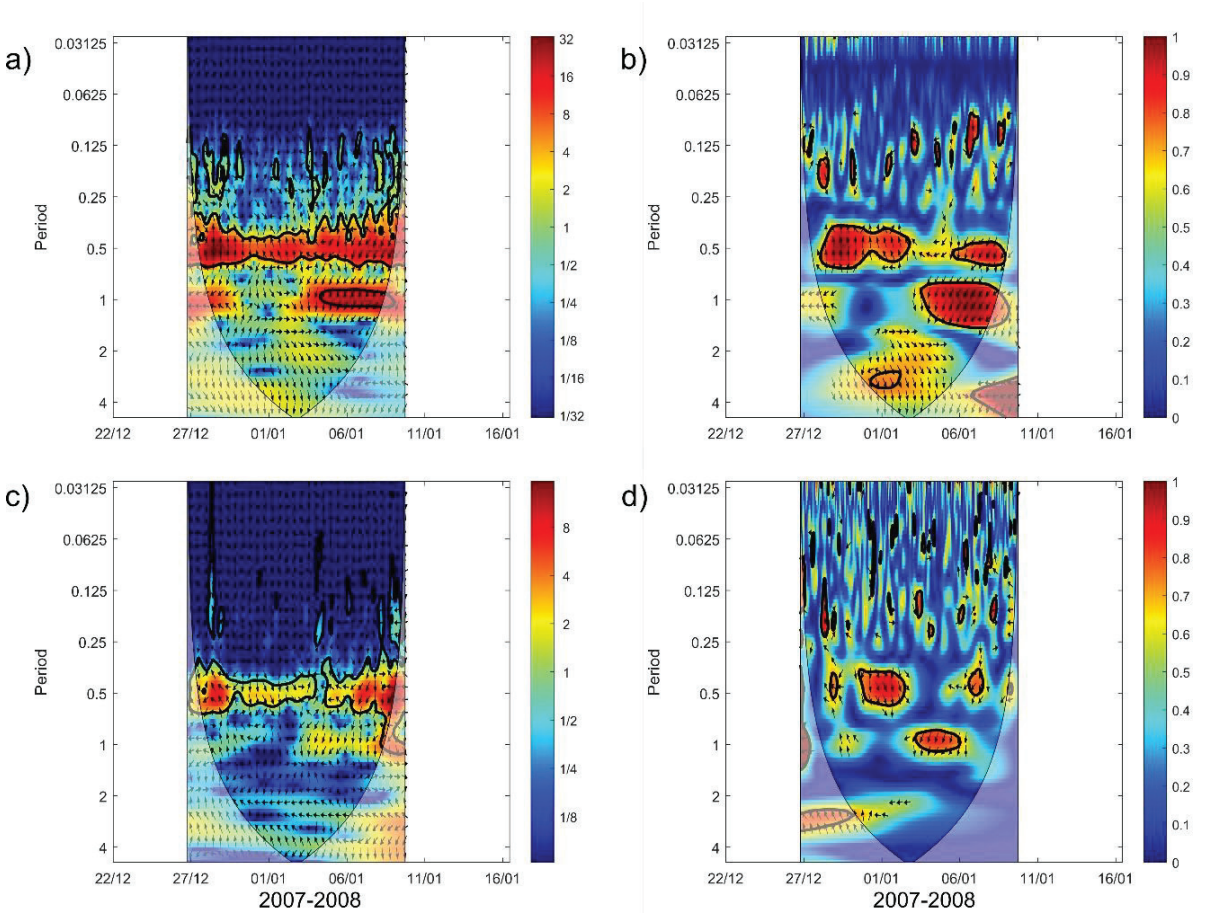

Figure 3.8. Cross wavelet transform (XWT) between currents in St. C with (a) surface-bottom density difference and (c) river discharge. Coherence wavelet transform (WTC) between currents in St. C with (b) surface–bottom density difference and (d) river discharge.

The XWT of the depth-averaged currents with discharge (Figure 3.8c) shows significant diurnal power during the observation period. However, the coherence signal (Figure 3.8d) is particularly evident under neap conditions (December 31, 2007 –January 2, 2008). The coherence suggests that the influence of river runoff significantly influences circulation. Regardless of the low river discharge condition (approximately 40 m^3/s), the effect of river runoff is noticeable during the neap condition due to the weakening of tidal influence.

3.5. Discussion

3.5.1. Interpretation of mixing

Estuary regime mapping using Fr_f and M [71] was applied to the Ota diversion channel floodway (Figure 3.9). The solid red line indicates the condition for vertical mixing that divides the estuary into areas that should always be stratified and areas in which mixing occurs during the tidal cycle. Figure 3.9 shows that the regime of the Ota River Floodway estuary can be classified as a salt wedge estuary, even though during spring (low discharge) periods, the estuary was strongly stratified, whereas during spring (high discharge) and neap (low discharge) periods, the regime shifted to the salt wedge type. We interpret this range of classification to be related to neap–spring tidal variation and river flow variation. Similar ranges of estuary type classification can also be observed in the Hudson River, Chesapeake River, and Ebro River [71]. Figure 3.9 shows that some points have M values that pass the condition for vertical mixing. This condition occurs during flood events during the spring (Figure 3.5) indicating that vertical mixing takes place during this period.

Mapping the Fr_f and M values of the estuary is a powerful tool for classifying estuaries based on variations in river discharge and tidal variation; however, this approach cannot determine the salt wedge geometry, such as its height and length. In this study, the salt wedge geometry was not calculated because of insufficient data. Determining the salt wedge geometry requires the longitudinal vertical salinity profile [56, 75].

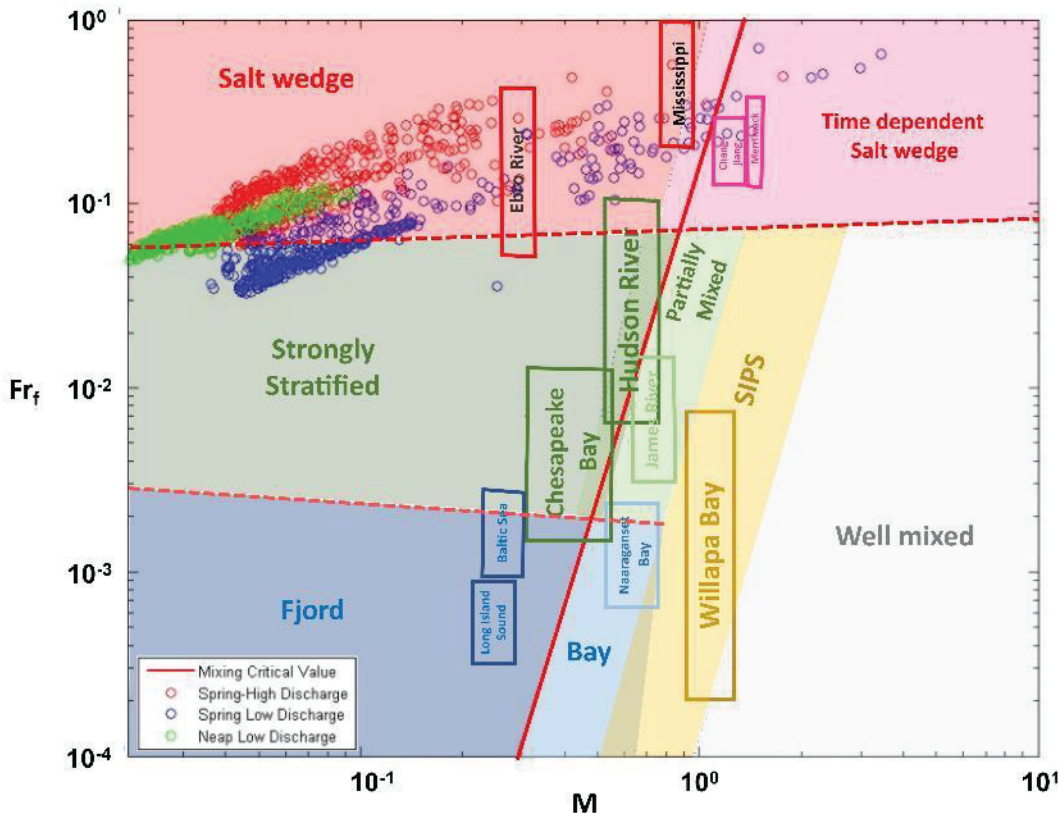

Figure 3.9. Estuarine parameter space, based on the freshwater Froude number (Fr_f) and Mixing tidal efficiency (M). The solid red line is the condition for vertical mixing. The estuarine classification and example estuary are adapted from Geyer and MacCready (2014)

3.5.2. Interpretation of the wavelet analyses

The CWT of the parameters shows that the currents mainly have 0.5-day periods and the surface-bottom density difference has 0.5- and 1-day periods, whereas the river discharge does not show clear periodicity. The 0.5- and 1-day periods captured in the currents and the surface-bottom density differences show clear tidal influence. However, the CWT of current data from St. B shows significant power at lower periods (higher frequency), such as 0.25 days. The appearance of a higher frequency component at St. B could be caused by the convergence of tidal and river discharges [80].

The WTC and XWT between currents and density differences show that tides play a key role in mixing, as the strength of mixing is controlled by the tides. These results demonstrate the role of the currents to the mixing: the mixing increases due to an increase in the tidal force during the spring. Furthermore, the tidal force is weak during the neap tide, prompted a decline in tidal straining. This is exhibited by weakening of the XWT power during the neap tide (Figure 3.7a and Figure 3.8). The observed phase differences during neap and spring in the WTC (Figure 3.7b and Figure 3.8b) confirm that strong straining occurs during the spring and weakened during the neap period.

3.5.3. Convergence Zone in the Ota River Floodway

Estuary systems with a stronger flood than the ebb velocity tend to promote the landward accumulation of suspended material [81]. This accumulation is a result of transport of suspended material and tidal pumping during flood events. River discharge influences the seaward transport of suspended materials. The effects of tidal and river discharge forces will likely lead to the formation of a convergence zone in an estuarine system; such convergence zones driven by tides and river discharge tend to act as suspended sediment traps [4]. As a result, estuarine turbidity maxima (ETM) arise in the convergence zone.

In the case of the Otagawa Floodway, a convergence zone is identified around St. A and St. B [25]. The contrasting characteristics of currents at Sts. A, B and C (Figure 3.2) confirm the presence of convergence zone occurrence in the middle of the Ota Floodway [4]. The subtidal velocity and tidal asymmetry at Sts. A, B, and C were compared and are presented in Figure 3.10a. The tidal peak current asymmetry, which shows the skewness between the peak flood and ebb currents, is used as a measure of asymmetry and is calculated using the statistical skewness method [81]. During spring, the subtidal velocity at St. A shows a seaward flow with a weakly flood-dominated asymmetry. Note that neap conditions are not shown because of the lack of available data during this period. The asymmetry at St. B shows flood

dominance and a strong landward subtidal flow during the neap and spring. In contrast, at St. C, the asymmetry is likely to be symmetrical with low subtidal flow during spring but strong seaward flow during neap conditions.

The asymmetry difference between St. B and St. C in spring conditions suggests that there is an imbalance of water transport in the middle of the channel of St. B and C, which could cause sediment trapping (Figure 3.10a). Furthermore, the subtidal currents at St. B and St. C converged to the middle of St. B and St. C (Figure 3.2f). This flow convergence induce strong near bottom mixing which enhances sediment resuspension, which results in an ETM in the convergence zone. The increased flood velocity during the spring tide enhances the bed shear stress and mixing, leading to a higher SPM concentration [4]. To support this analysis, we conducted a simple turbidity observation at St. A and St. B. The observations were conducted during flood and ebb periods in spring conditions on April 17, 2021, and are presented in Figure 3.10b and c. During both flood and ebb, the turbidity around St. B is higher than that recorded at St. A. During the flood event, the tidal current is landward and induces resuspension of sediment at St. B, while during the ebb, the current transports the SPM seaward. From this work, the patterns of turbidity, asymmetry, and subtidal flow indicate an ETM and convergence zone around St. B.

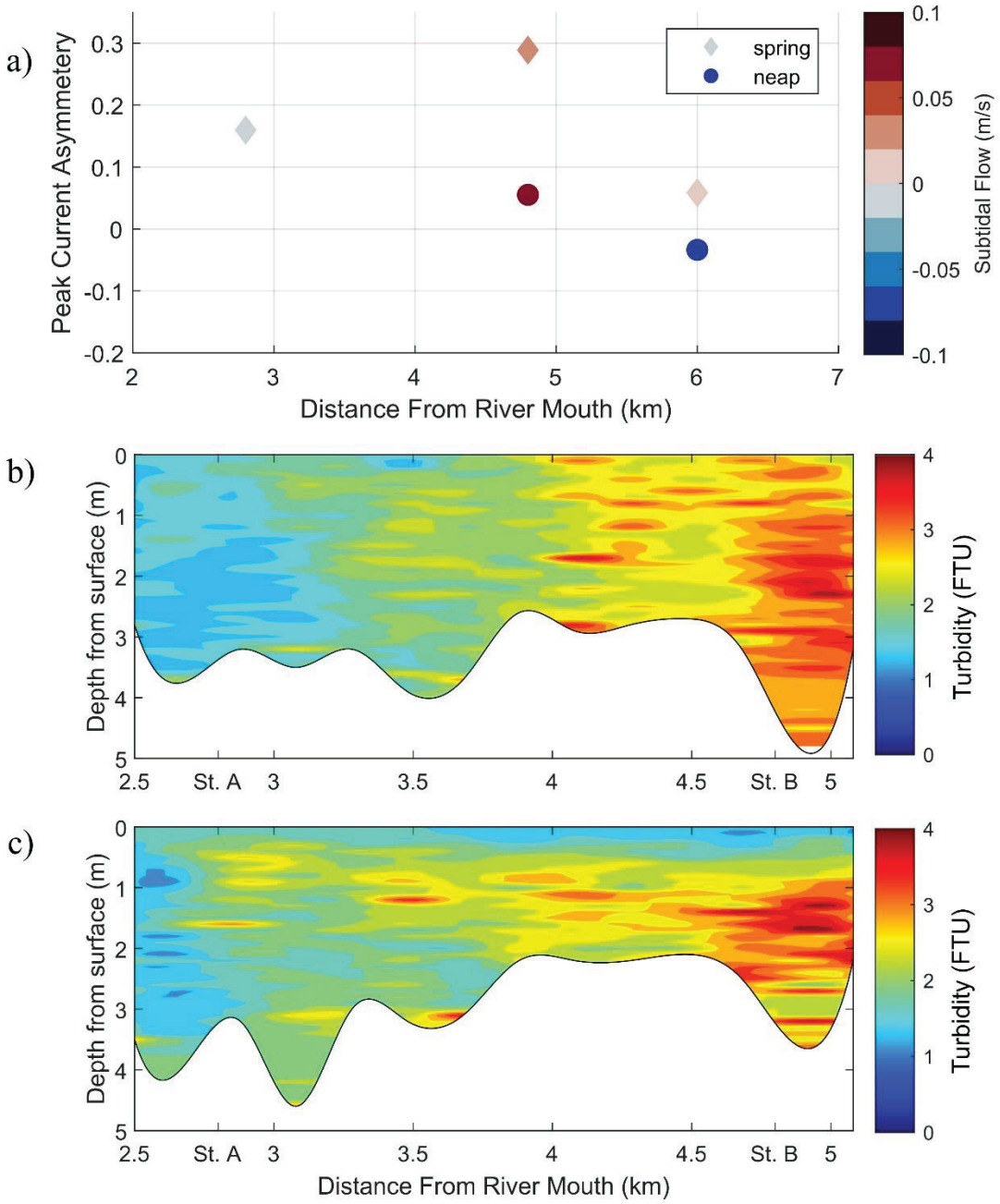

Figure 3.10. (a) Distribution of Spring/neap peak current asymmetry vs subtidal flow. Along-channel turbidity in (b) flood and (c) ebb conditions.

3.6. Conclusions

In this study, we investigated the response of the circulation and mixing of the Ota River Floodway estuary. The results reveal that the currents at three stations, located at 2.8 km, 4.8 km, and 6 km from the mouth of the river, are controlled by ebb–flood and neap–spring

tidal oscillations. However, when the river runoff is high (i.e., discharge at Yaguchi Station > 50 m^3/s), the currents can be modified by strengthening the ebb flow and prolonging its duration. During neap conditions, when the tidal force is weak, the influence of river runoff at station C (6 km from the river mouth) is clearly shown compared to the other stations that are closer to the river mouth. Mixing in the Ota River Floodway estuary is driven by tidal control, with this mixing following ebb–flood and neap–spring oscillations. Analysis of the mixing using the mixing tidal efficiency (M) and freshwater Froude number (Fr_f) reveal that the tides dominantly controlled mixing in the Ota River Floodway estuary, however, the river discharge contribution could be observed during the neap period. Overall, this study shows that the estuary regime of the Ota River Floodway can be defined as a salt-wedge estuary.

The continuous wavelet transform results show that the currents mainly have 0.5-day periods, indicating the dominance of astronomical tides as a driving factor. The surface–bottom density difference revealed periodic 1- and 0.5-day variations. The river discharge does not show periodicity, however, the signal was strong on January 9–16, 2008, during a period of increased discharge. The XWT and WTC reveal the relationship between circulation mixing and river runoff. During spring, the tidal straining increases and induces intense mixing, whereas during the neap tide, the tidal force is weakened, hence, the role of river runoff in circulation and mixing increases during the neap tide.

An extended analysis of the indication of the existence of a convergence zone using ADCP data reveals that the convergence zone is estimated to be approximately 4.8 km from the river mouth. The presence of the convergence zone is characterized by the occurrence of an ETM around the same area; however, the location of the convergence zone and the ETM dynamically change depending on the relative force of the tides and river runoff.

This study highlighted the characteristics of mixing and longitudinal currents in shallow floodway estuaries with limited discharge. Although the estuary is a tidal dominated and has a limited discharge, the role of discharge significantly affects the circulation and mixing, particularly during neap tide. Moreover, the role of the discharge is significant in inducing the appearance of the ETM, which usually appears in high discharge estuary. The existence of the ETM could affect the morphological change that could cause problems in the future. It is necessary to investigate these issues further. In addition, studies in small and limited discharge estuaries are still challenging, particularly those with unique geometries, such as multi-channel estuaries and estuaries with curvature.

Chapter 4: Propagation of tidal waves in tidal-dominated multi-channel estuary

4.1. Introduction

Tides are one of the main drivers of estuarine circulation in addition to river runoff. Tidal wave dynamics in estuaries are modified by shallow water friction and topographical settings [9, 10, 82]. Increasing the damping of water elevation in an estuary is a balance between channel convergence and friction [9]. Moreover, the same factors are responsible for the modulation of compound tides and overtide constituents, which induces tidal distortion and asymmetry [10, 82]

The interaction between river runoff and tides influences the tidal wave dynamics by increasing friction [11, 49]. Friction delays the phase, reduces the amplitude of the principal tidal constituent, and increases tidal distortion and asymmetry [28, 29, 83]. In the case of high-discharge estuaries such as the Yangtze River, the river plays a significant role in modifying the water level [84, 85]. Nonstationary and nonlinear tidal behaviours depend on variations in the river discharge. Tidal nonlinearity increases with increasing river discharge [84, 85]. Additionally, river runoff affects circulation and sediment transport, causing estuarine turbidity maxima [4, 50]. Although the effect of river discharge on the modulation of tidal evolution is known, the tidal nonlinearity behaviour of short tidal penetration channels in small estuaries has received less attention, although estuaries are the most common type of tidal river [53]. In this study, a small estuary was defined as an estuary with a surface area of less than 50 km^2 [19].

In tidal-dominated estuaries, where the ratio between river runoff and tidal discharge is less than one, river runoff plays a limited role in modifying the elevation of tidal waves [46, 86]. Tidal wave evolution is mainly affected by topographical settings, including changes in

the channel width and bathymetry [82, 86–88]. Shallow water friction in shallow bathymetry decays the principal tidal component and modulates tidal asymmetry [82]. In an estuary with a bifurcation channel, the tidal range decreases significantly at the apex of the bifurcation [17]. This is caused by the amassing of tidal waves from the convergence of the two channels [2, 17]. The meeting location of the tides is not exactly at the junction but depends on the length, width, and depth of the channel [2]. Although some studies have explored the changing tidal range in bifurcation, the tidal evolution along the estuary and the nonlinear behaviour of the water level at the junction require further analysis.

The Ota River Estuary is a multi-channel and tidal-dominated estuary located in the centre of Hiroshima City, Japan. The estuary functions as a tourism area, port, and for oyster cultivation. Water quality and river monitoring in the Ota River Estuary are important for supporting these economic activities. The normal discharge in the Ota River estuary upstream (Yaguchi Station) is approximately 20-50 m^3/s. The discharge from the upstream flows to two areas of the Ota River estuary: the Ota diversion channel (ODC), which is a straight channel, and the branching channel (Figure 4.1). The discharge of the Ota diversion channel (ODC) is controlled by watergate in the Gion (Figure 4.1), while the rest of the river runoff flows through the branching channel. With the controlled discharge and channel configuration that has straight and multi-channel, the Ota River estuary is suitable for examining the effect of different topographical setting on tidal wave dynamics. Moreover, river observation systems owned by the government installed in the Ota River Estuary can be utilised to support studies in the Ota River Estuary.

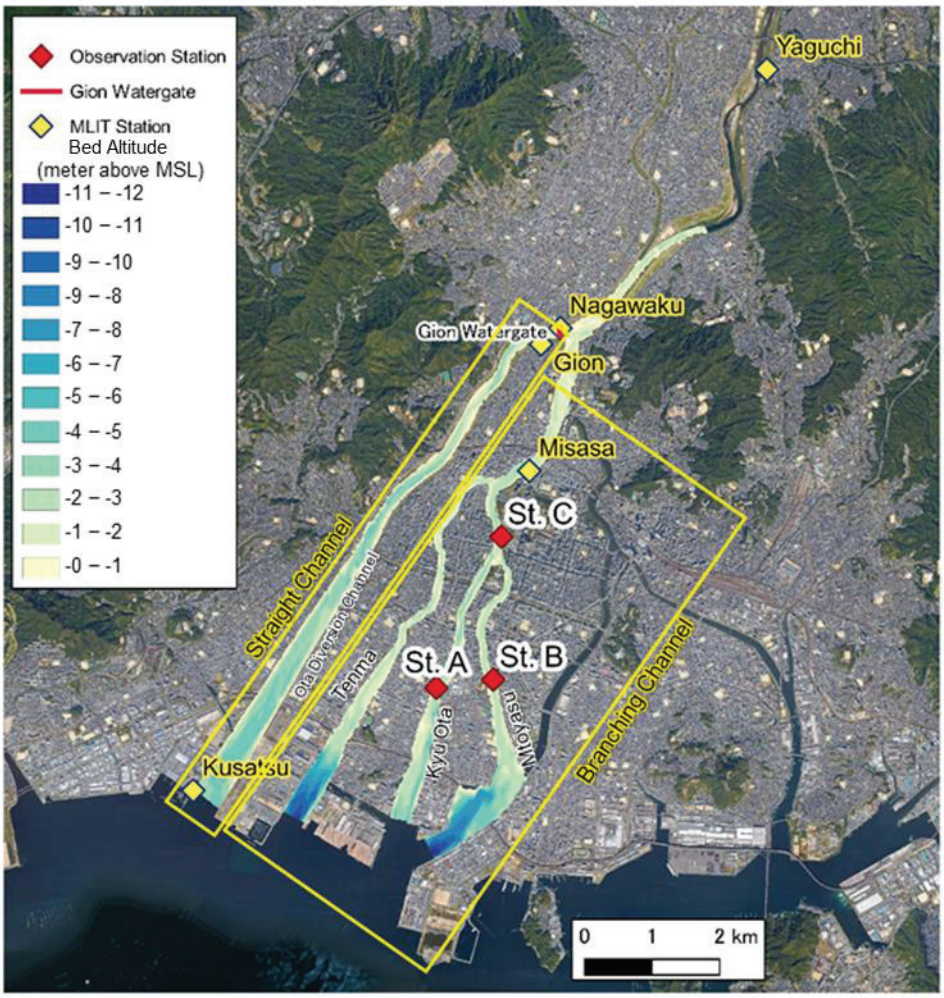

Figure 4.1. Observation stations and bathymetry of Ota River estuary network.

Previous studies [2, 17] have shown changes in the tidal range and the tidal nonlinearity behaviour when the tides converge in the bifurcation channel. However, it remains uncertain, for instance, what the mechanism of the changing nonlinear behaviour is, and how the compound tides and overtide constituents are modulated in various channel topographical settings. Therefore, in this study, we explored tidal wave dynamics regarding the 2 different topographical settings: a straight channel and a branching channel. We examined the temporal and spatial nonlinear behaviours of tidal waves in both channels using water elevation data from seven stations and current data from three ADCP stations. Bathymetric changes, channel

convergence changes, and subtidal friction decomposition were used to elucidate the mechanism of the tidal wave nonlinearity modulation.

The remainder of this paper is organised as follows. The study area is described in Section 4.2. The data and methods are explained in Section 4.3. The results and discussions are presented in Sections 4.4 and 4.5, respectively. Finally, the conclusions of this study are summarised in Section 4.6.

4.2. Study Area

The Ota River Estuary is located in Hiroshima Bay, Japan. The Ota River Estuary is divided into natural multi-branching channels, including the Tenma, Kyu Ota, Motoyasu, and Misasa channels, and one artificial straight channel, the Ota diversion channel (ODC) (Figure 4.1). The ODC is the main channel with mean channel depth and width around 2.1 m and 248 m, respectively, while the mean depth and width of the branching channel are 2.0 m and 212 m, respectively. However, the water depth at the mouth of the branching channel is up to 10 m, and Hiroshima harbour is located at the river mouth.

The Gion water gate is formed by rows of sluice gates located 8.8 km from the river mouth upstream of the ODC (Figure 4.1). The sluice gates control the volume of the river runoff in the ODC. Under normal conditions, the two gates is closed and one gate is slightly open. When the discharge at Yaguchi exceeded 400 m^3/s, all the sluice gates are opened. The Gion gates are designed to runoff approximately half of the total water discharge when all the gates are opened.

The Ota River Estuary is a tidal-dominated estuary with a semi-diurnal tidal regime. The maximum and minimum tidal ranges in the Ota River mouth are 3.6 m and 2.1 m respectively. The maximum tidal compartment is approximately 13 km upstream of the river mouth around the Kusatsu Station. The discharge at the Yaguchi gauging station ranged from

50 to 80 m^3, and during summer decreased to 20–30 m^3 during winter, respectively [25, 65, 89]. The discharge flows 20-50% to the ODC, and the rest flows to the branching channel [58]. A previous study reported that there was an equal discharge flow at the Misasa junction, where 50-63% discharge flowed to the east branch [90] and reached a maximum during spring. Discharge and tidal range play a role in the tidal distortion and asymmetry at this junction [86].

4.3. Materials and Methods

4.3.1. Data

Current and water elevation data at stations A, B, and C from the ADCP observations were used to study the propagation of tides in the branching channel. Water elevation data is obtained from water depth data. Stations A, B, and C were located 3.11 km, 3.12 km, and 5.04 km from the river mouth, respectively (Figure 4.1). Observations were conducted from 13-28 July 2021. Moreover, hourly elevation data from the Water Information System, Ministry of Land, Infrastructure, Transport, and Tourism (MLIT), Japan, during the same periods at St. Kusatsu, Gion, Nagawaku, Misasa, and Yaguchi, were acquired to cover the entire estuary area. Stations were located at 0 km, 8.2 km, 8.9 km, 5.04 km, and 13.7 km, respectively. The baseline of the water elevation data from the Water Information System is the mean sea level of Tokyo Bay. The water depths observed by ADCP (Station A, B and C) were transformed into water elevations using water level at the nearest gauging station. Namely, the transformation was done by matching the water depths at the high water to the high water level (HWL) of the nearest gauging station under low river runoff because the water surface gradient at HWL in the estuary is negligible under low river runoff. The water depths at the station A and B were transformed to the water elevations using HWL at Kusatsu station and the water depth at the station C was transformed using HWL at Misasa station. The water elevations at these stations

are shown in Figure 4.2. Water elevation data for Kusatsu are shown as tidal waves before entering the estuary. The water elevation in Gion and Nagawaku represents a tidal wave propagating in a straight channel. The water elevations at St. A, B, C, and Misasa represent the tidal waves after propagation in the branching channel. The water elevation at Yaguchi is the upstream station that is not affected by tidal waves but is associated with the river runoff flowing at Yaguchi. Detailed locations of the stations are shown in Figure 4.1, and a description of the ADCP data is presented in Table 4.1.

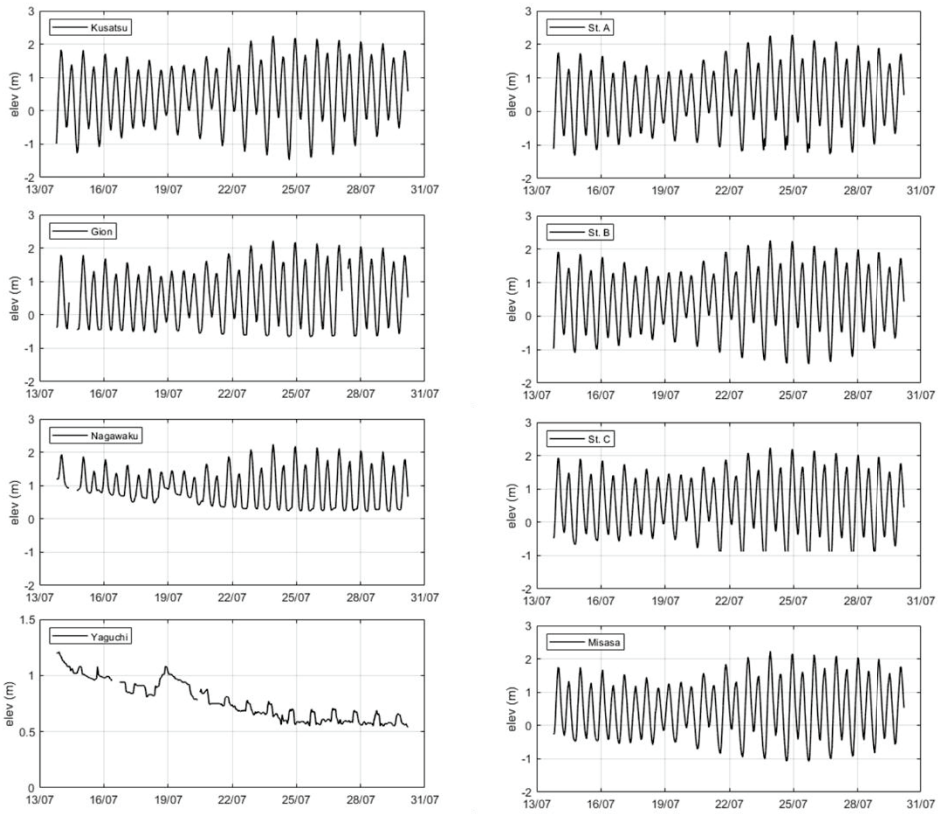

Figure 4.2. Time plot of water elevation data at (a) Kusatsu Station, (b) Gion Station, (c) Nagawaku Station, (d) Yaguchi Station, (e) Station A, (f) Station B, (g) Station C, and (h) Misasa Station

Table 4.1. ADCP settings and deployment

Station	Bin size (m)	Blank Space (m)	Sampling periods (min)	Installation	Observation periods
St. A	0.5	0.2	10	Upward Looking	13-28 July 2021
St. B	0.5	0.2	10	Upward Looking	13-28 July 2021
St. C	0.5	0.2	10	Upward Looking	13-28 July 2021

4.3.2. Tidal Analysis

4.3.2.1. Power Spectrum Analysis

Fourier analysis is a method for converting a continuous signal from time to the frequency domain. The discrete Fourier transform (DFT) is a Fourier analysis for decomposing a time series with a certain time step into different amplitudes and frequencies. This method is common in earth science, particularly for exposing the variability of time-series data. In this study, the fast Fourier transform (FFT) which is a fast DFT algorithm, was applied to decompose water elevation data. Water elevation data were analysed to determine the differences in energy distortion between the straight and branching channels.

4.3.2.2. Tidal Harmonic Analysis

Least-square harmonic analysis (HA) using the T_Tide package [91] was applied to water elevation data. The method expresses the water level time series as the summation of the mean value and cosine function series, as follows:

$$H(t) = b_0(t) + \sum_{n=1}^{N} [A_n \cos(\omega_n t - \Phi_n)] + r(t) \quad (4.1)$$

where $H(t)$ is the water elevation time series, $b_0$is the mean water level; and A, ω, and Φ are the tidal amplitude, frequency, and phase, respectively, of tidal constituents *n* (*n=1,2.. .N*) and $r(t)$ represents the residual components. The length of the time series determines the output of the tidal constituents. Water elevation time series with a length of 30 days produced 29 tidal constituents, while 25 h of data resolved six tidal constituents.

The tidal constituents resolved from HA can be used to estimate tidal asymmetry. Tidal asymmetry is estimated by calculating the phase difference and amplitude ratio of tidal constituents [28]. However, asymmetry assessment using HA is limited by the interaction of particular component e.g. M2-M4, and cannot calculate the net asymmetry resulting from the complex interaction of tidal constituents. In this study, we calculated the ratio between the total amplitude of the quarter-diurnal constituents and semi-diurnal tidal constituents to examine the distortion of the tidal amplitude along the channel.

4.3.2.3. Statistical Skewness of tidal duration

Tidal duration asymmetry (TDA) was estimated using a statistical approach by calculating the skewness value [27, 28] computed as follows:

$$\gamma(x) = \frac{\frac{1}{N-1}\sum_{i=1}^{N}(x_i - \bar{x})^3}{\left[\frac{1}{N-1}\sum_{i=1}^{N}(x_i - \bar{x})^2\right]^{\frac{3}{2}}} \quad (4.2)$$

where γ is the skewness, and x_i is the time series data, $\bar{x}$ is the expected value (mean value), and N is a number that equals the length of the time series. The TDA was computed by assuming x to be the derivation of water elevation ($x = d\eta/dt$).). A positive skewness indicates flood dominance, where the rising tides are longer than the falling tides, whereas a negative skewness indicates ebb dominance, where the rising tide is shorter than the falling tide. Guo et al. (2019) [27] showed that the calculation of TDA using the skewness method is equivalent to the calculation of tidal asymmetry using phase difference. Skewness methods can also be applied to diurnal, semidiurnal, and mixed-tidal regimes. The skewness method can be used to calculate the net asymmetry caused by multiple tidal compounds and subtidal variations. However, the skewness value is limited to measuring the absolute value of asymmetry in a relative manner, and lacks a physical background. The physical connection between skewness and tidal wave distortion must be explained.

4.3.3. Decomposition of Subtidal Friction

The friction term in the subtidal momentum balance equation is a nonlinear source of the tidal dynamics in estuaries. Friction plays a significant role in the damping and amplification of tides [10, 92]. The friction term is expressed as follows:

$$\langle gW\frac{U|U|}{C^2}\rangle = \frac{gW}{2\pi C^2}\int_0^{2\pi} U|U|dt \qquad (4.3)$$

where U is the current velocity, W is the channel width, C is the Chézy coefficient, and the angular bracket represents the average over the diurnal tidal cycle.

The product $U|U|$ in the friction term is approximated analytically using an odd function [93, 94], which adequately explains the interaction of tidal components and evaluates the compound tides associated with friction [94]. The approximation is expressed as follows :

$$\frac{gW}{2\pi C^2}\int_0^{2\pi} U|U|dt \approx \frac{gW{U_m}^2}{2\pi C^2}\int_0^{2\pi}\left(a\tilde{U}+b\tilde{U}^3\right)dt \qquad (4.4)$$

where $\tilde{U}$ is the current velocity nondimensionalised by the maximum velocity (U_m) , $a = 0.3395$ and $b = 0.6791$ [93, 94]. Moreover, the current velocity can be decomposed based on current velocity decomposition [85, 92]. which is approximated as

$$\tilde{U} = \tilde{u}_0 + \tilde{u}_1\cos(\omega_1 t+\phi_1) + \tilde{u}_2\cos(\omega_2 t+\phi_2) + \tilde{u}_4\cos(\omega_4 t+\phi_4) \qquad (4.5)$$

where, $\tilde{u}_i$, ω_i and ϕ_i are the nondimensional velocity, frequency, and phase of tidal current constituents, respectively, with the subscripts $i = 0,1,2,4$ indicating the subtidal current, diurnal, semi-diurnal, and quarter-diurnal, respectively.

To resolve subtidal friction, Equation 4.4 was integrated over the diurnal cycle. The integration resolved the three subtidal friction terms, as follows:

$$\frac{gWU_m{}^2}{2\pi C^2}\int_0^{2\pi}\left(a\tilde{U}+b\tilde{U}^3\right)dt \tag{4.6}$$

$$=\frac{gWU_m{}^2}{2\pi C^2}\left(\left(a\tilde{u}u_0+b\tilde{u}u_0{}^3\right)\right.$$

$$+\frac{3b}{2}\left(\tilde{u}u_0\tilde{u}u_1{}^2+\tilde{u}u_0\tilde{u}u_2{}^2+\tilde{u}u_0\tilde{u}u_4{}^2\right)$$

$$\left.+\frac{3b}{4}\left(\tilde{u}u_1{}^2\tilde{u}u_2\cos(2\phi_1+\phi_2)+\tilde{u}u_2{}^2\tilde{u}u_4\cos(2\phi_2+\phi_4)\right)\right)$$

The first term of the integration product is F_r which reflects the contribution of the subtidal flow to the friction term; the second term is F_{rt} that expresses the friction induced by the subtidal flow and tidal interaction; and the third term is F_t which indicates the friction term induced by tidal asymmetry.

4.4. Results

4.4.1. Subtidal Variations

The water elevation data in Figure 4.2 show that both straight and branching channels were controlled and dominated by tides, except at the Nagawaku and Yaguchi stations. The absence of tidal domination at the Yaguchi gauging station revealed that the tidal wave penetration did not reach the Yaguchi station. Moreover, the water level data from the Nagawaku station show that river runoff plays a significant role because the tidal wave is blocked by the Gion gates.

The water elevation at Kusastu (channel entrance) represents the water elevation prior to entering the estuary. The highest and lowest water levels at Kusatsu was 2.21 m and -1.48 m, respectively, and occur during spring tide. The highest water level did not significantly change after entering the estuary. However, the lowest water level had noticeable changes in Gion with -0.65 m, while in Misasa stations was -1.02 m, respectively. The changes in the lowest water level indicate the damping of the tidal wave amplitude.

The tidal ranges in the straight and branching channels are shown in Figure 4.3a, b. The tidal range was calculated by subtracting the maximum and minimum values of water elevation every 25 h. The tidal range at the Yaguchi station was not calculated because of the absence of tidal effects on water elevation. The tidal range in both the straight and branching channels showed that the tidal range varied in the neap-spring cycle, where the tidal range increased during spring. In straight channel, during spring tide, the tidal range decreased from 3.6 m at Kusatsu to 2.8 m at Gion, then dropped to 1.9 m at Nagawaku. The decreasing tidal range from Gion to Nagawaku is more significant than from Kusatsu to Gion, even though the distance Kusatsu –Gion is 8.2 km while Gion –Nagawaku is 0.6 km. The considerable decrease in the tidal range at Nagawaku indicates the effect of the Gion gate. Similarly, in the branching channel, the decrease in the tidal range was gradual toward the distance from the river mouth, except at St. C. During the spring tide, the tidal range at St. C was less than that at Misasa Station. St. C was dry during the lowest water level in spring. As we did not observe the lowest water level at St. C, the tidal range at St. C was lower than that at Misasa during spring tide.

The subtidal water elevation was calculated by averaging the water elevation data over a 25-hour window. The subtidal elevation in Kusatsu showed an increasing trend (Figure 4.3c, d). A similar trend was observed for the subtidal elevations at Gion, St. A, St. B, and Misasa. This increasing trend was caused by seasonal fluctuations in the mean water level of Hiroshima Bay. In contrast, the subtidal elevation in Nagawaku showed a decreasing trend similar to that of the water elevation in Yaguchi (Figure 4.2d). The similarity pattern indicates the effect of river runoff on the subtidal elevation at Nawagaku Station. Furthermore, the subtidal elevation at St. C shows a different pattern from the other stations, where it fluctuated around -0.05 – 0.05m.

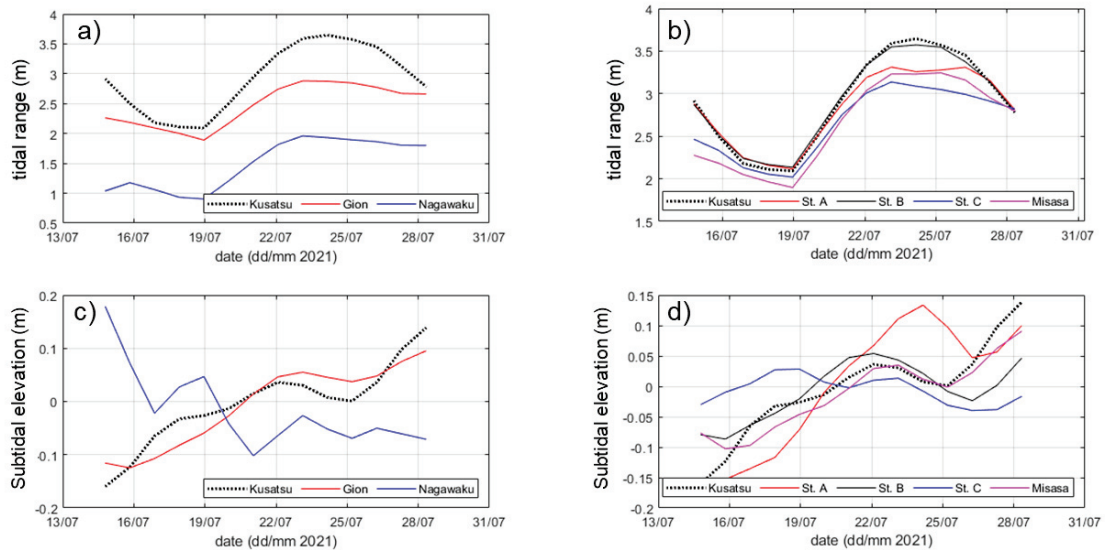

Figure 4.3. Time plot of tidal range (a, b) and subtidal elevation (c, d) of the water elevation stations in straight (a, c) and branching (b, d) channel. The straight channel includes Gion and Nagawaku Stations. The branching channels includes St. A, St. B, St. C and Misasa. Kusatsu Station located at river mouth.

4.4.2. Tidal Oscillation

The FFT method was applied to water elevation data from Kusatsu, Gion, Misasa, and Sts. A, B, and C to examine and compare the energy spectra of tidal oscillations in the straight and branching channels. The FFT results are affected by the durations of the observation and sampling periods. Longer observation periods revealed longer-period signals and a smaller sampling frequency yielded a larger frequency signal. The data at St. A, B, and C were resampled hourly to obtain the same variability results as the other data before applying the methods. The energy spectral analysis was expected to reveal changes in tidal oscillation from the river mouth to the inside of the estuary.

Figure 4.4a shows the change in the water elevation energy spectra from the river mouth upstream in the straight channel and Figure 4.4b shows the spectra in the branching channel. The water elevation spectrum at Kusatsu shows that the energy was dominated by 12- and 24-

hour period signals associated with semidiurnal and diurnal tides, respectively. Peak energy is observed in shorter periods of 8, 6, 5, and 4 h and is attributed to compound tides. In the straight channel, the decrease in energy in the 12- and 24-hour periods is clearly shown from downstream to upstream, whereas the shorter-period signals show increasing peaks. This result indicates energy transfer from the major tidal components (diurnal and semidiurnal tides) to the compound tides. In branching channels, an increase in energy in shorter-period signals is shown from downstream to upstream, particularly on 6 and 8-hour period signals, indicating energy distortion due to tidal distortion in the branching channel.

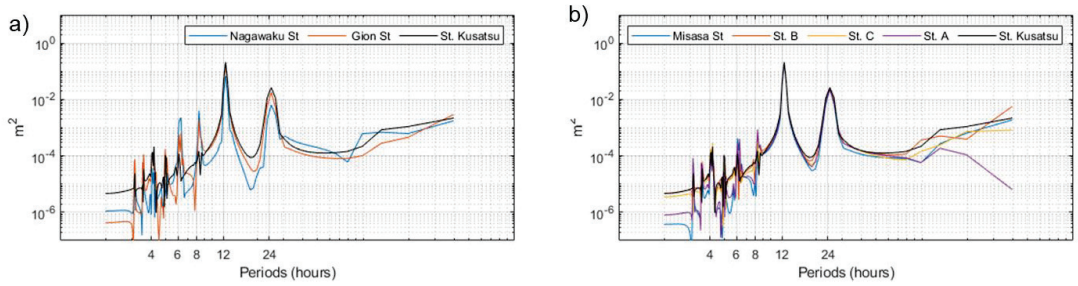

Figure 4.4. FFT power spectra of water elevation data in (a) straight channel, and (b) branching channel

Spectral analyses of water elevation data revealed the evolution of tidal oscillations from downstream to upstream. However, spectral analyses are limited to showing the tidal oscillation regime, and cannot analyse the exact tidal constituents involved in the oscillation. Harmonic analyses were applied to the data to examine the evolution of tidal constituents from downstream to upstream. The results of harmonic analysis are presented in Table 4.2. The eight tidal constituents are listed in Table 4.2, consisting of two semidiurnal constituents, two semi-diurnal constituents, three quarter diurnal constituents, and one subtidal constituent. In general, tidal oscillations are dominated by semi-diurnal tidal constituents, followed by diurnal and quarter-diurnal tidal constituents. At Kusatsu, M2 is the most dominant tidal constituent,

followed by K1, S2, O1, M4, MS4, and S4. The tidal constituent amplitudes at the upstream stations have a similar pattern to that of Kusatsu station, except at St. A, where the MS4 amplitude is higher than the M4 amplitude. The results indicate a different tidal evolution in which the M2 constituent interacts with S2, resulting in a compound tide MS4 constituent. However, the results of the harmonic analysis are consistent with those of the energy spectra analysis, revealing tidal energy distorted from major tidal constituents (semi-diurnal and diurnal tides) to compound tides.

Table 4.2. Harmonic analysis of the water elevation data in Kusatsu, Gion, Nagawaku, St. A, St. B, St. C and Misasa

		Kusatsu		Gion		Nagawaku		St. A		St. B		St. C		Misasa	
		A	P	A	P	A	P	A	P	A	P	A	P	A	P
sub	MSF	0.075	22.720	0.101	29.630	0.066	143.850	0.146	11.980	0.059	3.920	0.011	310.360	0.078	36.430
D1	O1	0.250	191.890	0.179	193.100	0.102	160.330	0.238	187.030	0.249	190.330	0.209	192.240	0.203	193.040
	K1	0.372	230.080	0.280	223.460	0.174	202.760	0.362	226.250	0.368	227.850	0.333	230.130	0.317	226.900
D2	M2	1.054	274.190	0.980	277.850	0.580	286.660	1.035	275.010	1.053	274.290	1.005	276.550	0.988	279.590
	S2	0.327	336.280	0.295	343.230	0.212	331.860	0.318	340.790	0.325	337.380	0.310	338.330	0.305	338.750
D4	M4	0.016	19.110	0.049	176.340	0.147	206.430	0.005	67.570	0.018	45.950	0.029	150.500	0.046	136.490
	MS4	0.015	111.250	0.038	208.460	0.072	275.560	0.026	150.950	0.018	137.060	0.032	204.540	0.029	200.430
	S4	0.001	195.540	0.002	166.260	0.013	50.610	0.008	236.040	0.002	273.930	0.007	281.960	0.004	50.660

4.4.3. Tidal Distortion and Tidal Asymmetry

4.4.3.1. Spatial variation of Tidal Distortion and Tidal Asymmetry

The amplitude ratio of the quarter-diurnal and semidiurnal tidal species (D4/D2) was used to estimate the net tidal distortion, without considering the differences in tidal evolution and tidal constituent interactions at every station. The amplitudes of the semi-diurnal (D2), diurnal (D1), and quarter-diurnal (D4) tidal species in the straight and branched channels are shown in Figure 4.5a. The amplitude of the tidal species was calculated by summing the amplitudes of the tidal constituents in the same species. The tidal constituents were produced from harmonic analysis of the water level data during the observation period. This analysis could diminish the effect of river discharge variation on tidal distortion estimation. Therefore, the effect of the channel setting on tidal distortion could be evaluated.

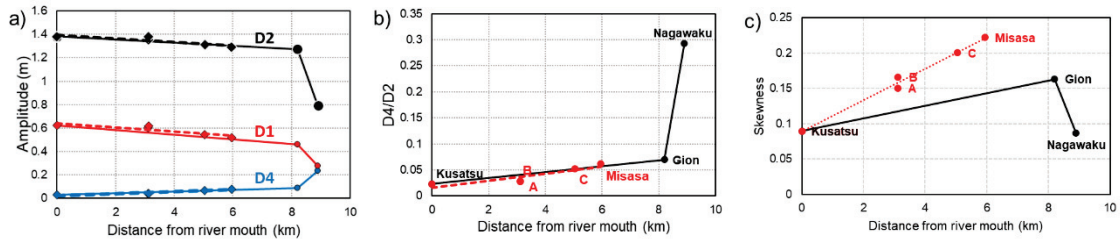

Figure 4.5. (a) total amplitude of semidiurnal (D2), diurnal (D1) and quarter diurnal (D4) tidal species, (b) Ratio of total amplitude quarter diurnal tidal species and semi diurnal tidal species, and (c) tidal duration skewness in straight and branching channel as a function of the distance from the river mouth.

The semidiurnal tide dominated the tidal oscillations in both straight and branching channels, followed by diurnal and quarter-diurnal tidal components (Figure 4.5a). The amplitudes of all tidal components change gradually from the river mouth upstream, except at Nagawaku station. The amplitude ratios of the semidiurnal and quarter-diurnal in the channels shows that the tidal distortion increases gradually in a similar pattern in both the straight and

branching channels (Figure 4.5b). However, tidal distortion increases at Nagawaku. Rapid changes in tidal component amplitude and tidal distortion in Nagawaku are influenced by the Gion watergate between the Gion and Nagawaku stations, which blocks river runoff from upstream and tidal flow from the Ota floodway entrance. The gate blocks the tidal propagation of the tidal wave, which causes a significant reduction in D2 and D1 amplitudes at Nagawaku station.

Tidal asymmetry in semidiurnal tidal regime estuaries is commonly estimated by the phase difference between constituents M2 and M4 [27]. However, tidal asymmetry was estimated using the skewness of the elevation-time derivative in this study. This method is considered more suitable because the results of the harmonic analysis show that there are stations where the amplitude of MS4 is much higher than that of M4, which indicates a difference in the tidal compound mechanism. The skewness method can estimate the net tidal asymmetry caused by all the tidal constituent interactions.

The calculation results of time duration asymmetry (TDA) using the data along the observation duration are shown in Figure 4.5c. The TDA at the river mouth (Kusatsu Station) showed flood dominance asymmetry, indicating a longer flood duration. In straight channel, TDA at Gion and Nagawaku are 0.16 and 0.08, respectively. In the branching channel, TDA increased with increasing distance from the river mouth. In both cases, the asymmetry increases gradually with increasing distance from the river mouth, except at Nagawaku, where the asymmetry increases rapidly. However, the increase in TDA in the branching channel is steeper than that in the straight channel. This indicates that the morphological setting of the branching channel plays a role in the tidal asymmetry. In the ODC, the Gion gate blocks the propagation of the tidal wave and reflects the tidal wave. The reflected tidal waves could have increased the asymmetry of the Gion stations. Moreover, the rapid increase in asymmetry at Nagawaku could have been caused by the existence of the Gion gate between the Nagawaku and Gion stations.

4.4.3.2. Temporal Variation of Tidal Distortion and Asymmetry

Theoretically, river runoff influences tidal interactions and the formation of compound tides and overtides [85]. River runoff influences tidal dynamics by enhancing subtidal friction, which plays a key role in tidal damping [11]. Moreover, when the tide propagates in an estuary, friction diminishes tidal energy and induces energy transfer related to overtides and compound tide formation [84, 85]. Some studies have observed landward enhancement of the M4 constituent, damping of M2, and an increasing amplitude ratio (D4/D2) from neap to spring [84, 85]. In this study, the tidal response to tidal forcing was evaluated using variations in tidal distortion and asymmetry. Tidal distortion was calculated using the ratio of daily D4 to D2, whereas tidal asymmetry was evaluated using daily TDA. According to the tidal distortion shown in Figure 4.6c, tidal distortion was high at the upstream stations and peaked during the spring tide, whereas during the neap tide, tidal distortion was minimal at all stations. The variation in tidal distortion is related to the daily variation in the D2 and D4 amplitudes, as shown in Figure 4.6 a and b, which show higher D2 and D4 values during the spring tides. However, D2 decreases inside the estuary, whereas D4 increases. The variation in amplitude D4 at the upstream station (Misasa and Gion Station, St. C) is higher than that at the downstream station (Kusatsu, St. A, and St. B).

Amplitudes D2 and D4 at Nagawaku station have exceptional patterns, where D2 decreases and D4 increases significantly (Figure 4.6a, b). Amplitudes D2 and D4 were higher during the spring tide; however, in the first spring period (13 July –18, 2022), the amplitude decreased. The decrease in amplitudes D2 and D4 in Nagawaku is related to the higher river runoff during this period, as shown by the water elevation in Yaguchi (Figure 4.2d). This result revealed that river runoff significantly affected the tidal dynamics at Nagawaku Station. Gion watergates cause tidal damping and intensify the role of river runoff in Nagawaku tidal

dynamics. Moreover, the tidal elevation in Nagawaku is influenced more by the tide from Misasa because of the limitation of tidal propagation from the Gion to Nagawaku.

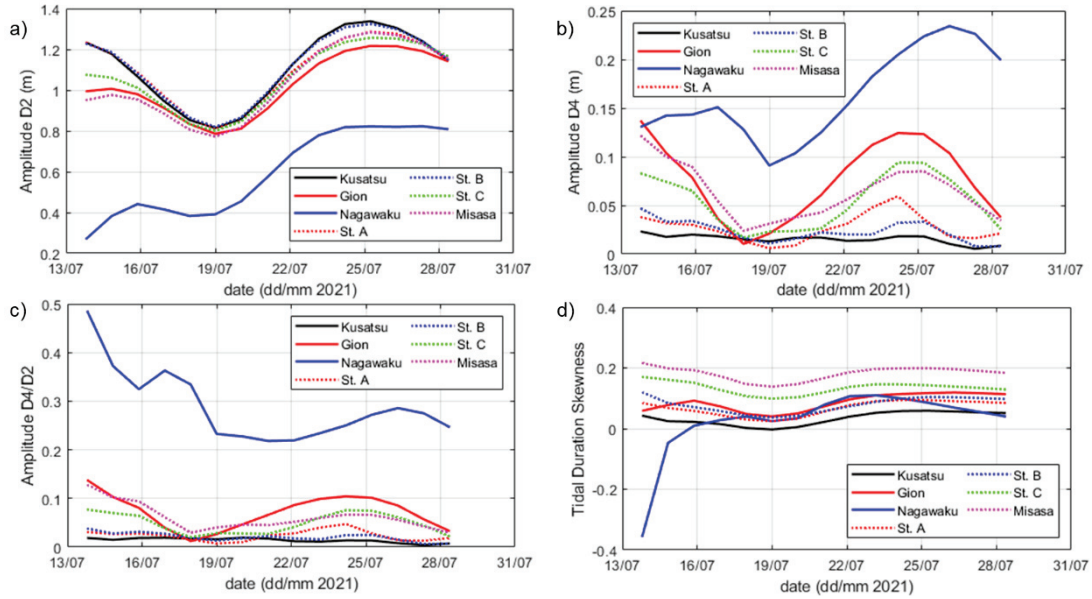

Figure 4.6. Temporal variation of (a) D2 amplitude, (b) D4 amplitude, (c) ratio of D4 and D2, (d) time duration skewness at Kusatsu, Gion. Nagawaku, St. A, B and C and Misasa stations.

The daily variation in tidal asymmetry (Figure 4.6d) shows flood dominance, suggesting a longer flood duration with a neap-spring variation. However, the neap-spring fluctuation was consistent at all stations except for Nagawaku and Gion. The TDA in Gion and Nagawaku tended to ebb dominance during 13 July –18, 2022, coinciding with the increase in river discharge.

4.5. Discussion

The interaction of tidal constituents, generation of compound tides, and over-tides can be modified by river runoff [11, 49, 85, 95]. Daily variations in tidal distortion and asymmetry captured the effect of river discharge at Nagawaku Station from 13 July to 18, 2022 (Figure 4.6c, d). Furthermore, a slightly different pattern of tidal asymmetry was observed at the Gion station during this period (Figure 4.6d). The exceptional pattern during this period is related to

the increase in discharge, as shown by the increase in the water level in Yaguchi (Figure 4.2d). During these periods at both stations, river runoff modifies the tidal asymmetry from flood dominance asymmetry to symmetrical/ebb dominance tidal duration. This means that the river shortens flood duration. The river discharge affected the tidal distortion and asymmetry in Nagawaku the most because of the existence of the Gion water gate. The water gate, located between the Gion and Ngawaku stations, blocks the river flow and accumulates river runoff, amplifying the effect of river runoff around the water gate. River flow enhances the friction that leads to energy transfer from the major tidal frequency to compound tides and overtides [85].

Despite river discharge, the nonlinearity of tidal behaviour can be affected by morphological settings, including channel convergence, bathymetry variation, and junctions [9, 10, 17, 82, 86, 96]. The changes in bathymetry and convergence channel of the Ota River Estuary are shown in Figure 4.7. The channel width of the straight channel narrows gradually, while the branching channel narrows rapidly from the first 4 km and then widens gradually. The straight channel bathymetry shallows gradually from 3 m in the river mouth to 1 m in Gion, while the branching channel bathymetry changes rapidly in the first 1 km. The change in the topographical setting implies a variation in tidal asymmetry which balances convergence, bathymetry change, and friction, determining tidal damping/amplification [9]. Moreover, the convergence of tides at a junction between two channels can generate compound tides that induce tidal asymmetry that plays a role in the transport of suspended sediments [2, 38, 86].

The implication of the different topographical settings between the straight and branching channels can be seen in the tidal asymmetry and tidal distortion variation in the Ota River Estuary network. The spatial variation of the tidal distortion and asymmetry in the Ota River estuary network shown in Figure 4.5 exhibits the difference in the tidal distortion and asymmetry in the straight and branching channels. The tidal distortions in the straight and

branching channels were not significantly different (Figure 4.5b), whereas the tidal asymmetry showed a considerable difference; the asymmetry in the branching channel increased rapidly from the river mouth to the inner estuary (Figure 4.5a). The TDA in Sts. A and B is comparable than the TDA of water elevation in Gion even though the location of St. A and B is 3.1 km while Gion station is 8.2 km. The rapid increase in TDA at St. A and B was induced by the rapid change in bathymetry (Figure 4.7b) and convergence channel (Figure 4.7a). Moreover, the convergence of tidal propagation at junctions at St. C and Misasa induces tidal interactions that increase tidal asymmetry [2, 86]. The aggregate effect of the morphological setting of the channel on tidal oscillations was evaluated; however, the effects of each parameter were not examined in this study. A sensitivity analysis of these parameters can be applied to tidal oscillations in future studies.

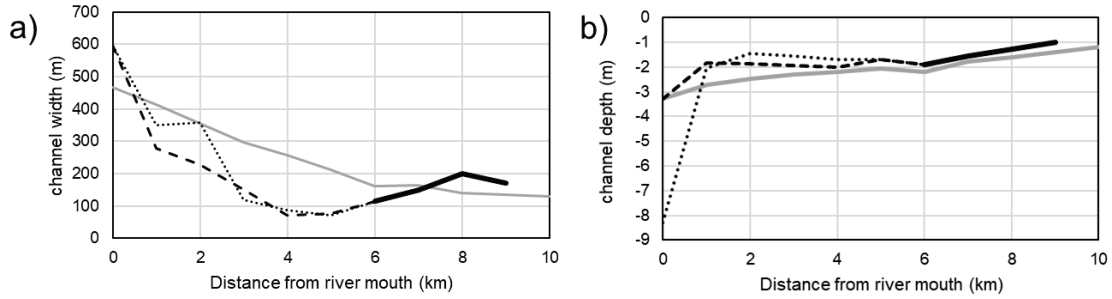

Figure 4.7. (a) Channel width and (b) channel depth a a function of the distance from river mouth

Friction is a crucial term that play a role in tidal distortion and asymmetry [10, 92]. Current velocity data were used to estimate the contributions of subtidal currents, tidal currents, and tidal asymmetry to the subtidal friction at St. A, B, and C using Equation 4.5. The equation decomposes subtidal friction into the contributions of subtidal flow (F_r), tidal-subtidal interaction (F_{rt}) and, tidal asymmetry(F_t). The correlation of the decomposition results with the subtidal elevation (Table 4.3) showed a high correlation between the subtidal elevation and

friction related to the subtidal flow at St. A and B. Moreover, the combination of subtidal friction with other frictions was also highly correlated (Table 4.3). In contrast, the subtidal elevation at St. C was highly correlated with the combination of friction related to tidal and tidal asymmetry ($F_t + F_{rt}$) with a negative correlation. The negative contribution of the tidal asymmetry friction term to water elevation indicates that friction results in a higher tidal asymmetry [92]. The results suggest that subtidal flow modulates the subtidal water level at St. A and B, where the channel is straight, whereas at St. C, where the junction area is located, the water level is modulated by the interaction between tides and tidal asymmetry. This finding again supports the previous argument which said the meeting of tides at the junction induces tidal interactions that generate tidal asymmetry.

Table 4.3. Correlation value subtidal water level in St. A, B and C with subtidal friction in term of subtidal flow (Fr), tidal-subtidal interaction (Frt), tidal asymmetry (Ft).

	Fr	Frt	Ft	Ft+Frt	Fr+Frt	Fr+Ft	Fr+Frt+Ft
St. A	0.91	0.60	0.40	0.55	0.90	0.90	0.89
St. B	0.65	0.50	-0.38	0.48	0.91	0.91	0.91
St. C	0.25	0.47	-0.30	-0.85	-0.56	-0.43	-0.59

Tidal asymmetry plays an important role in the residual sediment transport [30]. Owing to the limited river runoff in the Ota River Estuary, tidal current asymmetry induces suspended sediment transport [25]. This differs from a high-discharge estuary (discharge > 3000 m^3), in which discharges induce tidal asymmetry and play a role in suspended sediment transport [1]. However, in the ODC, the interaction between tides and river runoff results in estuarine turbidity maxima [89]. The river runoff-tidal interaction and its relationship with sediment transport may be related to erosion and deposition in the Ota River estuarine network.

4.6. Conclusions

We explored tidal wave dynamics in the straight and branching channels of the Ota River estuarine network. The tidal oscillations were evaluated using spectral and harmonic analyses. The spectral energy shows that there is an energy transfer from the primary tidal frequency to the compound tide and over-tide frequency when the tidal wave propagates from the river mouth upstream. The result of the harmonic analysis supports the result that shows that the diurnal and semidiurnal tidal species dominate the tidal oscillation, but the amplitude decreased upstream, while the amplitude of the quarter diurnal tidal species increased. Moreover, tidal distortion and asymmetry of the straight and branching channels of the Ota River estuarine network were investigated. The ratio of semidiurnal and quarter-diurnal tidal amplitudes and the skewness of the tidal duration were used to examine tidal distortion and asymmetry. The tidal distortions of the straight and branching channels are comparable in terms of spatial variation. In contrast, the tidal asymmetry in the branching channel increased rapidly from the river mouth to the inside of the estuary, compared to the tidal asymmetry in the straight channel. The rapid increase in tidal asymmetry in the branching channel was related to the topographical setting of the branching channels, including rapid changes in the bottom topography, channel width, and junctions.

In both the straight and branching channels, the tidal range decreased from the river mouth to the interior of the estuary. The mean water levels at all stations, except Nagawaku, showed an increasing trend with respect to seasonal water levels. The mean water level at the branching channel was correlated with friction related to tides and tidal asymmetry, whereas in the straight channel, the mean water level was correlated with friction related to subtidal flow. Nagawaku Station, located near the water gate, had an exception in the tidal range and mean water level variation. The tidal range decreased and the mean water level showed decreasing trends. The noticeably different patterns of tidal range and mean water level at the

Nagawaku station are related to the effect of the water gate, which amplifies the influence of river runoff on the water level.

The effect of river runoff was clearly observed at stations around Nagawaku and Gion stations around the water gate. River runoff affects tidal range, mean water level, tidal distortion, and tidal symmetry. The water gate blocked river flow and controlled the runoff volume of the ODC. The accumulation of water in the water gate amplified the effects of river runoff. River runoff dampens tidal amplitude constituents, leading to a decrease in the tidal range and water level. Moreover, river runoff shortens flood tide duration.

This study highlights the tidal wave dynamics difference between branching and straight channels in small and short tidal-dominated estuary. The results showed that different settings of topography, including channel configuration and bottom topography, played a role in the tidal evolution of straight and branching channels. However, this study was limited to the characteristics of the water elevation in both channels. Studies of estuarine dynamics in small estuaries with multi-channel branches are still challenging, particularly regarding river runoff-tidal interactions, and their relationship to sediment transport might be related to erosion/deposition.

Chapter 5: Sensitivity of Junction Width to Tidal Nonlinearity on Small and Shallow Tidal Junction

5.1. Introduction

Investigations of the tidal wave evolution in tidal river networks have received increasing attention in the literature. Many studies have been conducted in large estuarine networks such as the Yangtze [85] and Mahakam Rivers [83], because they have high discharge and sedimentation rates. In these estuaries, tidal wave dynamics are significantly modulated by river runoff [85]. River runoff modulates tidal nonlinearity behaviour by increasing tidal damping and asymmetry [49, 85]

In a tidal dominated estuary, where the ratio of river runoff to tidal discharge is less than one, the role of the river runoff inducing the tidal wave nonlinearity is limited.. The evolution of tidal waves is affected more by shallow water friction with respect to bottom topography changes [18, 82, 87, 88]. Using analytical approaches, the relation between friction and convergence channel in tidal dominated estuary was examined by Savenije et al. (2008)[9]. However, this study was limited to a single, straight channel. Small estuarine networks with limited discharge have achieved poor recognition, and the variation in the topographical setting is rarely discussed. Studies on tidal wave evolution in small and narrow estuary networks provide a better understanding of the tidal dynamics.

The water elevation in estuarine networks is more complicated than that in straight tidal rivers. In an estuarine tidal network, tides propagate from multiple tidal inlets to the estuaries. Topographical settings, including variations in bathymetry and channel length and width, affect the tidal propagation [2]. This study focused on the water elevation in shallow and narrow tidal junctions with limited river runoff. Moreover, in estuarine tidal junctions, the tidal range drops because of the convergence of tidal propagation at the apex of junction [17]. Understanding the

variables controlling tidal nonlinearity behaviour is important because tides may become a dominant factor that controls sediment transport and nutrient mixing in estuarine networks. However, this study limits the studies on the sensitivity of water elevation to variations in the upstream channel width.

The remainder of this paper is organised as follows. Section 5.2 explains the methods, including the observation data, analysis methods, and numerical model setup. In Section 5.3, the results of the tidal asymmetry analysis from the observation data and models are presented. A discussion and conclusion of the results are presented in Sections 5.4 and 5.5.

5.2. Methods

5.2.1. Observation Location and Data

The Ota River Estuary is an estuarine network dominated by tidal forcing and is located in Hiroshima city, Japan. The junction is located 5.3 km upstream from the river mouth (Figure 5.1) The junction involved the upstream Kyu Ota branch (northern branch), downstream Kyu Ota (west side branch), and Motoyasu (east side branch). Danial et al. (2019) [90] studied the Misasa junction that is located 1 km upstream from the studied junction, and showed the existence of tidal discharge asymmetry induced by branch channel geometry variation. At the same junction, Xiao et al. (2021) [18] showed that limited river runoff plays a role in tidal asymmetry at the tidal junction.

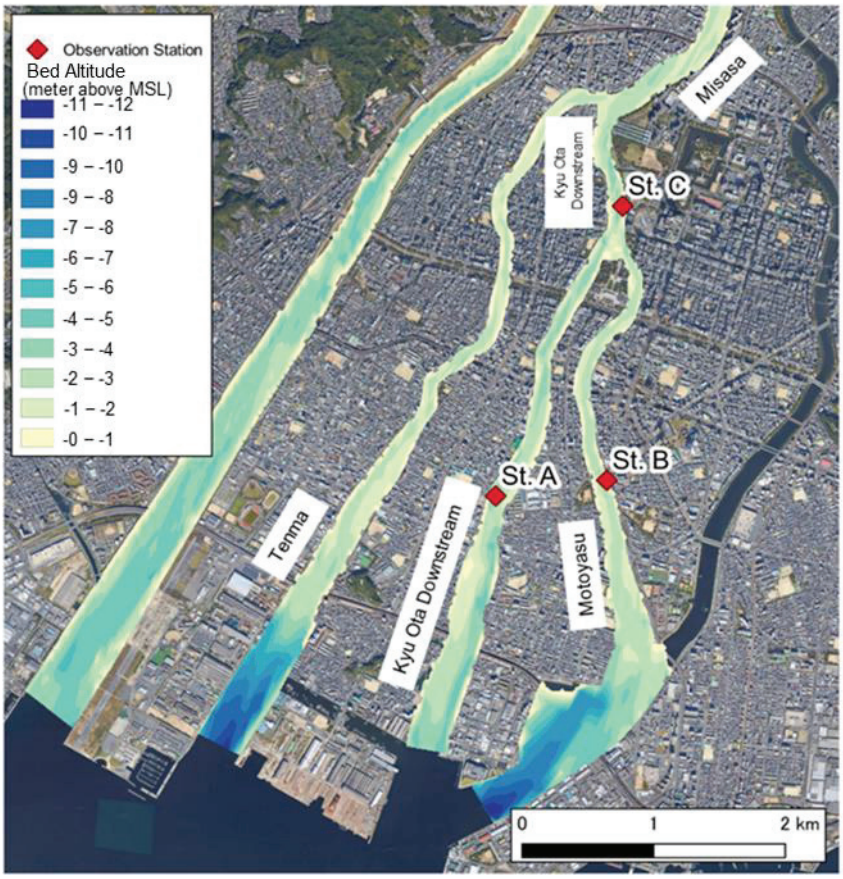

Figure 5.1. Ota River channel network.

The water elevations at three stations at Sts. A, B, and C were observed using a pressure sensor from aquadop ADCPs during 12–30 July 2021. Sts. A and B were located downstream of Kyu Ota and Motoyasu branches, respectively. St. C was located at the junction upstream of the Kyu Ota branch. Observational data are shown in Figure 5.2. During the neap tide, the water elevations at St. A and St. B have the same amplitude and phase, whereas the water elevation at St. C has slightly different amplitudes and phases (Figure 5.2b). On the other hand, during spring tide, at the highest high-water level, St. A and St. B water elevations are higher than St. C (Figure 5.2c); however, at the second high-water level, St. C water elevation is higher than St. B and St. A. Unfortunately, during the lowest low water level, we could not capture the water elevation data at St. C and St. A because the station was dry. Visually, this

observation shows a difference in tidal asymmetry between the straight channels in the Sts. A-B and St. C. Tidal asymmetry assessment requires further analysis to quantify asymmetry. Moreover, this result motivated the modelling examination, which aimed to understand the variables controlling tidal asymmetry at junctions.

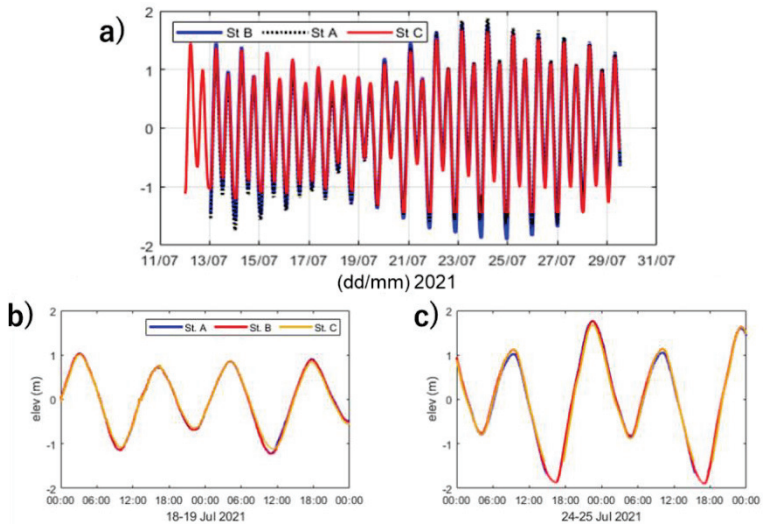

Figure 5.2. Water elevation observation in Sts. A, B, and C (a) during the observations, (b) during neap tide, (c) during spring tide.

5.2.2. Tidal Asymmetry Analysis

Harmonic analysis using the T_Tide package [91] was applied to the water elevation data to decompose them into tidal constituent amplitudes and phases. The method shows that the time series data are composed by summation harmonic signals with a certain frequency, amplitude, and phase, as follows:

$$H(t) = b_0(t) + \sum_{n=1}^{N} [A_n \cos(\omega_n t - \Phi_n)] + r(t) \qquad (5.1)$$

where the water elevation time series is denoted as $H(t)$, $b_0$is the mean water level, and A, ω, and Φ are the tidal amplitude, frequency, and phase, respectively, of tidal constituents n (n=1,2...N), and $r(t)$ represents the residual components.

The outcome of the harmonic analysis is the amplitude and phase, which were utilised to estimate tidal asymmetry. The tidal asymmetry was calculated from the amplitude ratio of the tidal constituents [38]. In this study, the ratio amplitudes of M4 and M2 are used to estimate tidal distortion because the tidal regime in the Ota River Estuary is semi-diurnal [86].

5.2.3. Numerical Experiments

A depth-averaged version of the Delft3D model is used in this study. The depth-averaged model is selected instead of a 3-dimensional model because the 3-dimensional flow is not important for studying the propagation of tidal waves. Furthermore, this model uses a barotropic mode and neglects density gradient.

Table 5.1. Parameter setting of idealized junction model

Symbol	Variable	Value
Δx	along channel grid size	40-170 m
Δy	cross channel grid size	10 m
h	still water depth	5 m
L	length of seaward channel	10 km
Q	river discharge	50 m^3s^{-1}
M2	amplitude of M2	0.7 m
S2	amplitude of S2	0.4 m
Width Branch	width seaward branch	70 m
Width Apex	width upstream branch	160 m
C	Chezy coefficient	55 $m^{1/2}s^{-1}$

An idealised model of the junction is built based on the Ota River Estuary junction. The model grid is shown in Figure 5.3. The junction was located 10 km from the open-sea boundary, and the total length of the channel is 560 km. The upstream channel is set to be very long to ensure that the tides are smoothly damped. The depth and width of the channel are designed

based on the average depth and width of the Kyu-Ota junction. The upstream branch width is 160 m, and the width of the downstream branches is 70 m. In this model, tidal forcing is limited to only the M2 and S2 tidal constituents because the Ota River Estuary is dominated by semi-diurnal tides. The parameter settings are listed in Table 5.1. Moreover, a series of simulations is conducted to analyze the sensitivity of the model to width changes, while the other parameters are fixed. The width of the upstream channel varies from to 70–208 m. The sensitivity test aims to explain how the change in the width of the upstream branch affects the nonlinear behaviour of the water elevation in the junction.

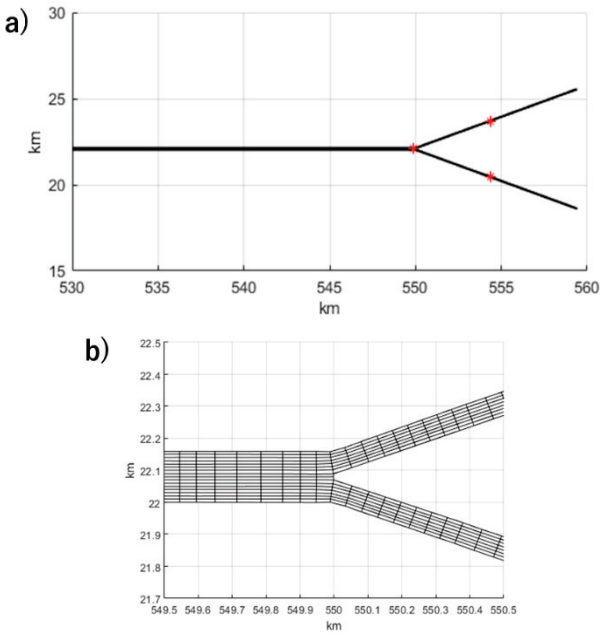

Figure 5.3. a) Downstream part of the model domain, including the upstream channel and the branch that connects to the sea. b) The grid surroundings of the tidal junction.

5.3. Results

5.3.1. Water Level Nonlinearity

Harmonic analysis on 25-hour window water elevation data shows that the amplitudes of M2 and M4 vary in the spring-neap cycle (Figure 5.4Figure 5.4). The highest amplitudes of

M2 and M4 occur during the spring tide. M2 amplitudes at Sts. A and B are similar, whereas the M2 amplitude is lower at St. C. In contrast, the M4 amplitude at St. C is higher than those at Sts. A and B. Although the amplitudes M2 at Sts. A and B have similar values, the M4 amplitudes at Sts. A and B have slightly different values and peaks. The topographical setting, including the bathymetric profile, channel length, and width, could have affected the different M4 amplitude profiles at Sts. A and St. B. A significant increase in M4 at St. C indicates that the nonlinearity increases at the apex of the junction.

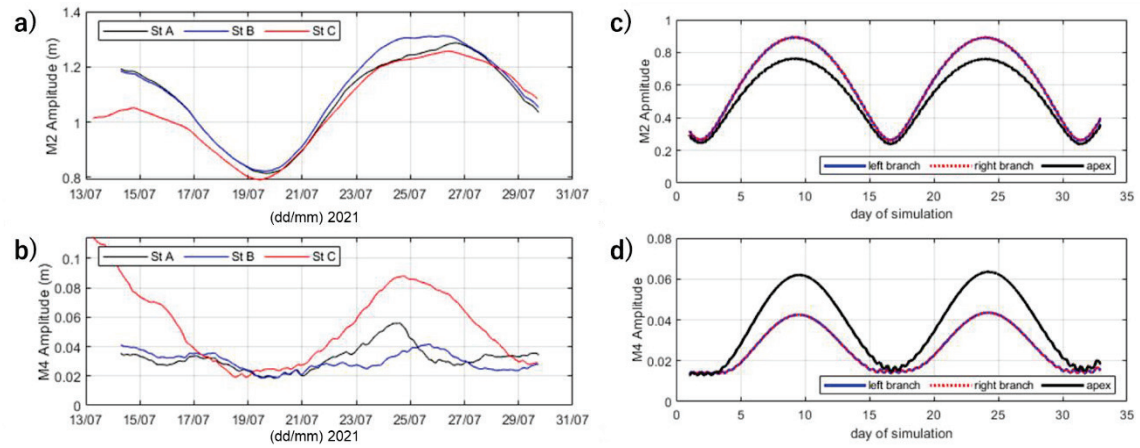

Figure 5.4. Amplitude of (a, c) M2 and (b, d) M4 from the (a, b) observation data and (c, d) idealized model.

The application of harmonic analysis to the water elevation of the idealised junction model shows a pattern similar to the observations, where the amplitude of M2 at the apex of the junction is less than the M2 amplitude in the downstream branches, and the M4 amplitude at the apex of the junction is higher than the M4 amplitude in the branches. However, both the amplitudes of M2 and M4 of the model exhibit lower values than those of the observations. The difference between the model and the observations can be attributed to the high degree of simplification of the model. However, the model reproduces the increase in tidal nonlinearity from the downstream to the apex of the junction.

5.3.2. Sensitivity Analysis

A sensitivity analysis by varying the upstream channel width is shown in Figure 5.5. Only the amplitudes of M2 and M4 at the apex of the junction and left branch are shown because the amplitudes of M2 and M4 at the right and left branches had the same value. The results show that the M2 amplitudes at the left branch and apex decrease with an increase in upstream channel width. In contrast, the M4 amplitude showed an increasing pattern with an increasing upstream channel width. However, an exception pattern was observed at the 206 m upstream channel width. The M4 amplitude was 0.07 m during the spring and 0.02 m during neap, which is less than the amplitude of M4 at 160 m and 112 m channel widths.

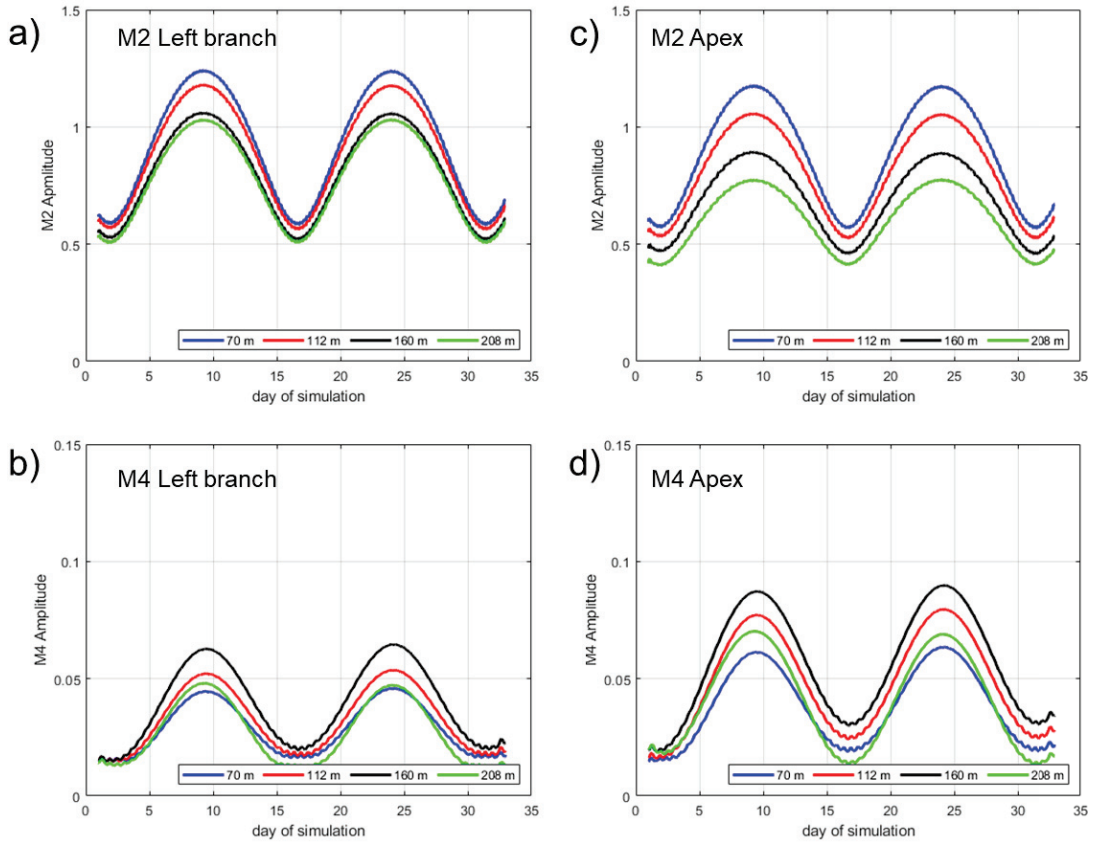

Figure 5.5. Amplitude of (a, c) M2 and (b, d) M4 from at (a, b) left branch and (c, d) apex of junction.

The damping/amplification of water elevation is affected by the changes in friction and the cross-sectional area of the channel[9]. Sensitivity analysis examined the changes in the cross-section area to the water elevation damping/amplification by varying the width of the upstream channel. The results show that the damping of the tidal wave increases with a larger cross-sectional area: it is clearly observed that the M2 amplitude decreases with an increase in the upstream channel width. However, this behaviour is not observed for the overtide constituent; in this case, M4, which increases when the width of the upstream channel is more than twice that of the downstream channel.

5.4. Discussion

The spring tide, neap tide, and 30 days period time-windows harmonic analysis was applied in water elevation data. The neap tide window harmonic analysis shows the lowest amplitude owing the low tidal forcing during neap tide, while the spring tide window harmonic analysis shows the highest amplitude. The 30 days window harmonic analysis showed shows the mean value of the M2 amplitudes (Figure 5.6). Figure 5.6 summarises the sensitivity analysis of the junction with changes in the upstream channel width. When the channel width increases, the amplitude of M2 gradually decreases. In contrast, the amplitude of M4 increases with the width of the channel, except for the 220 m width of the upstream channel.

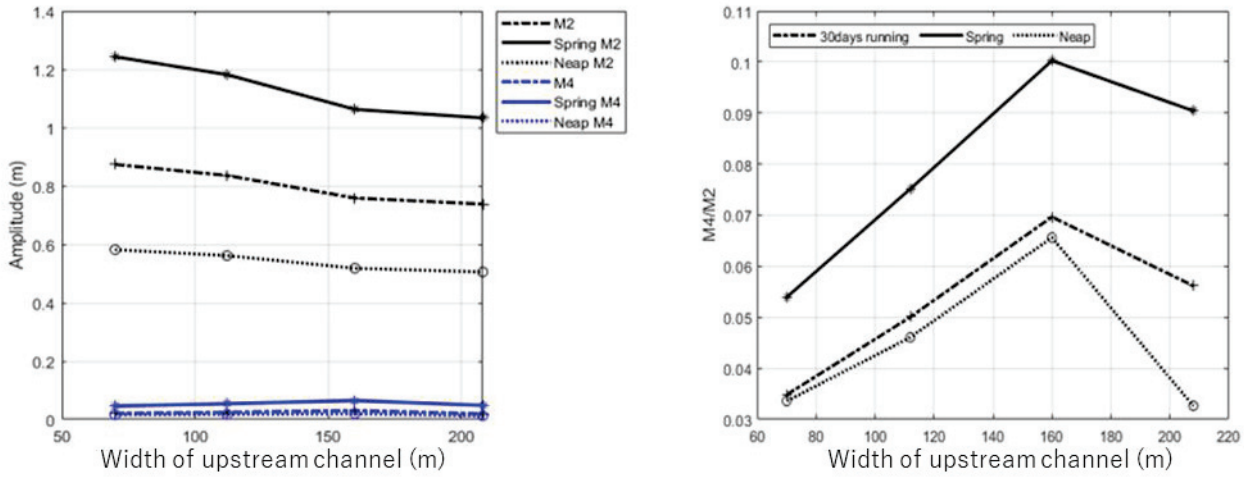

Figure 5.6. (left) Variation of M2 and M4 amplitude to the width of upstream channel. (right) Variation ratio of M4 and M2 to the width of upstream channel.

The application of the model at the junction is highly simplified. The Ota River junction is more complex with variations in geometry and bathymetry. The complexity of the junction is not considered in this model. Moreover, at the Ota River junction, the branches of the junction (downstream Kyu Ota and Motoyasu) are connected downstream. However, the simplified model can capture the nonlinear phenomena that occur at the junction.

The sensitivity of the tidal wave amplitude at the junction is used to analyse the changes in upstream channel width to tidal nonlinearity at the junction. The ratios of the M4 and M2 amplitudes are used to measure the nonlinearity (Figure 5.6). We found that nonlinearity increased as the width of the channel increased until the width of the upstream channel was twice that of the downstream channel. Meanwhile, when the width of the upstream channel was more than twice that of the downstream channel, nonlinearity decreased significantly (Figure 5.6).

When the tidal converges from the branches to the junction, the meeting of tidal waves causes increasing tidal nonlinearity [17]. In a wider channel, the change of width from the narrow channel in the branches to a wider channel in the junction induces decreasing of major

tidal constituents' amplitude significantly. However, when the junction becomes wider, the role of river runoff is more influential. The river runoff dampens the tidal wave amplitude; hence, the nonlinearity decreases. A decrease in the amplitude ratio in Figure 5.6 indicates an increase in role river runoff to the tidal evolution [97]. Horrevoets et al. (2004) [98] explained that the critical point where river runoff dominated tidal damping was when the river runoff velocity was larger than the tidal velocity. River runoff velocity could be a factor that determines the maximum tidal nonlinearity. However, the study was conducted in a straight channel, and studies on tidal junctions require further research.

5.5. Conclusions

Water elevation observations were conducted at the Ota River junction during neap and spring tides. We found an increase in tidal nonlinear behaviour from the river mouth to the junction. The increasing of tidal nonlinearity during the spring tide indicates that tidal nonlinearity is controlled by tidal amplitude. Based on these results, an idealised model using a simplified scenario was applied to examine whether the junction geometry induces the tidal nonlinearity. The model was simulated using constant discharge at the land boundary, M2 and S2 tidal constituents as open-sea boundaries, and uniform depth. The result of the numerical model can capture the observed phenomena. The results of the model indicate that the width channel changes in the junction play a significant role in increasing the nonlinearity of tidal elevation.

The upstream channel width variation in the sensitivity analysis showed a splitting result. The tidal nonlinearity increases for the width of the upstream channel is less than twice of the downstream channel. Meanwhile, tidal nonlinearity decreases for the width of the upstream channel is more than twice that of the downstream channel. The increasing tidal nonlinearity was caused by the convergence of tides in the junction. However, at a wider

junction, the river runoff plays a significant role by damping both M2 and M4, which results in a decrease in tidal nonlinearity. The results suggest that the tidal convergence of the channel plays a role increasing the tidal nonlinearity in a narrow junction (the width of upstream channel less than twice of downstream channel), whereas in a wider channel (the width of upstream channel more than twice of downstream channel), river runoff plays a significant role in the reduction of the tidal amplitude.

This study limited the investigation of the role of the upstream channel width on water elevation in junctions using numerical model under simplified condition. The simplified condition helps us reduce the complexity of tidal nonlinearity dynamics and focuses how the effect of the channel width on tidal nonlinearity. However, the model is highly simplified by neglecting the depth variation, real channel length variation, and complexity of the topographical settings. Therefore, a sensitivity analysis that considers these variables should be conducted in the future to examine those variability to the tidal nonlinearity.

Chapter 6: Conclusions and future works

6.1. Main conclusions

This research aims to characterize the tidal dynamics and its interactions with the river runoff in a variate topographical setting. We conducted field observations and numerical experiments to examine the mechanism of the tidal-river runoff interaction. The field observations were conducted in the Ota river estuary. The numerical experiments were applied in Segara Anakan Lagoon and a synthetic domain. The synthetic domain was adapted from the junction in the Ota river estuary.

This study focuses on (1) characterization of tidal dynamics in the lagoon, single straight channel, and multi-channel estuary (2) Interactions between tide and river runoff and how the interactions affect the tidal currents and tidal elevation as well as mixing of the water column.

The specific conclusions and contributions of this study can be summarized as follows:

1. The tidal wave simultaneously propagates to the lagoon through two open channels from eastern and western inlets. During the rising tide, the tidal wave converges in the middle of the lagoon and diverges during the falling tides. The amassing tidal wave from eastern and western inlets in the middle of the lagoon induces an abrupt change in the tidal range and the tidal asymmetry.
2. TDA and SWA in the eastern and western parts of the lagoon indicate ebb dominance but shifting to flood dominance in the interior of the lagoon. The bottom friction delays the tidal wave celerity, leading to a longer flood duration in the interior of the lagoon.
3. In straight and branching channels, there is an energy transfer from the primary tide to the compound tide and over-tide when the tidal wave propagates from the river mouth upstream, as shown from the spectral energy and harmonic analysis.

4. The spatial variation of tidal distortions (ratio of amplitude: D4/D2) of the straight and branching channels are comparable. In contrast, the tidal asymmetry in the branching channel increased rapidly from the river mouth to the inside of the estuary compared to that in the straight channel. The rapid increase in tidal asymmetry in the branching channel is related to the topographical setting of the branching channels, including rapid changes in the bottom topography, channel width, and junctions.
5. The variation of mean water level is affected by the friction. The variation of mean water level at the branching channel is correlated with the friction related to tides and tidal asymmetry, whereas in the straight channel, the variation of mean water level is correlated with the friction related to subtidal flow
6. The water level station near the water gate has an exception in the tidal range and mean water level variation. The noticeably different patterns of tidal range and mean water level at the station are related to the effect of the water gate, which amplifies the influence of river runoff on the water level.
7. Sensitivity analysis shows that the width of the upstream channel in the junction plays a significant role in the variation of the tidal nonlinearity. The tidal nonlinearity increases when the width of the upstream channel is less than twice that of the downstream channel. The increasing nonlinearity is caused by the convergence of tides in the junction. In contrast, the tidal nonlinearity decreases when the width of the upstream channel is more than twice that of the downstream channel. When the width of the upstream channel is equal to 2 times the branch channel, the cross-sectional area in the upstream is equal to the total cross-sectional area in the branches. Therefore, the tidal interaction due to convergence in the junction is minimal. Hence, the river runoff could play a significant role in damping both M2 and M4 amplitude, which results in a decrease in tidal nonlinearity.

8. Mixing analysis using Freshwater Froude Number (Fr_f) — Mixing tidal efficiency (M) is adequate to reveals that mixing in the ODC is driven by tidal control due to the limited discharge during the observation ($Q_{yaguchi}$ = ~30 m^3/s), with this mixing following ebb–flood and neap–spring oscillations. The river discharge contribution could be significantly observed during the neap period, even in limited discharge. The river discharge contribution could be significantly observed during the neap period. During the spring tide, the contribution of river discharge to the mixing is considerable when the river discharge increases more than the amplitude of tidal discharge. The contribution of river discharge to the mixing is significant when the ratio between river discharge in Yaguchi and tidal discharge amplitude is more than one ($Q_{Yaguchi} > Q_{tidal}$).
9. The cross wavelet transforms (XWT) and wavelet transform coherence (WTC) is able to reveal the nonstationary interaction of circulation, mixing, and river runoff, even though the analysis is applied in short time-series data (less than 30 days).
10. Interactions between tides and river runoff induce the existence of a convergence zone that is estimated to be approximately 4.8 km upstream from the river mouth based on the observation of turbidity along the ODC. The presence of the convergence zone is characterized by the occurrence of an ETM around the same area; however, the location of the convergence zone and the ETM dynamically change depending on the relative force of the tides and river runoff. The dynamics location of ETM could be determined using polynomial regression between the observation of the ETM location and the discharge. However, in this study, the equation could not be proposed because the longitudinal turbidity observation was only conducted once to confirm the existence of the convergence zone..

6.2. Future works

The research does not stop. An enormous number of points must be investigated in future research:

1. This research has investigated the tidal dynamics in the Segara Anakan lagoon. Studies exploring tidal mixing, sediment transport, and sedimentation are important to conduct in the future. Hence, more detailed and longer observations of the discharge, currents, sediment characteristics, salinity, and temperature spatially and temporally would become a database for more comprehensive research. The data can facilitate a solid understanding of hydro-sediment dynamics in the Segara Anakan Lagoon.
2. Study of estuarine circulation and the interaction with the discharge and mixing in a single straight channel have been explored in Chapter 3, showing the existence of ETM as the result of the convergence zone. However, the interaction in the multi-channel estuary has not been explored because the available data cannot be used to study mixing and sediment dynamics in multi-channel estuary. Observation of the discharge, currents, sediment characteristics, salinity, and temperature upstream and downstream of the junction could give insight into the interaction of those parameters in the junction. In addition, it is important to understand how the tide–river runoff interaction affects the transport of sediment and sedimentation in the long term.
3. The ETM location dynamically changes depending on the relative force of the tides and river runoff. The location could be determined using polynomial regression between the river discharge and ETM location. In the future, along channel turbidity observations will be conducted on various river discharges to develop the empirical equation of the ETM location in the ODC. Moreover, since the ETM formation is on the head of the salt intrusion, the analytical solution of the advection-diffusion equation for salt transport [99] will be applied as a proxy to predict the location of the ETM. The prediction of the

analytical solution will be validated using the empirical model that was built from the observation.

4. Examining the tidal nonlinearity behaviour is conducted by variating the width of the upstream channel in numerical experiments. However, the experiment is limited on examining the influence of the upstream channel area to the tidal nonlinearity behaviour. We focused on how the transformation of tidal wave when the tidal wave converged in various junction area. In future researches, I will investigate the effect of length and depth of the channel geometry to the tidal nonlinearity.

References

[1] Guo L, Wegen M van der, Roelvink JA, He Q. The role of river flow and tidal asymmetry on 1-D estuarine morphodynamics L. 2014;300–16.

[2] Wagner W, Mohrig D. Flow and Sediment Flux Asymmetry in a Branching Channel Delta. Water Resour Res. 2019;55(11):9563–77.

[3] Matte P, Jay DA, Zaron ED. Adaptation of classical tidal harmonic analysis to nonstationary tides, with application to river tides. J Atmos Ocean Technol. 2013;30(3):569–89.

[4] Burchard H, Schuttelaars HM, Ralston DK. Sediment trapping in estuaries. Ann Rev Mar Sci. 2018;10(September):371–95.

[5] Du JL, Yang SL, Feng H. Recent human impacts on the morphological evolution of the Yangtze River delta foreland: A review and new perspectives. Estuar Coast Shelf Sci [Internet]. 2016;181:160–9. Available from: http://dx.doi.org/10.1016/j.ecss.2016.08.025

[6] Chen Z, Xu H, Wang Y. Ecological degradation of the Yangtze and Nile delta-estuaries in response to dam construction with special reference to monsoonal and arid climate settings. Water (Switzerland). 2021;13(9):1–10.

[7] Yang SL, Milliman JD, Xu KH, Deng B, Zhang XY, Luo XX. Downstream sedimentary and geomorphic impacts of the Three Gorges Dam on the Yangtze River. Earth-Science Rev. 2014;138:469–86.

[8] Winterwerp JC, Wang ZB. Man-induced regime shifts in small estuaries - I: Theory. Ocean Dyn. 2013;63(11–12):1279–92.

[9] Savenije HHG, Toffolon M, Haas J, Veling EJM. Analytical description of tidal dynamics in convergent estuaries. J Geophys Res Ocean. 2008;113(10):1–18.

[10] Cai H, Toffolon M, Savenije HHG, Yang Q, Garel E. Frictional interactions between tidal constituents in tide-dominated estuaries. Ocean Sci. 2018;14(4):769–82.

[11] Cai H, Savenije HHG, Toffolon M. Linking the river to the estuary: Influence of river discharge on tidal damping. Hydrol Earth Syst Sci. 2014;18(1):287–304.

[12] Tarya A, Sunaringati LC, Ningsih NS. Mangrove density impacts on tidal dynamic in Segara Anakan Lagoon , Indonesia. J Phys Conf Ser. 2019;1245 01206.

[13] Maicu F, Abdellaoui B, Bajo M, Chair A, Hilmi K, Umgiesser G. Modelling the water dynamics of a tidal lagoon: The impact of human intervention in the Nador Lagoon (Morocco). Cont Shelf Res. 2021;228(August).

[14] Lopes CL, Dias JM. Tidal dynamics in a changing lagoon: Flooding or not flooding the marginal regions. Estuar Coast Shelf Sci. 2015;167:14–24.

[15] Contreras Ruiz Esparza A, Douillet P, Zavala-Hidalgo J. Tidal dynamics of the Terminos Lagoon, Mexico: Observations and 3D numerical modelling. Ocean Dyn. 2014;64(9):1349–71.

[16] Serrano D, Ramírez-Félix E, Valle-Levinson A. Tidal hydrodynamics in a two-inlet coastal lagoon in the Gulf of California. Cont Shelf Res [Internet]. 2013;63:1–12. Available from: http://dx.doi.org/10.1016/j.csr.2013.04.038

[17] Buschman FA, Hoitink AJF, Van Der Vegt M, Hoekstra P. Subtidal flow division at a shallow tidal junction. Water Resour Res. 2010;46(12):1–12.

[18] Xiao C, Kawanisi K, Torigoe R, Al Sawaf MB. Mapping tidal current and salinity at a shallow tidal channel junction using the fluvial acoustic tomography system. Estuar Coast Shelf Sci [Internet]. 2021;258(May):107440. Available from: https://doi.org/10.1016/j.ecss.2021.107440

[19] Pye K, Blott SJ. The geomorphology of UK estuaries: The role of geological controls, antecedent conditions and human activities. Estuar Coast Shelf Sci [Internet]. 2014;150(PB):196–214. Available from: http://dx.doi.org/10.1016/j.ecss.2014.05.014

[20] Jewell SA, Walker DJ, Fortunato AB. Tidal asymmetry in a coastal lagoon subject to a mixed tidal regime. Geomorphology [Internet]. 2012;138(1):171–80. Available from: http://dx.doi.org/10.1016/j.geomorph.2011.08.032

[21] Möller OO, Castaing P, Fernandes EHL, Lazure P. Tidal frequency dynamics of a southern Brazil coastal lagoon: Choking and short period forced oscillations. Estuaries and Coasts. 2007;30(2):311–20.

[22] Guo X, Futamura A, Takeoka H. Residual currents in a semi-enclosed bay of the Seto

Inland Sea, Japan. J Geophys Res C Ocean. 2004;109(12):1–23.

[23] White AT, Martosubroto P, Sadorra MSM. The coastal environmental profile of Segara Anakan-Cilacap, South Java, Indonesia. Vol. 25, ICLARM Technical Reports. ICLARM Technical Reports; 1989.

[24] Holtermann P, Burchard H, Jennerjahn T. Hydrodynamics of the Segara Anakan lagoon. Reg Environ Chang. 2009 Nov;9(4):245–58.

[25] Xiao C, Kawanisi K, Al Sawaf MB. Suspended particulate matter concentration in response to tidal hydrodynamics in a long mesotidal floodway. Estuar Coast Shelf Sci [Internet]. 2020;233(November 2019):106525. Available from: https://doi.org/10.1016/j.ecss.2019.106525

[26] Dronkers J. Tidal asymmetry and estuarine morphology. Netherlands J Sea Res. 1986;20(2–3):117–31.

[27] Guo L, Wang ZB, Townend I, He Q. Quantification of Tidal Asymmetry and Its Nonstationary Variations. J Geophys Res Ocean. 2019;124(1):773–87.

[28] Nidzieko NJ. Tidal asymmetry in estuaries with mixed semidiurnal/diurnal tides. J Geophys Res Ocean. 2010;115(8):1–13.

[29] Nidzieko NJ, Ralston DK. Tidal asymmetry and velocity skew over tidal flats and shallow channels within a macrotidal river delta. J Geophys Res Ocean. 2012;117(3):1–17.

[30] Hoitink AJF, Jay DA. Tidal river dynamics: Implications for deltas. Rev Geophys. 2016;54(1):240–72.

[31] Tenorio-Fernandez L, Zavala-Hidalgo J, Olvera-Prado ER. Seasonal variations of river and tidal flow interactions in a tropical estuarine system. Cont Shelf Res. 2019 Oct;188:103965.

[32] Ardli ER, Wolff M. Land use and land cover change affecting habitat distribution in the Segara Anakan lagoon, Java, Indonesia. Reg Environ Chang. 2009 Nov;9(4):235–43.

[33] Lukas MC. Widening the scope: linking coastal sedimentation with watershed dynamics in Java, Indonesia. Reg Environ Chang. 2017 Mar 1;17(3):901–14.

[34] Guo L, Brand M, Sanders BF, Foufoula-Georgiou E, Stein ED. Tidal asymmetry and residual sediment transport in a short tidal basin under sea level rise. Adv Water Resour [Internet]. 2018;121(July):1–8. Available from: https://doi.org/10.1016/j.advwatres.2018.07.012

[35] Deltares. Delft3D-FLOW User Manual Hydro-Morphodynamics. 2014;

[36] Egbert GD, Erofeeva SY. Efficient inverse modeling of barotropic ocean tides. J Atmos Ocean Technol. 2002;19(2):183–204.

[37] Kuang C, Chen W, Gu J, Zhu DZ, He L, Huang H. Numerical Assessment of the Impacts of Potential Future Sea-Level Rise on Hydrodynamics of the Yangtze River Estuary, China. J Coast Res. 2014;30(3):586.

[38] Hoitink AJF, Hoekstra P, Van Maren DS. Flow asymmetry associated with astronomical tides: Implications for the residual transport of sediment. J Geophys Res C Ocean. 2003;108(10):13–1.

[39] Losada, M. A., Dıez-Minguito, M., Reyes-Merlo MA. Tidal-fluvial interaction in the Guadalquivir River Estuary: Spatial and frequency-dependent response of currents and water levels. J Geophys Res Ocean. 2017;122:1–22.

[40] McKay P, Blain CA, Di Iorio D, Hansell H. Mixing and Turbulence in a Flooding Coastal River. J Hydraul Eng. 2013;139(12):1213–22.

[41] Winant CD. Three-Dimensional Residual Tidal Circulation in an Elongated, Rotating Basin. J Phys Oceanogr. 2008;38(6):1278–95.

[42] Jay DA, Giese BS, Sherwood CR. Energetics and sedimentary processes in the Columbia River Estuary. Prog Oceanogr. 1990;25(1–4):157–74.

[43] Zou T, Zhang H, Meng Q, Li J. Seasonal Hydrodynamics and Salt Exchange of a Shallow Estuary in Northern China. J Coast Res. 2016;2016-Sprin(Special Issue 74):95–103.

[44] Simpson JH, Williams E, Brasseur LH, Brubaker JM. The impact of tidal straining on the cycle of turbulence in a partially stratified estuary. Cont Shelf Res. 2005;25(1):51–64.

[45] Simpson JH, Brown J, Matthews J, Allen G. Tidal Straining , Density Currents , and Stirring in the Control of Estuarine Stratification. Estuaries. 1990;13(2):125–32.

[46] Calero Quesada MC, García-Lafuente J, Garel E, Delgado Cabello J, Martins F, Moreno-Navas J. Effects of tidal and river discharge forcings on tidal propagation along the Guadiana Estuary. J Sea Res [Internet]. 2019;146(December 2018):1–13. Available from: https://doi.org/10.1016/j.seares.2019.01.006

[47] Mao Q, Shi P, Yin K, Gan J, Qi Y. Tides and tidal currents in the Pearl River Estuary. Cont Shelf Res. 2004;24(16):1797–808.

[48] Pu X, Shi JZ, Hu GD, Xiong LB. Circulation and mixing along the North Passage in the Changjiang River estuary, China. J Mar Syst [Internet]. 2015;148:213–35. Available from: http://dx.doi.org/10.1016/j.jmarsys.2015.03.009

[49] Sassi MG, Hoitink AJF. River flow controls on tides and tide-mean water level profiles in a tidal freshwater river. J Geophys Res Ocean. 2013;118(9):4139–51.

[50] Wan Y, Zhao D. Observation of saltwater intrusion and ETM dynamics in a stably stratified estuary: the Yangtze Estuary, China. Environ Monit Assess. 2017;189(2).

[51] Burchard H, Hetland RD. Quantifying the contributions of tidal straining and gravitational circulation to residual circulation in periodically stratified tidal estuaries. J Phys Oceanogr. 2010;40(6):1243–62.

[52] Jay DA, Leffler K, Diefenderfer HL, Borde AB. Tidal-Fluvial and Estuarine Processes in the Lower Columbia River: I. Along-Channel Water Level Variations, Pacific Ocean to Bonneville Dam. Estuaries and Coasts. 2015;38(2):415–33.

[53] Callaway R, Grenfell S, Lønborg C. Small estuaries: Ecology, environmental drivers and management challenges. Estuar Coast Shelf Sci. 2014;150(PB):193–5.

[54] Giddings SN, Fong DA, Monismith SG. Role of straining and advection in the intratidal evolution of stratification , vertical mixing , and longitudinal dispersion of a shallow , macrotidal , salt wedge estuary. 2011;116:1–20.

[55] Krvavica N, Gotovac H, Lončar G. Salt-wedge dynamics in microtidal Neretva River estuary. Reg Stud Mar Sci [Internet]. 2021;43:101713. Available from: https://doi.org/10.1016/j.rsma.2021.101713

[56] Haralambidou K, Sylaios G, Tsihrintzis VA. Salt-wedge propagation in a Mediterranean micro-tidal river mouth. Estuar Coast Shelf Sci [Internet]. 2010;90(4):174–84. Available from: http://dx.doi.org/10.1016/j.ecss.2010.08.010

[57] Uncles RJ, Stephens JA, Harris C. Freshwater, tidal and wave influences on a small estuary. Estuar Coast Shelf Sci [Internet]. 2014;150(PB):252–61. Available from: http://dx.doi.org/10.1016/j.ecss.2014.05.035

[58] Soltaniasl M, Kawanisi K, Yano J, Ishikawa K. Variability in salt flux and water circulation in Ota River Estuary, Japan. Water Sci Eng [Internet]. 2013;6(3):283–95. Available from: http://dx.doi.org/10.3882/j.issn.1674-2370.2013.03.005

[59] Kawanisi K. Evaluation of M-Y closure model in tidal estuary with turbulence data from high-resolution current profiler. WIT Trans Built Environ. 2003;70(March):101–10.

[60] Razaz M, Kawanisi K. Turbulence characteristics in the bottom layer of a shallow tidal channel. J Turbul. 2012;13(October 2014):1–22.

[61] Kawanisi K. Structure of Turbulent Flow in a Shallow Tidal Estuary. J Hydraul Eng. 2004;130(4):360–70.

[62] Umehara A, Asaoka S, Fujii N, Otani S, Yamamoto H, Nakai S, et al. Biological productivity evaluation at lower trophic levels with intensive Pacific oyster farming of Crassostrea gigas in Hiroshima Bay, Japan. Aquaculture [Internet]. 2018;495(November 2017):311–9. Available from: https://doi.org/10.1016/j.aquaculture.2018.05.048

[63] Razaz M, Kawanisi K, Nistor I. Tide-driven controls on maximum near-bed floc size in a tidal estuary. J Hydro-Environment Res [Internet]. 2015;9(3):465–71. Available from: http://dx.doi.org/10.1016/j.jher.2014.04.001

[64] Soltaniasl M. Salt Flux, Salinity Intrusion and Estuarine Circulation in the Ota Diversion Channel [Internet]. Hiroshima University Institutional Repository (HiR). Ph.D. Thesis, Hiroshima University, 163 p; 2013. Available from: http://ir.lib.hiroshima-u.ac.jp/en/list/ndc/519/p/2/item/35139

[65] Kawanisi K, Razaz M, Kaneko A, Watanabe S. Long-term measurement of stream flow and salinity in a tidal river by the use of the fluvial acoustic tomography system. J Hydrol. 2010;380(1–2):74–81.

[66] Kawanisi K, Zhu XH, Fan X, Nistor I. Monitoring Tidal Bores using Acoustic Tomography System. J Coast Res. 2017;331(July):96–104.

[67] Bahreinimotlagh M, Kawanisi K, Danial MM, Al Sawaf MB, Kagami J. Application of shallow-water acoustic tomography to measure flow direction and river discharge. Flow Meas Instrum [Internet]. 2016;51:30–9. Available from: http://dx.doi.org/10.1016/j.flowmeasinst.2016.08.010

[68] Al Sawaf MB, Kawanisi K. Novel high-frequency acoustic monitoring of streamflow-turbidity dynamics in a gravel-bed river during artificial dam flush. Catena. 2019;172(January 2018):738–52.

[69] Al Sawaf MB, Kawanisi K. Assessment of mountain river streamflow patterns and flood events using information and complexity measures. J Hydrol [Internet]. 2020;590(September):1–12. Available from: https://doi.org/10.1016/j.jhydrol.2020.125508

[70] Ge J, Zhou Z, Yang W, Ding P, Chen C, Wang ZB, et al. Formation of Concentrated Benthic Suspension in a Time-Dependent Salt Wedge Estuary. J Geophys Res Ocean. 2018;123(11):8581–607.

[71] Geyer WR, MacCready P. The estuarine circulation. Annu Rev Fluid Mech. 2014;46:175–97.

[72] Pritchard D.W. Estuarine Classification — A Help or a Hindrance. In: Neilson BJ., Kuo A, Brubaker J., editors. Estuarine Circulation Contemporary Issues in Science and Society [Internet]. Humana Press.; 1989. p. 1–38. Available from: https://doi.org/10.1007/978-1-4612-4562-9_1

[73] Hansen D V, Rattray MJ. New dimension in estuary classification. Limnol Oceanogr. 1966;3(July):319–26.

[74] Geyer W. Estuarine salinity structure and circulation. In: Valle A, Levinson, editors. In Contemp. Cambridge: Cambridge University Press; 2010. p. 12–26.

[75] Shaha DC, Cho YK. Comparison of empirical models with intensively observed data for prediction of salt intrusion in the Sumjin River estuary, Korea. Hydrol Earth Syst Sci. 2009;13(6):923–33.

[76] Grinsted A, Moore JC, Jevrejeva S. Application of the cross wavelet transform and wavelet coherence to geophysical time series. Nonlinear Process Geophys. 2004;11(5/6):561–6.

[77] Paiva BP, Siegle E, Schettini CAF. Channel curvature effects on estuarine circulation in a highly stratified tropical estuary: The São Francisco river estuary (Brazil). Estuar Coast Shelf Sci. 2020;238(September 2019):106723.

[78] Zhou M. Influence of bottom stress on the two-layer flow induced by gravity currents in estuaries. Estuar Coast Shelf Sci. 1998;46(6):811–25.

[79] Wang B, Giddings SN, Fringer OB, Gross ES, Fong DA, Monismith SG. Modeling and understanding turbulent mixing in a macrotidal salt wedge estuary. J Geophys Res Ocean. 2011;116(2):1–23.

[80] Spicer P, Huguenard K, Ross L, Rickard LN. High-Frequency Tide-Surge-River Interaction in Estuaries: Causes and Implications for Coastal Flooding. J Geophys Res Ocean. 2019;124(12):9517–30.

[81] Guo L, Brand M, Sanders BF, Foufoula-Georgiou E, Stein ED. Tidal asymmetry and residual sediment transport in a short tidal basin under sea level rise. Adv Water Resour. 2018 Nov 1;121:1–8.

[82] Khadami F, Kawanisi K, Tarya A. Tidal Asymmetry in Two-Inlet Lagoon: a Case Study on Segara Anakan Lagoon, Central Java, Indonesia. J Japan Soc Civ Eng Ser B1 (Hydraulic Eng. 2020;76(2):I_1411-I_1416.

[83] Sassi MG, Hoitink AJF, Vermeulen B, Hidayat H. Sediment discharge division at two tidally influenced river bifurcations. Water Resour Res. 2013;49(4):2119–34.

[84] Lu S, Tong C, Lee DY, Zheng J, Shen J, Zhang W, et al. Propagation of tidal waves up in Yangtze Estuary during the dry season. J Geophys Res Ocean. 2015;2121–8.

[85] Guo L, Wegen M van der, Jay DA, Matte P, Wang ZB, Roelvink D, et al. River-tide dynamics: Exploration of nonstationary and nonlinear tidal behavior in the Yangtze River estuary. J Geophys Res C Ocean. 2015;120:3499–521.

[86] Xiao C, Kawanisi K, Torigoe R, Al Sawaf MB. Mapping tidal current and salinity at a shallow tidal channel junction using the fluvial acoustic tomography system. Estuar

Coast Shelf Sci [Internet]. 2021;258(May):107440. Available from: https://doi.org/10.1016/j.ecss.2021.107440

[87] Bilskie M V., Bacopoulos P, Hagen SC. Astronomic tides and nonlinear tidal dispersion for a tropical coastal estuary with engineered features (causeways): Indian River lagoon system. Estuar Coast Shelf Sci. 2019 Jan 5;216:54–70.

[88] MacMahan J, van de Kreeke J, Reniers A, Elgar S, Raubenheimer B, Thornton E, et al. Fortnightly tides and subtidal motions in a choked inlet. Estuar Coast Shelf Sci [Internet]. 2014;150(PB):325–31. Available from: http://dx.doi.org/10.1016/j.ecss.2014.03.025

[89] Khadami F, Kawanisi K, Al Sawaf MB, Gusti GNN, Xiao C. Spatiotemporal Response of Currents and Mixing to the Interaction of Tides and River Runoff in a Mesotidal Estuary. Ocean Sci J [Internet]. 2022;57(0123456789):37–51. Available from: https://doi.org/10.1007/s12601-022-00056-0

[90] Danial MM, Kawanisi K, Al Sawaf MB. Characteristics of tidal discharge and phase difference at a tidal channel junction investigated using the fluvial acoustic tomography system. Water (Switzerland). 2019;11(4).

[91] Pawlowicz R, Pawlowicz R, Beardsley RC, Beardsley R, Lentz S, Lentz S. Classical tidal harmonic analysis including error estimates in MATLAB using T_TIDE. Comput Geosci. 2002;28(8):929–37.

[92] Buschman FA, Hoitink AJF, Van Der Vegt M, Hoekstra P. Subtidal water level variation controlled by river flow and tides. Water Resour Res. 2009;45(10):1–12.

[93] Godin G. The propagation of tides up rivers with special considerations on the upper Saint Lawrence river. Estuar Coast Shelf Sci. 1999;48(3):307–24.

[94] Godin G. Compact approximations to the bottom friction term, for the study of tides propagating in channels. Cont Shelf Res. 1991;11(7):579–89.

[95] Cai H, Savenije HHG, Jiang C, Zhao L, Yang Q. Analytical approach for determining the mean water level profile in an estuary with substantial fresh water discharge. Hydrol Earth Syst Sci. 2016;20(3):1177–95.

[96] Talke SA, Familkhalili R, Jay DA. The Influence of Channel Deepening on Tides, River Discharge Effects, and Storm Surge. J Geophys Res Ocean. 2021;126(5):1–24.

[97] Kukulka T, Jay DA. Impacts of Columbia River discharge on salmonid habitat: 1. A nonstationary fluvial tide model. J Geophys Res Ocean. 2003;108(9).

[98] Horrevoets AC, Savenije HHG, Schuurman JN, Graas S. The influence of river discharge on tidal damping in alluvial estuaries. J Hydrol. 2004;294(4):213–28.

[99] Cai H, Savenije HHG, Zuo S, Jiang C, Chua VP. A predictive model for salt intrusion in estuaries applied to the Yangtze estuary. J Hydrol [Internet]. 2015;529:1336–49. Available from: http://dx.doi.org/10.1016/j.jhydrol.2015.08.050